




FACULTY OF SCIENCE AND TECHNOLOGY

MASTER THESIS

Study programme / specialisation: Marine and Offshore Technology	Spring semester, 2023 Open / Confidential
Author: Arash Shahbazi Doust	 (Writers' signature)
Supervisor at UiS: Dr. Daniel Karunakaran External supervisor(s): Dr. Dasharatha Achani -WoodPLC M.Sc. Vinicius Vileti- Aker Solutions	
Thesis title: Analysis of predicting terminal velocities and impact energies of dropped objects falling through sea column	
Credits (ECTS): 30	
Keywords: Drop objects, terminal velocity, impact energy, probability of exceedance, trajectory, OrcaFlex.	Pages: 80 + appendix: 30 Stavanger, <i>15th June 2023</i>

Abstract

Many offshore operations include risks that might lead to catastrophic consequences. One of the most common offshore risks is the unintentional drop of objects during various marine operations. This work is divided into two main parts. The first part of the thesis is to perform numerical simulations using OrcaFlex to determine the trajectory, terminal velocity, and maximum velocity of the cylindrical dropped object. The numerical study is based on the 3D theory for dropped objects. The study begins by investigating the small-scale model of size 1:20.32 followed by simulating the full-scale model selected from Aanesland et al. (1987). The numerical results for the small-scale model are validated with the experimental data available in the literature. The numerical results show that drop angle, normal drag force and normal drag moment coefficients, and Munk moment coefficient are the most critical factors that determine the trajectories of the dropped object. The results also show that drop angle has no effect on maximum velocity, but it determines the landing location, especially in shallow water regions. For the 0° drop angle of the small-scale model, the terminal velocity obtained using numerical simulation shows good agreement with experimental results and analytical calculation. However, for the same, 90° drop angle, the terminal velocity obtained using numerical simulation is 12 % higher than the experiment due to smooth cylinder assumption. The object's trajectory obtained for a small-scale model for different drop angles also shows good agreement with the experimental results. For the full-scale model, the highest maximum velocity that an object can attain during an excursion in certain water depths is observed for the Munk moment coefficient in the range of 0.08 to 0.20. It is also observed that the maximum impact energy of the full-scale model will be constant after 400 m water depth for different combinations of Munk moment coefficients and drag moment coefficients.

Finally, the probability of exceedance and probability of impact is calculated for the full-scale model based on DNV-RP-F107 and results are compared with the numerical simulations. The results show that the probability of exceedances increases with water depth, while it decreases by increasing the horizontal distance from the drop location. The results also show a higher probability of impact at far horizontal locations using numerical simulation as compared to DNV-RP-F107 and vice-versa for short horizontal distances from the drop location.

Acknowledgement

I want to offer my heartfelt appreciation to my supervisor, Dr. Daniel Karunakaran, for his tremendous assistance and support through my thesis. His knowledge, perceptive input, and devotion have all helped shape my thoughts and bring my thesis to conclusion.

I consider myself fortunate to collaborate with Dr. Dasharatha Achani as my co-supervisor. His dedication to perfection and true enthusiasm for the thesis was a source of inspiration for me. I am convinced that the information and abilities I have obtained via Dr. Achani guidance will have a long-term influence on my future pursuits. I would like to take this opportunity to especially thank him for his significant support and guidance.

Furthermore, I want to say thanks to my co-supervisor, and Engineer Vinicius Vileti for his insightful suggestions, guidance, and assistance during the process of this study. His comments and ideas were critical in improving my work.

I would like to express my deepest gratitude to all professors and faculty members at the Department of Mechanical and Structural Engineering and Materials Science for their assistance and guidance during my education at the University of Stavanger. I appreciate my friends and classmates, Karan Sandipkumar Patel, Hassan Hassan Yousef, and Sohail Salahshoor Langroodi, for their fascinating ideas and ongoing inspiration.

Ultimately, I am grateful to my dear family and respected friends for their constant support, compassion, and unwavering love during my academic journey. Their encouragement and support provided me with strength to overcome difficulties and achieve success.

Contents

Abstract.....	ii
Acknowledgement.....	iii
1. Chapter 1: Introduction.....	1
1.1. Background.....	1
1.2. Scope.....	4
2. Chapter 2: Literature review.....	6
2.1. Drop frequency	8
2.2. Parameter identification	9
3. Chapter 3: Theory and Methods.....	11
3.1. Method of motion projection.....	11
3.1.1. Free fall in the air	11
3.1.2. Impact with water surface	12
3.1.3. Free fall in the water.....	12
3.2. Dynamics of object falling through water column	13
3.2.1. Potential flow theory	13
3.2.2. A two-dimensional (2D) theory for dropped objects.....	16
3.2.3. A three-dimensional (3D) theory for dropped objects.....	19
3.3. Basic assumption and definitions	24
3.4. Drag forces and moments.....	24
3.5. Slamming forces	26
3.6. Energy calculation.....	26
3.7. Object excursion and hit probability	27

4. Chapter 4: Introduction to OrcaFlex.....	31
4.1. Coordinate system.....	31
4.2. Direction convention.....	32
4.3. 6D buoys.....	32
4.4. Static analysis.....	33
4.5. Dynamic analysis.....	33
4.6. Hydrodynamic loads.....	34
5. Chapter 5: Numerical validation of small-scale model.....	36
5.1. Model setup.....	38
5.2. Small-scale model velocity verification.....	44
5.3. Small-scale model excursion verification.....	46
6. Chapter 6: Parametric study and probability calculations of drop object.....	51
6.1. Small-scale model.....	51
6.2. Full-scale drill pipe.....	60
7. Chapter 7: Conclusion and recommendation.....	75
Conclusion.....	75
Future work.....	76
References.....	78
Appendix I.....	81
Appendix II.....	85
Appendix III.....	86
Appendix IV.....	96
Appendix V.....	97

Appendix VI 99

List of figures

Figure 1.1 Examples of dropped objects on submarine installations.....	1
Figure 1.2 Marine anchor [3]	3
Figure 3.1 Two-dimensional (2D) Coordinate systems	17
Figure 3.2 Three-dimension (3D) coordinate system	19
Figure 3.3 Distribution function parameters in Eq.[3.72].....	28
Figure 3.4 Probability of landing of drop object on a ring with inner radius of r_i and outer radius of r_o [5].....	29
Figure 3.5 Definition of hit area [5].....	30
Figure 4.1 Coordinate system in OrcaFlex [28].....	31
Figure 4.2 Direction and Headings [28]	32
Figure 4.3 Simulation stages and time in dynamic analysis [28]	34
Figure 5.1 Model setup for dropped drilling pipe [4]	36
Figure 5.2 Illustration of drag areas	38
Figure 5.3 Location of Morrison elements on the cylinder	39
Figure 5.4 Drag coefficient in axial flow for smooth cylinder as a function of Reynolds number [31].....	40
Figure 5.5 Skin friction streamwise behavior along the thin cylinder in terms of Reynolds numbers Re_x and Re_a with comparison to flat plate empirical model [32].....	41

Figure 5.6 Plots of skin friction coefficient for smooth and rough flat plate at laminar, transition, and turbulent flow regimes [33].....	41
Figure 5.7 Velocity of small-scale model for $\beta = 0^\circ$ and $\beta = 90^\circ$ (fully submerged).....	45
Figure 5.8 Velocity of small-scale model for $\beta=0^\circ$ and $\beta=90^\circ$ (height from surface = 1.48 m) ..	45
Figure 5.9 Investigation of Munk moment coefficient (C_{mm}) at $\beta = 45^\circ$ and $C_{d, moment} = 1.0$	47
Figure 5.10 Investigation of Munk moment coefficient (C_{mm}) at $\beta = 30^\circ$ and $C_{d, moment} = 1.0$	47
Figure 5.11 Investigation of Munk moment coefficient (C_{mm}) at $\beta = 60^\circ$ and $C_{d, moment} = 1.0$	48
Figure 5.12 Investigation of drag moment coefficient ($C_{d, moment}$) when $\beta = 30^\circ$	49
Figure 5.13 Investigation of drag moment coefficient ($C_{d, moment}$) when $\beta = 45^\circ$	49
Figure 5.14 Investigation of Drag moment coefficient ($C_{d, moment}$) when $\beta = 60^\circ$	50
Figure 6.1 Effect of water depth on velocity of small-scale model.....	52
Figure 6.2 Effect of Munk moment coefficient (C_{mm}) on velocity for small-scale model in 40 m water depth.....	53
Figure 6.3 Effect of axial drag moment coefficient $C_{f, moment}$ on velocity.....	55
Figure 6.4 Effect of axial drag moment coefficient $C_{f, moment}$ on excursion	56
Figure 6.5 Small-scale model drag force coefficient time history for different drop angles.....	57
Figure 6.6 Small-scale model excursion when $\beta = 30^\circ$	58
Figure 6.7 Small-scale model excursion when $\beta = 45^\circ$	59

Figure 6.8 Small-scale model excursion when $\beta = 60^\circ$	59
Figure 6.9 Full-scale drilling pipe excursion in 100 m water depth for different drop angle.....	62
Figure 6.10 Probability of exceedance for different water depth according to DNV (RP)	71
Figure 6.11 Probability of exceedance different water depth according to OrcaFlex simulation	72
Figure 6.12 Comparison of probability of hit in 100 m water depth	72
Figure 0.1 Effect of Munk moment coefficient on velocity for small-scale model with drop angle of 45° in 5 m water depth	81
Figure 0.2 Effect of Munk moment coefficient on velocity for small scale model with drop angle of 45° in 10 m water depth	82
Figure 0.3 Effect of Munk moment coefficient on velocity for small scale model with drop angle of 45° in 20 m water depth	83
Figure 0.4 Effect of Munk moment coefficient on velocity for small scale model with drop angle of 45° in 40 m water depth	84
Figure 0.1 Drag force coefficient (Cd) time history for different β and $Cmm = 0.08$	85
Figure 0.1 Excursion and velocity of full-scale model when $\beta = 45^\circ$ and $Cd, moment = 0.3$ for different Munk moment coefficient Cmm in different water depth	87
Figure 0.2 Excursion and velocity of full-scale model when $\beta = 45^\circ$ and $Cd, moment = 0.4$ for different Munk moment coefficient Cmm in different water depth	88
Figure 0.3 Excursion and velocity of full-scale model when $\beta = 45^\circ$ and $Cd, moment = 0.6$ for different Munk moment coefficient Cmm in different water depth	89
Figure 0.4 Excursion and velocity of full-scale model when $\beta = 45^\circ$ and $Cd, moment = 0.8$ for different Munk moment coefficient Cmm in different water depth	91

Figure 0.5 Excursion and velocity of full-scale model when $\beta = 45^\circ$ and $Cd, moment = 1.0$ for different Munk moment coefficient Cmm in different water depth	92
Figure 0.6 Excursion and velocity of full-scale model when $\beta = 45^\circ$ and $Cd, moment = 1.2$ for different Munk moment coefficient Cmm in different water depth	93
Figure 0.7 Excursion and velocity of full-scale model when $\beta = 45^\circ$ and $Cd, moment = 1.4$ for different Munk moment coefficient Cmm in different water depth	95
Figure 0.1 Comparison of probability of exceedance based on DNV (RP) and OrcaFlex simulations for full-scale model in different water depth.....	96

List of tables

Table 1.1 Container Properties [2].....	2
Table 1.2 Anchor properties [2].....	3
Table 2.1 Relation between the landing point of the object and water depth [13]	8
Table 2.2 DNV reported frequency of dropped object in sea [5]	9
Table 2.3 Selective parameters [15].....	10
Table 3.1 Angular deviation of a dropping object from vertical line [5].....	28
Table 5.1 Drilling pipe properties.....	36
Table 5.2 List of investigated parameters	38
Table 5.3 Geometry setting, and coefficient used in OrcaFlex.....	42
Table 5.4 Drag and slam setting, and coefficient used in OrcaFlex	43
Table 5.5 Added mass and damping setting and coefficient used in OrcaFlex.	43
Table 5.6 Morison Element geometry and orientation used in OrcaFlex	43
Table 5.7 Morison elements specification used in OrcaFlex	44
Table 5.8 Terminal velocity of small-scale model for different drop cases	46
Table 6.1 Maximum velocity of the small-scale model in 5 m water depth	54
Table 6.2 Maximum velocity of the small-scale model in 10 m water depth	54
Table 6.3 Maximum velocity of the small-scale model in 20 m water depth	54
Table 6.4 Maximum velocity of the small-scale model in 40 m water depth	55

Table 6.5 Effect of drop angle and drag moment coefficient on average drag force coefficient .	57
Table 6.6 Effect of Munk moment coefficient on average drag force coefficient.....	58
Table 6.7 Geometry setting used in OrcaFlex	60
Table 6.8 Drag and slam setting, and coefficient used in OrcaFlex	60
Table 6.9 Added mass and damping setting and coefficient used in OrcaFlex.....	61
Table 6.10 Morison Element geometry and orientation used in OrcaFlex	61
Table 6.11 Morison elements specification used in OrcaFlex	61
Table 6.12 Terminal velocity of full scaled drill pipe	62
Table 6.13 Maximum velocity of full-scale model in 100 m water depth.....	63
Table 6.14 Maximum velocity of full-scale model in 200 m water depth.....	64
Table 6.15 Maximum velocity of full-scale model in 400 m water depth.....	64
Table 6.16 Maximum velocity of full-scale model in 800 m water depth.....	65
Table 6.17 Landing velocity of full-scale model in 100 m water depth	66
Table 6.18 Landing velocity of full-scale model in 200 m water depth	66
Table 6.19 Landing velocity of full-scale model in 400 m water depth	67
Table 6.20 Landing velocity of full-scale model in 800 m water depth	67
Table 6.21 Effective energy of full-scale model in 100 m water depth.....	68
Table 6.22 Effective energy of full-scale model in 200 m water depth.....	68
Table 6.23 Effective energy of full-scale model in 400 m water depth.....	69

Table 6.24 Effective energy of full-scale model in 800 m water depth	69
Table 6.25 Effect of drag moment coefficient on Average drag force coefficient	70
Table 6.26 Comparison of probability of impact in 100 m water depth for different locations from drop point	73
Table 6.27 Comparison of probability of impact in 200 m water depth for different locations from drop point	73
Table 6.28 Comparison of probability of impact in 400 m water depth for different locations from drop point	74
Table 6.29 Comparison of probability of impact in 800 m water depth for different locations from drop point	74

Nomenclature:

Ω_1 : Rotational velocity in x-direction (rolling frequency)

Ω_2 : Rotational velocity in y-direction (pitch frequency)

Ω_3 : Rotational velocity in z-direction (yaw frequency)

A_r : Area within the ring (m^2), Figure 3.2

C_a : Added mass coefficient for the body

C_d : Drag coefficient

C_{dx} : Drag coefficient on x -direction

C_{dz} : Drag coefficient on z -direction

C_{mm} : Munk moment coefficient

D_o : Outer diameter of cylinder

F_{Ly} : Lift force in y -direction

F_{Lz} : Lift force in z -direction

F_{dx} : Drag force in x -direction

F_{dy} : Drag force in y -direction

F_{dz} : Drag force in z -direction

F_e : Vector of equation of forces

F_{ex} : Equation of forces in x -direction

F_{ey} : Equation of forces in y -direction

F_{ez} : Equation of forces in z -direction

F_w : Wave force or current force

I_x : Mass moment of inertia in x -axis when object rotates around x -axis

I_{xy} : Mass moment of inertia in x -axis when object rotates around y -axis

I_y : Mass moment of inertia in y -axis when object rotates around y -axis

I_{yx} : Mass moment of inertia around y -axis when object rotates around x -axis

I_z : Mass moment of inertia in z -axis when object rotates around z -axis

I_{zx} : Mass moment of inertia around z -axis when object rotates around x -axis

L_{sl} : Length of subsea line within the ring (m)

M_{44} : Moment of inertia in roll direction

M_{55} : Moment of inertia in pitch direction

M_{55} : Moment of inertia in pitch direction

M_{66} : Moment of inertia in yaw direction

M_{Ly} : Lift moment around y -axis

M_{Lz} : Lift moment around z -axis

M_{dy} : Drag moment around y -axis

M_{dz} : Drag moment around z -axis

$M_{\alpha ix}$: Munk moment around x direction

$M_{\alpha iy}$: Munk moment around y direction

$M_{\alpha iz}$: Munk moment around z direction

$P_{hit,r}$: Probability of hit within the ring

$P_{hit,sl,r}$: Probability of dropped object hitting subsea line (sl) within certain ring, r .

U_1 : Translational velocity in x-direction

U_2 : Translational velocity in y-direction

U_3 : Translational velocity in z-direction

$U_y(x)$: Local relative velocity in y-axis direction

$U_z(x)$: Local relative velocity in z-axis direction

V_T : Terminal velocity

V_r : Fluid velocity relative to the body

\dot{X} : Velocity in X-direction

\dot{Y} : Velocity in Y-direction

\dot{Z} : Velocity in Z-direction

a_r : Fluid acceleration relative to the body

a_w : Fluid acceleration relative to the earth

m_{11} : Added mass in surge direction

m_{22} : Added mass in sway direction

m_{22} : Added mass in sway direction from strip theory

m_{33} : Added mass in heave direction from strip theory

m_{55} : Added mass in pitch direction from strip theory

m_{66} : Added mass in yaw direction from strip theory

m_{mm} : Added mass

m_{t2} : 2D added mass coefficient in sway direction at the trailing edge

m_{t3} : 2D added mass coefficient in heave direction at the trailing edge

r_i : Inner radius of the ring

r_o : Outer radius of the ring

x_t : Longitudinal position of effective trailing edge

Δ : Mass of fluid displaced by body

∇ : Gradient operator in potential flow theory

∇ : Immersed volume of the object

For symmetric cylinders $I_{xz} = I_{zx}$, $I_{xy} = I_{yx}$, $I_{yz} = I_{zy}$

h : Vertical distance from water surface

Δ : Mass of the displaced water by the body

A : Drag area

B : Breadth of falling object (m), Figure 3.3

$C(p, v)$: System damping load

C : Arbitrary function of time

D : Diameter of subsea line (m), Figure 3.3

E : Effective energy

$F(p, v, t)$: External load

F : Net force

$K(p)$: System stiffness

L : Length of the cylinder

$M(p, a)$: System inertia load

P : Position

U : velocity of the moving body

V : Fluid velocity at time t

a : Acceleration

c : Rolling frequency decaying rate

g : Gravitational acceleration

i : Unit vector in x direction

j : Unit vector in y direction

k : Unit vector in z direction

m : Mass of the object

n : Normal vector of the body surface

$p(x)$: Probability of falling object hitting a location at horizontal distance x from drop point

t : Time

x : Horizontal distance at seabed (meter)

z : Vertical distance (positive is upward)

α : Angle of attack

β : Instantaneous rotational angle between x -axis in local coordinate and X -axis in global coordinate systems

γ : Coefficient of air friction

δ : Lateral deviation (meter)

ζ : Wave elevation

η : Side slip angle

θ : Instantaneous Euler angle around Y-axis

ρ : Water density

ν : Kinetic viscosity of water

φ : Velocity potential function

ψ : Instantaneous Euler angle around Z- axis

ϕ : Instantaneous Euler angle around X-axis

D_o : Outer diameter

D_i : Inner diameter

I_n : Normal drag area third moment of Inertia

I_a : Axial drag area third moment of Inertia

Chapter 1: Introduction

1.1. Background

Development of the oil and gas sector has increased dramatically in recent years to fulfill the global energy demand. New expansions pushed the industry to deeper water depths. Deeper waters increase the challenges of marine operations which prompts the industry to demand higher level safety standards to reduce the risks and improve safety. Accidental drops of objects are one of the most prevalent problems during marine operations. These accidents may result in fatalities or environmental pollution. Figure 1.1 illustrates two examples of dropped objects. Some guidelines such as DNV-RP-F107 have provided an approximation for the extent of damage due to falling objects which are not suitable for detailed analysis of the different cases. To mitigate environmental damage and economic loss, the offshore industry needs to investigate these critical events in detail. To study the accidents thoroughly we must understand the dynamics of the objects and their kinetic energies.

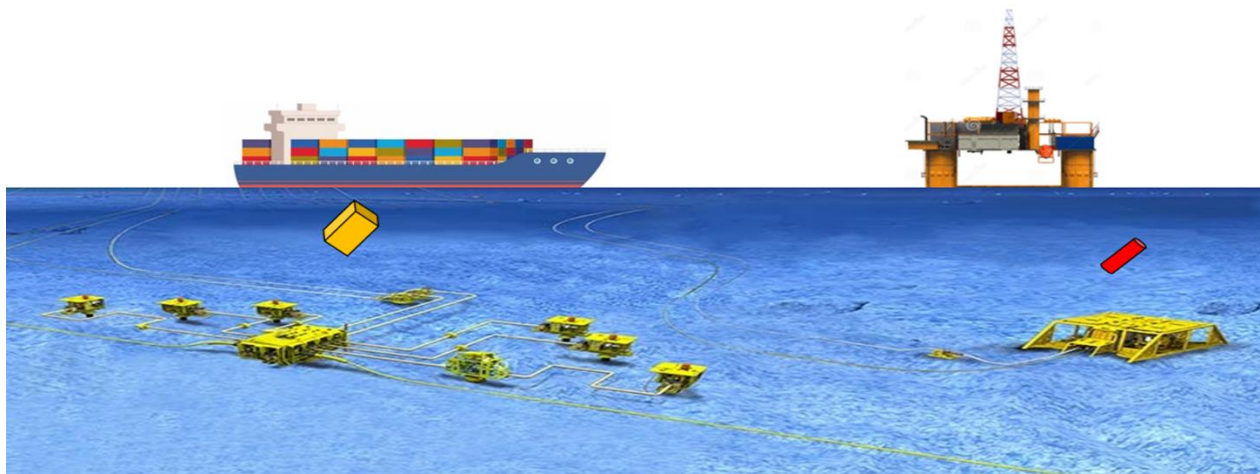


Figure 1.1 Examples of dropped objects on submarine installations

A dropped object is defined as anything which falls from its static condition and is subjected to gravitational force and can inflict death, injury, or damage to equipment and the environment [1]. In this work, the term dropped object only refers to marine operations. There are two categories of dropped objects, static and dynamic. Static-dropped objects are objects that fall from their initial position due to their weight without any external force being applied. Dynamic dropped

objects are objects that fall from their initial position because of applied force. For example, impact from equipment or loads during transport.

Table 1.1 Container Properties [2]

Container type	Max. Gross mass (kg)	L (mm)	W (mm)	H (mm)
20 ft. Standard	24000	6100	2370	2590
40 ft. standard	30500	12190	2440	2590

Drop object accidents happen due to many causes but the below cases are the most common causes [1]:

- Inadequate securing
- Failed fixture and fitting
- Corrosion
- Poor housekeeping
- Procedure not followed

The falling of small objects such as hand tools into the sea during offshore operations usually has minor consequences. The major consequences however are due to the falling of large, heavy objects such as casing, drilling equipment, containers, X-mas trees, subsea modules, and templates because of their high impact energy. Falling objects into the ocean in offshore fields are considered a threat to subsea equipment, pipelines, jackets, mooring system, and in certain cases, ROVs near platform.

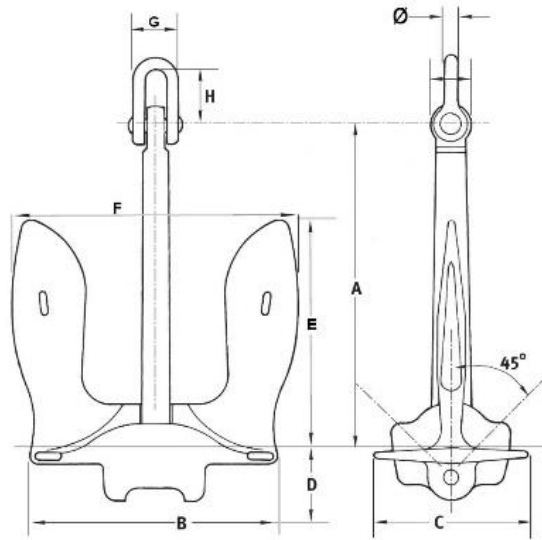


Figure 1.2 Marine anchor [3]

Table 1.2 Anchor properties [2]

Mass of anchor (kg)	E (mm)	C (mm)	H (mm)	B (mm)	A (mm)
3060	1283	841	380	1832	2374
4890	1498	984	415	2135	2769
6900	1681	1105	480	2391	3100
10500	1934	1273	600	2752	3571
14100	2135	1404	660	3036	3939
20000	2399	1578	730	3411	4420

While installing the subsea equipment, it is vital to assess the extent of object excursion in case of an accidental drop. To ensure the safety of subsea equipment, installation vessels are required to perform their operation in some distance to the subsea assets. The required distance is called “standoff point”. To provide an estimate of the standoff point for installation of various objects, their dynamics should be investigated. Determining the standoff point also involves investigating the hydrodynamic forces.

Investigating the dropped objects encompasses a variety of subjects. For example, nonlinear dynamics, maneuvering theory, fluid dynamics, probability, and statistical approaches, and hence

have a broad importance and applicability. The falling objects go through three phases during the falling process offshore. Drop through air, through splash zone, and through the sea column. The kinetic energy of falling objects is a function of their velocity. The falling object velocity depends on number of variables such as depth, the initial velocity of the object, the geometry and weight of the object, and angle of object when it is diving to the water.

1.2. Scope

In this dissertation the author covers numerical and analytical study of velocity and spatial motion of dropped cylindrical objects. The research has mainly investigated the object's behavior in water. Simulations are performed by OrcaFlex which is widely used in marine operation analysis and several control parameters are investigated. The control parameters consist of Munk moment coefficient, drag moment coefficient, and initial drop condition (drop angle and drop height). Also, the DNV (RP) for analysis of dropped object is investigated and are compared with simulations. This work comprises 6 chapters. Following the background and motivation in **Chapter 1**, a review of pervious literatures on dropped objects is provided in **Chapter 2**. The theory and mathematical modeling of dropped cylindrical objects is presented in **Chapter 3**. A brief introduction to OrcaFlex is presented in **Chapter 4** and 6D Buoy object which is used for simulations is described in that chapter. **Chapter 5** includes the modeling of small-scale drilling pipe and validation of OrcaFlex results with experiment data extracted from literature. In **Chapter 6**, the effect of different combination of coefficient and water depth on small scale model's velocity is studied. In addition, a full-scale drilling pipe is modeled, and the effect of different coefficients and water depth is investigated. Finally, a comparison between DNV (RP) and OrcaFlex simulation for probability of impact to a subsea pipeline is carried out. Lastly, **Chapter 7** provides an overview of the performed research and concludes the work with recommendations for future research. **Appendix I** illustrates the effect of Munk moment coefficient on velocity for small scale model for different water depth. **Appendix II** provides drag force coefficient (C_d) time history for different drop angles. **Appendix III** provides details of excursion and velocity of full-scale model during simulation for different water depth. **Appendix IV** provides the detail of comparison between DNV (RP) and simulation results in probability of exceedance for full scale drilling pipe. **Appendix V** presents the details of

analytical calculation for small-scale and full-scale model terminal velocity in 0° and 90° drop angle. **Appendix VI** provides the PYTHON code for modifying the model and performing several simulations for different combinations of studied parameters.

Chapter 2: Literature review

Heavy dropped object accidents such as falling of pipes during offshore operations are considerably reduced due to effective safety procedures and advanced technology implemented by industry. However, knowing the behavior and statistics of the dropped object events are critical for offshore operations. The offshore operations that have risk of dropped object can be categorized to below activities [1]:

- Drilling operation
- Well service operation
- Lifting operation
- Maintenance operation
- Scaffolding
- Vessel operation
- Quayside operations
- Road transport
- Other operations

In 1987, Aanesland et al. [4] used Newman's ship maneuvering equation in their study. They performed numerical and experimental study on a falling drilling pipe and corrected Newman's equation to include viscous effect. Their experimental study includes model tests with scale of 1:20.32. They concluded that the height of the object above the water surface has significant influence on object motion just below the surface, but the effect diminishes as the cylinder sinks deeper [4]. DNV-RP-F107 [5] provided a methodology for studying the probability of dropped objects hitting the subsea equipment and referred to these experiments as calculation methods. Luo and Davis (1992) performed 2D simulations of falling objects by solving differential equations of motion. They identified the important parameters by illustrative parametric studies. Computer software DELTA was used to perform the study. They concluded that drop angle and current significantly affect the horizontal displacement of the falling object, while wave's effect is comparatively negligible. Furthermore, the horizontal velocity of the object is a function of drop height and angle of drop [6]. Colwill and Ahilan (1992) also used DELTA software tool to

perform a series of numerical studies on trajectory of drill casings falling into the sea. They concluded that drop height and drop angle of the object are dominating factors in horizontal velocity of dropped object. The relationship between impact velocity and the chance of exceeding it was effectively developed using reliability-based impact analysis [7]. Gilles (2001) performed a series of tests on circular cylinders and used two underwater cameras at two different locations to record each drop. In his study, he modified the center of mass (COM) location, initial velocity, orientation angle of drop, and diameter to length ratio of the cylinders. He concluded that the location of center of mass is the dominant factor in excursion of dropped cylinders [8]. Ray (2006) performed a total of 42 experimental tests on objects made of polyester resin. In total 42 experiments were performed. Based on the study from Ray (2006), the trajectory of cylinder is more stable and predictable compared to other objects. He concluded that for rigid dropped objects with high velocity in water, their trajectory and dispersion pattern is highly dependent of object geometry [9]. Kim et al. (2002) used direct numerical method to study general 3D dropped objects with 6 degrees of freedom in time domain and determine their characteristic motions. Further, they performed physical experiments to determine the viscous effect on cylindrical bodies. The parameters such as different body aspect ratio, end shape, and orientation to incoming flow were investigated to estimate various drag force coefficients. Based on the results, they concluded that the simulated motion pattern highly depends on initial drop angle, body aspect ratio, and mass center [10]. Chu et al. (2005) and Chu and Fan (2006) used IMPACT35 to simulate dropped objects travelling in single phase and stratified fluids such as air, water, or sediment. To simplify the equations, a series of linearization is performed by using different coefficients in the time domain for calculating drag force, lift force, and moment. Their results show that, the location of center of mass of the object plays a crucial role in spatial motion of the object [11], [12]. Yasseri (2014) performed a series of tests on scaled models of falling cylinders in water with small initial velocity to study their landing points and influence of their orientation. Based on the study they defined a relation between the landing point of the object and water depth which is presented in Table 2.1 [13].

Table 2.1 Relation between the landing point of the object and water depth [13]

Radius from drop point (Percentage of water depth)	Probability of landing within the radius
10 %	50 %
20 %	80 %
30 %	90 %
40 %	95 %
50 %	98 %

Yaseri (2014) also investigated stand-off points for various objects in three current velocities in his work. He concluded that cavity formed by dropped object influences the dynamic motion and excursion of the object in fluid. He also notes that statistical distribution of landing points cannot cover the effect of all governing parameters in excursion of dropped objects [13]. Awotahegn et al. (2015) performed series of tests on falling containers and drill pipes in sea. Their study includes a 2D model developed from a 3D study of object motion with different angles of orientation. To identify the dominant factors in dynamics of the falling object a parametric study is performed, and a case study is included to compare the results with DNV (RP). They concluded that the distribution of landing point of the falling objects is a function of drop angle, drop height, water entry, impact velocity, object mass, and hydrodynamics of the object. By comparing the experiment results with suggested method from DNV, they concluded that DNV method provides conservative results.

2.1. Drop frequency

The UK department of energy tracked dropped object incidents that happened between 1980 to 1986. Based on this study, 81 incidences involving falling objects and 825 crane operations per year were recorded during this time. There were 3.7 million lifts during this period, which equates to 4500 lifts to / from vessel for each crane in one year. This corresponds to the probability of 2.2E-05 falling object incident for each lift. The probability of the event is increased to 3.0E-05 for objects heavier than 20 tons for each lift. The study reported that 70 % of the falling objects were landed on deck while the remaining 30 % of objects were dropped into the sea. It was assumed the objects dropped during utilization of drilling derrick were solely

landed in the water [5]. The dropped objects' reports that have been used by DNV (RP) contains details of the object specification. No update has been provided regarding dropped object accidents. Importance of available data for evaluation of failure rate, reliability, and risk is clearly approved. However, the report of accidents in industry is intended to be kept confidential by companies unless they are enforced by rules to disclose the case to the public.

Table 2.2 DNV reported frequency of dropped object in sea [5]

Type of lift	Frequency (per lift)
Ordinary lift to/from supply vessel with platform crane < 20 tons	1.2E-05
Heavy lift to/from supply vessel with the platform crane > 20 tons	1.6E-05
Handling of load < 100 tons with the lifting system in the drilling derrick	2.2E-05
Handling of BOP/load > 100 tons with the lifting system in the drilling derrick	1.5E-05

Formation of worldwide work group, consisting of more than 200 operators, contractors, and service companies, and industrial bodies, which was dedicated and enthusiastic about preventing dropped object incidents had efficiently improved the industry performance in risk mitigation subjects [14].

2.2. Parameter identification

Accidents happening offshore can be categorized into different types. Parameters that affect these accidents can include many different conditions. However, there are specific factors that have substantial effect on the accidents. Kawsar et al. (2015) classified these affective parameters into three categories, deterministic, constant, and variable to anticipate the implemented risk and consequence of these accidents. Table 2.3 provides a summary of effective parameters considered by Kawsar et al. (2015), which dominate the frequency and consequence of accidents on offshore pipelines.

Table 2.3 Selective parameters [15]

Variable		Deterministic	Constant
Mass and dimension	Corrosion parameter		
Weight	Pit depth	Drag surface	Sea surface height
Length	Pit length	Drag force	Pipeline material properties
Breadth/ Diameter	Pit breadth	Terminal velocity	Pipeline shape and diameter
Height		Hit angle	Hydrostatic pressure
		Energy	Internal pressure

Chapter 3: Theory and Methods

3.1. Method of motion projection

In a dropped object scenario, the object experiences three phases until it landed on the final location.

- 1) Falling in air;
- 2) Passing the splash zone (a transient period in which a portion of the object is immersed in water);
- 3) Fully submerged in water;

3.1.1. Free fall in the air

Calculation of falling object velocity in air is a well-established topic and it can be determined while including the air resistance or neglecting its effect.

Newton's second law:

$$F = m \cdot a = m \cdot \left(\frac{dV}{dt}\right) \quad [3.1]$$

Gravity force (downward force):

$$F = m \cdot g \quad [3.2]$$

Force due to air resistance (upward force):

$$F = \gamma \cdot V \quad [3.3]$$

From Eq. [3.1], [3.2], and [3.3]

$$m \cdot \left(\frac{dV}{dt}\right) = m \cdot g - \gamma \cdot V \quad [3.4]$$

Since the air resistance is small,

$$\left(\frac{dV}{dt}\right) = g \quad [3.5]$$

The velocity of impact to water surface

$$V = \sqrt{2} \cdot (g \cdot h) \quad [3.6]$$

3.1.2. Impact with water surface

The process of falling objects passing through water surface is considered as a complicated phenomenon which consists of four stages. The shake phase, the flow forming phase, the open cavity phase, and the close cavity phase. The detail of this process is not included in this work.

3.1.3. Free fall in the water

Dropped objects sinking in water are affected by the following forces:

- Object weight;
- Upward force due to change in momentum of water relative to the falling object (projected area of the object affects this force);
- Upward force due to friction between water and object surface (this force is a function of object surface area, Reynolds number, and relative surface roughness);
- Upward force due to buoyancy (this force is function of object volume and density of water) [16];

It is possible to use the numerical methods to calculate the velocity of the dropped objects in water from equation of motion. A dropped object will reach its terminal velocity when the summation of vertical forces is zero and the object stops accelerating. This definition implies that gravitational force is equal to the buoyancy and drag force.

Drag force at terminal velocity is:

$$F = \frac{1}{2} C_d \cdot A \cdot \rho \cdot V_T^2 \quad [3.7]$$

Buoyancy force is:

$$F = \rho \cdot g \cdot \nabla \quad [3.8]$$

From Eq.[3.2], [3.7], and [3.8] we get:

$$\frac{1}{2} C_d \cdot A \cdot \rho \cdot V_T^2 + \rho \cdot g \cdot \nabla = m \cdot g \quad [3.9]$$

By simplifying Eq.[3.9] we get:

$$V_T^2 = 2 \cdot g \cdot \left(\frac{m - \rho \cdot \nabla}{C_d \cdot A \cdot \rho} \right) \quad [3.10]$$

3.2. Dynamics of object falling through water column

To understand the motion of three-dimensional objects in water, it is necessary to analyze dynamics of the body. Several factors such as geometry of the object, potential flow effect, and environmental effects are contributing to the motion of objects in water. So, accurate evaluation of objects' dynamic behavior is challenging from an engineering point of view.

For three-dimensional objects with six degrees of freedom in water, it is possible to develop a numerical solution for time domain analysis. For specific problems, based on the objective of the study, a mathematical model tailored for that problem should be developed [17].

To analyze dropped object accidents in sea column it is important to define the water depth, time interval from drop moment to landing, and weight of the dropped object, buoyancy force, drag force, and geometry of the object. Furthermore, object orientation at its initial location, object aspect ratio, and mass distribution, are considered as the dominant parameters in dynamic behavior of the object [18].

3.2.1. Potential flow theory

To study the hydrodynamics of the objects in water we need to provide a mathematical model for fluid surrounding the object. Potential flow theory provides such a model; however, some simplifications should be applied. According to the theory, flow is inviscid, incompressible, and irrotational [19]. These three assumptions provide a convenient mathematical model that is very practical.

To characterize the velocity, a time t and location $X = (x, y, z)$ velocity vector $V(x, y, z, t) = (U_1, U_2, U_3)$ are defined. So, in global cartesian coordinate system:

$$V = \nabla\phi = i \frac{\partial\phi}{\partial x} + j \frac{\partial\phi}{\partial y} + k \frac{\partial\phi}{\partial z} \quad [3.11]$$

The velocity potential function has no physical meaning, but it is defined to make mathematical calculations for irrotational fluid motion easier. A fluid is considered irrotational when the vorticity vector is zero in all flow domain.

$$\omega = \nabla \times V \quad [3.12]$$

Sea water is also considered to be incompressible:

$$\nabla \cdot V = 0 \quad [3.13]$$

According to the theory the velocity potential should satisfy the Laplace equation:

$$\frac{\partial^2\phi}{\partial x^2} + \frac{\partial^2\phi}{\partial y^2} + \frac{\partial^2\phi}{\partial z^2} = 0 \quad [3.14]$$

The complete mathematical problem of finding the velocity potential of irrotational, incompressible, fluid motion consists of solution of the Laplace equation with relevant boundary conditions on the fluid.

By solving the Laplace equation for irrotational, incompressible, fluid flow, the velocity potential can be calculated. To solve the Laplace equation, suitable boundary conditions should be considered.

Pressure (p) in flow domain can be calculated by solving Bernoulli's equation.

$$p + \rho gz + \rho \frac{\partial\phi}{\partial t} + \frac{\rho}{2} \cdot V \cdot V = C \quad [3.15]$$

In this equation, C is a function of time and set as constant value. z at mean sea surface is zero and the gravitational force is considered as the dominant force on the flow field. Eq.[3.15] is valid for defining unsteady, irrotational, and inviscid fluid motion.

3.2.1.1. Kinematic boundary condition

The below equation defines the boundary condition for fixed body in moving fluid.

$$\frac{\partial \phi}{\partial n} = 0 \quad [3.16]$$

Eq.[3.16] provides the differentiation equation of potential flow over the normal direction to the body surface. In this work the positive normal direction is into the fluid domain. In another word, Eq.[3.16] shows impermeability of the body, which means no flow is entering or exiting the body surface. The tangential component of the velocity on the bod surface is neglected in this work. For moving bodies, Eq.[3.16] can be modified to:

$$\frac{\partial \phi}{\partial n} = U \cdot n \quad [3.17]$$

In Eq.[3.17], U can represent transitional velocity or rotational velocity. which implies different location on the body will experience different U values. To define the rate of change of a parameter in fluid domain for a particle, function $F(x, y, z, t)$ is defined. Substantial derivative of function F is defined as below:

$$\frac{DF}{Dt} = \frac{\partial F}{\partial t} + V \cdot \nabla F \quad [3.18]$$

If the sea water surface is defined as:

$$z = \zeta(x, y, t) \quad [3.19]$$

The function F will be:

$$F(x, y, z, t) = z - \zeta(x, y, t) = 0 \quad [3.20]$$

To satisfy the Eq.[3.20], water particle on the water surface is assumed to remain on the surface, which lead to substantial derivative of F to be 0. The following equation is used to apply the kinematic boundary condition on sea water surface.

$$\frac{\partial}{\partial t}(z - \zeta(x, y, t)) + \nabla\varphi \cdot \nabla(z - \zeta(x, y, t)) = 0 \quad [3.21]$$

For $z = \zeta(x, y, t)$ we get:

$$\frac{\partial \zeta}{\partial t} + \frac{\partial \varphi}{\partial x} \frac{\partial \zeta}{\partial x} + \frac{\partial \varphi}{\partial y} \frac{\partial \zeta}{\partial y} - \frac{\partial \varphi}{\partial z} = 0 \quad [3.22]$$

3.2.1.2. Dynamic free- surface condition

Based on the theory the water pressure at sea surface is equal to the atmospheric pressure P_0 and it is constant. By substituting constant C in Eq.[3.15] with $\frac{P_0}{\rho}$, which implies there is no fluid motion. For $z = \zeta(x, y, t)$ we get:

$$g\zeta + \frac{\partial \varphi}{\partial t} + \frac{1}{2} \left(\left(\frac{\partial \varphi}{\partial x} \right)^2 + \left(\frac{\partial \varphi}{\partial y} \right)^2 + \left(\frac{\partial \varphi}{\partial z} \right)^2 \right) = 0 \quad [3.23]$$

By linearizing free surface conditions [3.22] and [3.23], the equations will be simplified and possible to solve with acquired data in each case. Otherwise, due to nonlinearity of the free surface condition, the problems will be complicated, and we cannot solve them to find the free surface location.

3.2.2. A two-dimensional (2D) theory for dropped objects.

There are two different coordinate systems used in two-dimensional (2D) theory to define the motion. As shown in Figure 3.1, XOZ is used to define the global coordinate system where it is fixed on the water level and coincide with the local coordinate system when the drop accident occurs at water surface. The xoz is used to define the local coordinate system where it is fixed to the center of mass of the object and if the object rotates, the local coordinate system also rotates.

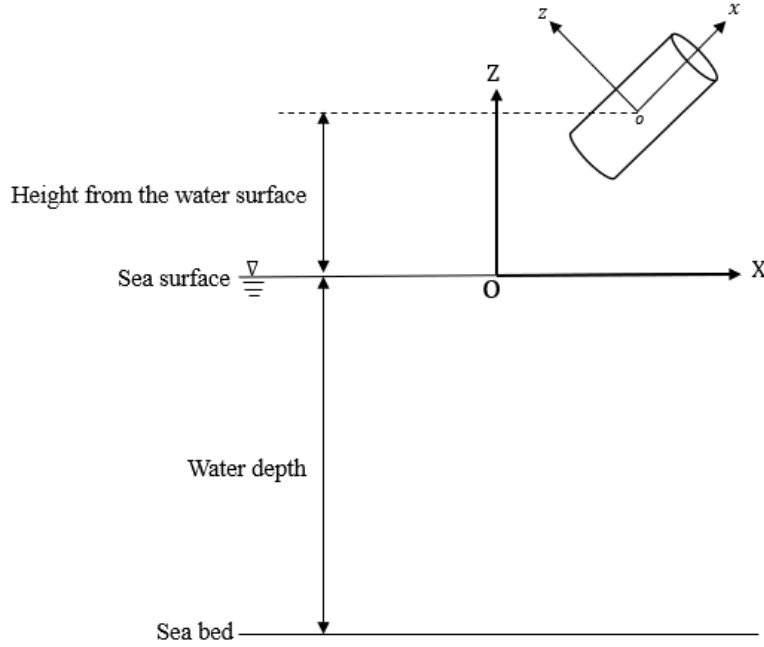


Figure 3.1 Two-dimensional (2D) Coordinate systems

3.2.2.1. Equation of motion in 2D

Based on Newton's second law the equation of motion in global coordinate system can be derived for rigid objects. The following equations provide translational motion of the center of gravity and rotational motion about the center of gravity. Presented equations are based on Aanesland et al. (1987), which only considers the motion in two-dimensions (2D). The object in his calculations is slender, rigid and has uniform mass distribution.

$$(m - \rho V)g \sin(\theta) + F_{dx} = m\dot{U}_1 \quad [3.24]$$

$$\begin{aligned} & -(m - \rho V)g \cos(\beta) + F_{dz} \\ = & \{U_1 m_t U_3 - U_1 (x_t m_t) \Omega_2 + m_{33} \dot{U}_3\} + m(\dot{U}_3 - U_1 \Omega_2) \end{aligned} \quad [3.25]$$

$$M_{dy} = \{-U_1 (m_{33} + x_t m_t) U_3 + U_1 x_t^2 m_t \Omega_2 + m_{55} \dot{\Omega}_2\} \quad [3.26]$$

The above equations are providing motion about local coordinate system (xoz). The Slender body theory assumes that object's geometrical variation is smooth along the length. While for

cylinders, there is an abrupt change in the end points. To accommodate this change in to the equations, the effective trailing edge (x_t) is defined [20].

Calculation of viscose forces and moments are carried out by the following formulas:

$$F_{dx} = 0.664\pi\sqrt{v\rho^2L}U_1\sqrt{|U_1|} + \frac{1}{8}\rho\pi C_{dx}D^2U_1|U_1| \quad [3.27]$$

$$F_{dz} = 0.5 \int_{-0.5L}^{0.5L} \rho C_{dz}DU_z(x)|U_z(x)|dx \quad [3.28]$$

$$M_{dy} = -0.5 \int_{-0.5L}^{0.5L} \rho C_{dz}DxU_z(x)|U_z(x)|dx \quad [3.29]$$

To include the frictional drag the term $0.664\pi\sqrt{v\rho^2L}U_1\sqrt{|U_1|}$ is added to Eq.[3.27] which can be derived based on boundary layer theory in turbulent flow [21]. The second part of Eq.[3.27] is defining the form drag component [22]. Eq.[3.28] and Eq.[3.29] are representing Morrison equation [23]. Velocity of cylinder relative to water in z-axis direction is presented by $U_z(x)$ which is defined as follow:

$$U_z(x) = -(U_3 - \Omega_2), \quad for \quad -0.5L < x < 0.5L \quad [3.30]$$

By substituting Eq.[3.30] to Eq.[3.28] and [3.29], we get:

$$F_{dz} = 0.5\rho C_{dz}D_o \int_{-0.5L}^{0.5L} -(U_3 - \Omega_2) |U_3 - \Omega_2| dx \quad [3.31]$$

$$F_{dz} = 0.5\rho C_{dz}D_o \int_{-0.5L}^{0.5L} x(U_3 - \Omega_2x) |U_3 - \Omega_2x| dx \quad [3.32]$$

By solving velocities (U_1, U_3, Ω_2) we get the motion in local coordinate system for each time step. Calculated motion should be transferred to global coordinate system using the following equation:

$$\begin{bmatrix} \dot{X} & \dot{Y} \end{bmatrix} = \begin{bmatrix} U_1 & U_3 \end{bmatrix} \begin{bmatrix} \cos(\beta) & -\sin(\beta) \\ \sin(\beta) & \cos(\beta) \end{bmatrix} \quad [3.32]$$

Since the y -axis in local coordinate system is parallel to Y -axis in global coordinate system the angular velocity $\dot{\beta} = \Omega_2$ so the angle β can be derived.

3.2.3. A three-dimensional (3D) theory for dropped objects.

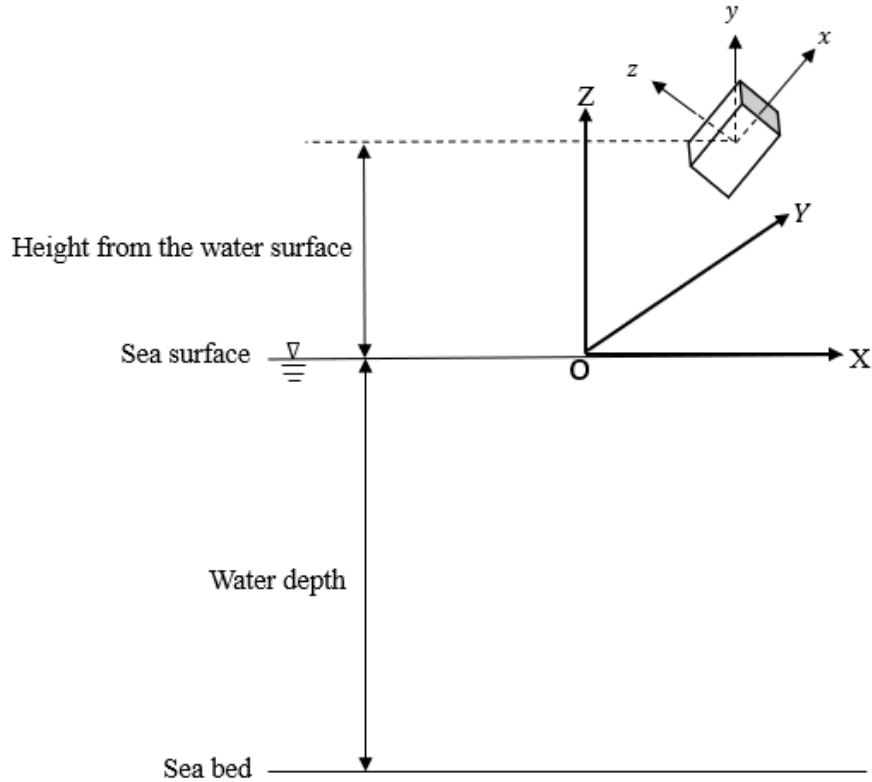


Figure 3.2 Three-dimension (3D) coordinate system

Global coordinate system for three-dimensional (3D) body is illustrated in Figure 3.2. The X-Y plane in global coordinate system (O-XYZ) is presenting the water surface and water depth is in negative Z direction. Local coordinate system (o-xyz) is fixed on object and local coordinate system origin (o) coincide with objects center of mass. The local coordinate system (o-xyz) and global coordinate system (O-XYZ) coincide when the cylinder is on the water surface.

3.2.3.1. Equation of 3D motion of rigid body

Assume \vec{V}_0 defines the velocity of body origin (o) in local coordinate system (o -xyz) and $\vec{\Omega}_0$ defines the angular velocity of body in global coordinate system (O -XYZ). The vectors of \vec{V}_0 and $\vec{\Omega}_0$ are defined in unit vectors of $\vec{i}, \vec{j}, \vec{k}$ for local coordinate system.

$$\vec{V}_0 = [U_1 \quad U_2 \quad U_3] \begin{bmatrix} \vec{i} \\ \vec{j} \\ \vec{k} \end{bmatrix} \quad [3.33]$$

$$\vec{\Omega}_0 = [\Omega_1 \quad \Omega_2 \quad \Omega_3] \begin{bmatrix} \vec{i} \\ \vec{j} \\ \vec{k} \end{bmatrix} \quad [3.34]$$

Equilibrium of forces and moments on object is defined by the following Eq.[3.24][3.25]:

$$F_e = [F_{ex} \quad F_{ey} \quad F_{ez}] \begin{bmatrix} \vec{i} \\ \vec{j} \\ \vec{k} \end{bmatrix} \quad [3.35]$$

$$F_{ex} = m[\dot{U}_1 - U_2\Omega_3 + U_3\Omega_2] \quad [3.36]$$

$$F_{ey} = m[\dot{U}_2 + U_1\Omega_3 - U_3\Omega_1] \quad [3.37]$$

$$F_{ez} = m[\dot{U}_3 - U_1\Omega_2 + U_2\Omega_1] \quad [3.38]$$

$$M_e = [M_{ex} \quad M_{ey} \quad M_{ez}] \begin{bmatrix} \vec{i} \\ \vec{j} \\ \vec{k} \end{bmatrix} \quad [3.39]$$

$$M_{ex} = M_{44}\dot{\Omega}_1 - M_{45}(\dot{\Omega}_2 - \Omega_1\Omega_3) - M_{46}(\dot{\Omega}_3 + \Omega_1\Omega_2) + M_{56}(\Omega_3^2 - \Omega_2^2) + (M_{44} - M_{55})\Omega_2\Omega_3 \quad [3.40]$$

$$M_{ey} = M_{55}\dot{\Omega}_2 - M_{54}(\dot{\Omega}_1 + \Omega_2\Omega_3) - M_{56}(\dot{\Omega}_3 - \Omega_1\Omega_2) + M_{46}(\Omega_1^2 - \Omega_3^2) + (M_{44} - M_{66})\Omega_1\Omega_3 \quad [3.41]$$

$$M_{ez} = M_{66}\dot{\Omega}_3 - M_{64}(\dot{\Omega}_1 - \Omega_2\Omega_3) - M_{65}(\dot{\Omega}_2 + \Omega_1\Omega_3) + M_{45}(\Omega_2^2 - \Omega_1^2) + (M_{55} - M_{44})\Omega_1\Omega_2 \quad [3.42]$$

3.2.3.2. Equations of 3D motion of a dropped cylinder with uniform mass distribution

Eq.[3.24] to Eq.[3.26] are used to develop two-dimensional motion of the object and Eq.[3.35] and Eq.[3.39] are used to extend Eq.[3.24] to Eq.[3.26] and develop three-dimensional motion of the object. The following equations define the 3D motion of the dropped object.

$$(m - \rho V)g \sin(\theta) + F_{dx} = m(\dot{U}_1 + U_3\Omega_2 - U_2\Omega_3) \quad [3.43]$$

$$-(m - \rho V)g \cos(\theta) \sin(\phi) + F_{Lx} + F_{dy} = \{m_{22}\dot{U}_2 + U_1m_{t2}U_2 - U_1(x_tm_{t2})\Omega_3\} + m(\dot{U}_2 + U_1\Omega_3 - U_3\Omega_1) \quad [3.44]$$

$$-(m - \rho V)g \cos(\theta) \cos(\phi) + F_{Lz} + F_{dz} = \{m_{33}\dot{U}_3 + U_1m_{t3}U_3 - U_1(x_tm_{t3})\Omega_2\} + m(\dot{U}_3 + U_2\Omega_1 - U_1\Omega_2) \quad [3.45]$$

$$\dot{\Omega}_1 = c \quad [3.46]$$

$$M_{Ly} + M_{dy} = \{-U_1(m_{33} + x_tm_{t3})U_3 + U_1x_t^2m_{t3}\Omega_2 + m_{55}\dot{\Omega}_2\} + M_{55}\dot{\Omega}_2 + (M_{44} - M_{66})\Omega_1\Omega_3 \quad [3.47]$$

$$M_{Lz} + M_{dz} = \{-U_1(m_{22} + x_tm_{t2})U_2 + U_1x_t^2m_{t2}\Omega_3 + m_{66}\dot{\Omega}_3\} + M_{66}\dot{\Omega}_3 + (M_{55} - M_{44})\Omega_1\Omega_2 \quad [3.48]$$

By numerical simulation in time domain the translational motion and rotational motion of the object can be calculated in each time step. To transfer the motions from local coordinate system

(o-xyz) to global coordinate system (O-XYZ), a series of partial rotations are defined so that each rotation is performed based on the previous rotation.

- a) yaw motion is used to define the Euler angle if angular motion is around Z-axis. After rotation, Y-axis is named n and considered as nutation axis.
- b) Pitch motion is used to define the Euler angle if angular motion is around nutation axis n .
- c) Roll motion is used to define the Euler angle if angular motion is around x-axis (Local x axis coincides with global X axis).

The following Equation defines the relation between three Euler angles and angular velocity in local coordinate system [24].

$$\begin{bmatrix} \Omega_1 \\ \Omega_2 \\ \Omega_3 \end{bmatrix} = \begin{bmatrix} -\dot{\psi} \sin(\theta) \\ \dot{\psi} \sin(\phi) \cos(\theta) \\ \dot{\psi} \cos(\phi) \cos(\theta) \end{bmatrix} + \begin{bmatrix} 0 \\ \dot{\theta} \cos(\phi) \\ -\dot{\theta} \sin(\phi) \end{bmatrix} + \begin{bmatrix} \dot{\phi} \\ 0 \\ 0 \end{bmatrix} \quad [3.49]$$

In 3D theory, there are three more additional motions compared to 2D theory (transitional motion in y direction and rotational motion around x-axis and z-axis). By solving Morrison equation, we get drag forces and lift forces and moments due to axial roll motions in ideal flow. The forces and moments are calculated using Kutta-Joukowski's lift theorem [25].

$$F_{dx} = 0.664\pi\sqrt{v\rho^2L}U_1\sqrt{|U_1|} + \frac{1}{8}\rho\pi C_{dx}D_o^2U_1|U_1| \quad [3.50]$$

$$F_{dy} = 0.5 \int_{-0.5L}^{0.5L} \rho C_{dy}D_o U_y(x) |U_y(x)| dx \quad [3.51]$$

$$F_{dz} = 0.5 \int_{-0.5L}^{0.5L} \rho C_{dz}D_o U_z(x) |U_z(x)| dx \quad [3.52]$$

$$F_{Ly} = \int_{-0.5L}^{0.5L} \rho U_z(x) \Gamma dx = \int_{-0.5L}^{0.5L} \rho U_z(x) \pi D_o \Omega_1 \frac{D_o}{2} dx \quad [3.53]$$

$$F_{Lz} = - \int_{-0.5L}^{0.5L} \rho U_z(x) \Gamma dx = - \int_{-0.5L}^{0.5L} \rho U_y(x) \pi D_o \Omega_1 \frac{D_o}{2} dx \quad [3.54]$$

$$M_{Ly} = \int_{-0.5L}^{0.5L} \rho U_z(x) \Gamma x dx = \int_{-0.5L}^{0.5L} \rho U_y(x) \pi D_o \Omega_1 \frac{D_o}{2} x dx \quad [3.55]$$

$$M_{Lz} = \int_{-0.5L}^{0.5L} \rho U_z(x) \Gamma x dx = \int_{-0.5L}^{0.5L} \rho U_z(x) \pi D_o \Omega_1 \frac{D_o}{2} x dx \quad [3.56]$$

$$M_{dy} = -0.5 \int_{-0.5L}^{0.5L} \rho C_{dz} D_o U_z(x) |U_z(x)| x dx \quad [3.57]$$

$$M_{dz} = 0.5 \int_{-0.5L}^{0.5L} \rho C_{dy} D_o U_y(x) |U_y(x)| x dx \quad [3.58]$$

$$U_z(x) = -(U_3 - \Omega_2 x), \quad for \quad -0.5L < x < 0.5L \quad [3.59]$$

$$U_y(x) = -(U_2 + \Omega_3 x), \quad for \quad -0.5L < x < 0.5L \quad [3.60]$$

Eq.[3.50] to Eq.[3.58] calculated the forces and moment in x,y,z direction. Ordinary differential equations (ODE) presented here are nonlinear so the explicit Runge Kutta 4th order method is used for solution. In each time step translational velocity components (U_1, U_2, U_3) are calculated [26]. The following relation is used to convert local translational velocities into global coordinate system by considering the rotation sequence of the coordinate system used in the proceeding phase [27].

$$[\dot{X} \quad \dot{Y} \quad \dot{Z}] = [U_1 \quad U_2 \quad U_3] \cdot \left\{ \begin{bmatrix} 1 & 0 & 0 \\ 0 & \cos(\phi) & \sin(\phi) \\ 0 & -\sin(\phi) & \cos(\phi) \end{bmatrix} \begin{bmatrix} \cos(\theta) & 0 & -\sin(\theta) \\ 0 & 1 & 0 \\ \sin(\theta) & 0 & \cos(\theta) \end{bmatrix} \begin{bmatrix} \cos(\psi) & \sin(\psi) & 0 \\ -\sin(\psi) & \cos(\psi) & 0 \\ 0 & 0 & 1 \end{bmatrix} \right\} \quad [3.61]$$

3.3. Basic assumption and definitions

The main effective force on a falling object in air is the gravitational force. Since the aerodynamic forces play a small role in dynamic behavior of majority of dropped objects, this work is mainly focused on dropped object's dynamic behavior when they are submerged in water.

In general, the flow of a fluid in both space and time can be described using various physical characteristics, including the velocity of the fluid particles, pressure, density, and temperature, all of which vary based on both space and time. These characteristics are calculated using principles of mass and momentum conservation, energy conservation, and the state of the fluid.

Regarding the dynamics of the fluid flow, parameters such as temperature and pressure are assumed constant during the analysis. So, the focus is on calculating the speed and pressure of the fluid within the fluid domain. Respective equations for defining the dynamics of the object can be developed by utilizing mass and momentum conservation law which can be obtained from equation of motion for fluids.

3.4. Drag forces and moments

Drag force is considered as a hydrodynamic load that is proportional to the square of the relative velocity of the fluid with respect to object. To calculate the drag force on a falling object, it is assumed that the flow is following the crossflow assumption. Assuming the drag area and drag coefficients are known, the relative flow velocity is divided into normal and tangential components and utilized to compute the drag force in respective directions.

To determine the drag force in normal and tangential direction, with respect to local coordinate system, different reference drag area and drag coefficients are calculated. Reference drag area is the area that is used in drag force formula. To calculate the drag moments, the same procedure as drag force calculation is followed, however, the reference area is replaced by moment of reference area.

To get the initial data for calculation of drag force, two methods can be utilized. The first and most accurate method is performing an experiment to get the required data (e.g., using a downscaled model or actual size model). The second method is to use the data from available literature or theoretical values for drag data, which can be used in case that physical experiment data is not available.

Munk moment

When slender bodies experience an axial flow, two forces of equal size are applied on the front half and rear half of the body. These forces cause a moment that highly destabilizes the motion of the body, which is known as the Munk moment. By solving the equation of motion, the spatial motion of trajectories can be obtained. Munk moment appears as dimensionless position derivative of the motion state in kinetic part of equation of motion.

To calculate the Munk moment it is assumed:

- The object is considered rigid body;
- The object is symmetric in o-xy and o-yz plane;
- The inertial products are negligible ($M_{45} = M_{54} = M_{46} = M_{56} = M_{65} = 0$);
- The object is fully submerged;
- Longitudinal mass distribution of the body is constant;

Based on the above assumptions the following formulas are derived:

$$\begin{cases} M_{\alpha ix} = (m_{22} - m_{33})U_2U_1 \\ M_{\alpha iy} = (m_{33} - m_{11})U_3U_1 \\ M_{\alpha iz} = (m_{11} - m_{22})U_1U_2 \end{cases} \quad [3.62]$$

$$\alpha = -\arctan\left(\frac{U_2}{U_1}\right) \quad [3.63]$$

$$\eta = \arctan\left(\frac{U_3}{\sqrt{U_1^2 + U_2^2}}\right) \quad [3.64]$$

Considering small angle of attack and side slip angle the Munk moment is:

$$[M] = \frac{1}{2} v^2 \begin{bmatrix} \sin(2\eta) & 0 & 0 \\ 0 & \sin(2\eta) & 0 \\ 0 & 0 & \sin(2\alpha) \end{bmatrix} \cdot \begin{bmatrix} m_{22} - m_{33} & 0 & 0 \\ 0 & m_{33} - m_{11} & 0 \\ 0 & 0 & m_{11} - m_{22} \end{bmatrix} \quad [3.65]$$

According to the above formula, Munk moment is dependent on velocity, side slip angle, angle of attack, and added mass. The above formula agrees with Munk moment definition in OrcaFlex, which is presented below.

$$M = \frac{1}{2} C_{mm} \cdot \nabla \cdot \sin(2\alpha) \cdot v^2 \quad [3.66]$$

$$m_{mm} = C_{mm} \cdot \Delta \quad [3.67]$$

3.5. Slamming forces

Slamming is an intense, nonlinear, impact that occurs as result of interaction between water, air, and structure. Slamming forces are governed by several factors which include water compressibility, flexibility of the object, air bubbles, generation of cavity or vacuum and evacuation of the air from water. It is possible to calculate the slamming forces by including the slamming data in computations. Also, the slamming coefficient can be considered constant or variable during the submergence of the object.

3.6. Energy calculation

To estimate the energy of the dropped object we need to determine its mass and velocity. We should note that dropped object velocity in water is a function of their submerged mass and geometry. To calculate the terminal energy of the falling object, the terminal velocity is required. The terminal energy is:

$$E_T = \frac{1}{2} \cdot m \cdot V_T^2 \quad [3.68]$$

Substituting Eq.[3.10] in Eq.[3.68]:

$$E_T = \frac{m \cdot g}{C_d \cdot A} \left(\frac{m}{\rho} - \nabla \right) \quad [3.69]$$

The effective energy of the object at the moment of impact is a function of kinetic terminal energy and kinetic added mass energy. The effective energy at the moment of impact is:

$$E = E_T + E_A = \frac{1}{2} \cdot (m + m_{mm}) \cdot V_T^2 \quad [3.70]$$

$$m_{mm} = \rho \cdot C_a \cdot \nabla \quad [3.71]$$

3.7. Object excursion and hit probability

Falling objects geometry plays an important role in horizontal translation of the object. According to Aanesland et al. (1987), cylindrical object excursion is dependent on the water entry angle, and they may follow different patterns during falling while heavy box shape objects are almost sinking vertically. The distribution of falling objects on the seabed is assumed to follow normal distribution which is defined as below:

$$p(x) = \frac{1}{\sqrt{2\pi}\delta} e^{-\frac{1}{2}\left(\frac{x}{\delta}\right)^2} \quad [3.72]$$

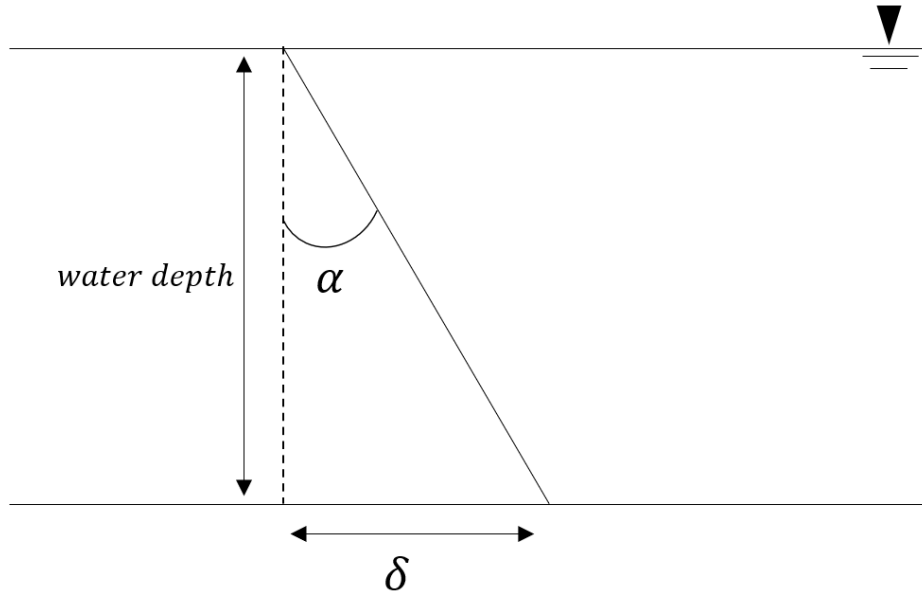


Figure 3.3 Distribution function parameters in Eq.[3.72]

DNV-RP-F107 provided a table that indicates angular deviation of a dropping object from vertical line. Table 3.1 shows angular deviation of dropped object with respect to their geometry and weight based on DNV-RP-F107

Table 3.1 Angular deviation of a dropping object from vertical line [5]

No	Description	Weight(tons)	Angular deviation (α) (degree)
1	Flat/Long shaped	<2	15
2		2-8	9
3		>8	5
4	Box/Round shaped*	<2	10
5		2-8	5
6		>8	3
7	Box/Round shaped	>>8	2

* A spread on the surface before the objects sinks is included.

Probability of a falling object land on a location within the horizontal distance r from drop location is:

$$P(x \leq r) = \int_{-r}^r p(x) dx \quad [3.73]$$

Area that has risk of drop object impact on subsea equipment can be divided into several rings as shown in Figure 3.4. Probability of the dropped object land on one of these rings are calculated as shown below:

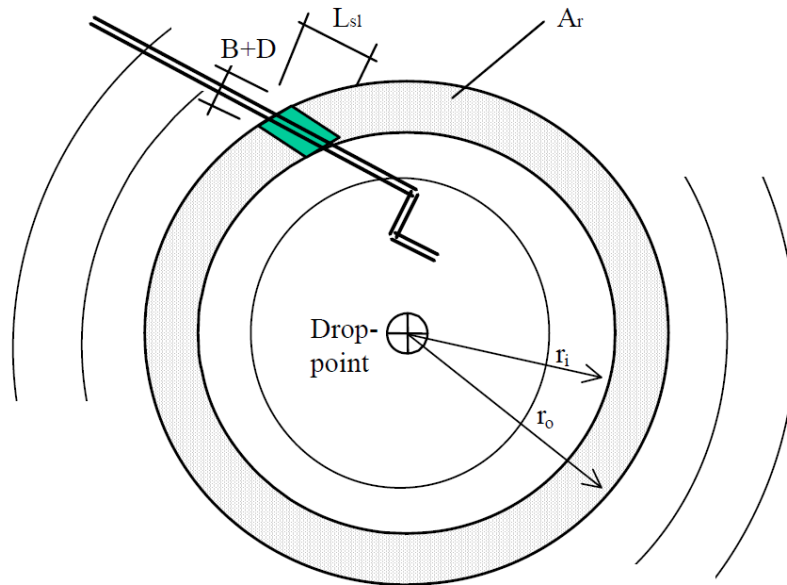


Figure 3.4 Probability of landing of drop object on a ring with inner radius of r_i and outer radius of r_o [5]

$$P_{hit,r} = P(r_i \leq x \leq r_o) = P(x \leq r_o) - P(x \leq r_i) \quad [3.74]$$

Probability of a dropped object hit a pipeline within a specific ring can be calculated as below:

$$P_{hit,sl,r} = P_{hit,r} \cdot \frac{L_{sl} \cdot \left(D + \frac{B}{2} + \frac{B}{2} \right)}{A_r} \quad [3.75]$$

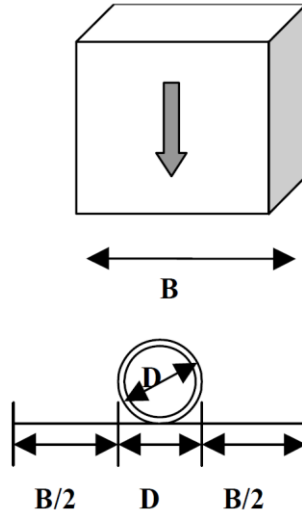


Figure 3.5 Definition of hit area [5]

Breadth of the falling object, B , for box shaped objects can be estimated as an average of two smallest sides, while for tubular objects it is the diameter of the object.

Chapter 4: Introduction to OrcaFlex

A vast variety of software is developed for simulating offshore operation and response of fixed and floating marine structures. Some of these software's are OrcaFlex, Simo- RiFlex, Fast, etc. Orcina is the developer of OrcaFlex which is specialized for performing static, quasi-static, and dynamic analyses. In this work, OrcaFlex is used as the main software for developing models and simulation. OrcaFlex can simulate a wide range of offshore structures such as buoys, ships, wind turbines, pipelines and risers, and mooring systems.

4.1. Coordinate system

OrcaFlex software considers GXYZ as the global coordinate system while GX, GY, GZ are the main axes in X direction, in Y direction, and in Z direction, respectively. Local coordinate system is also defined in the software for each component of the model and denoted by Lxyz. Defined coordinate systems are right-handed. Figure 4.1 illustrates the coordinate systems defined above and includes the Global coordinate system GXYZ, local coordinate system Vxyz of the vessel V as an example of object. In this coordinate system clockwise, angular displacement is considered as the positive direction of rotation.

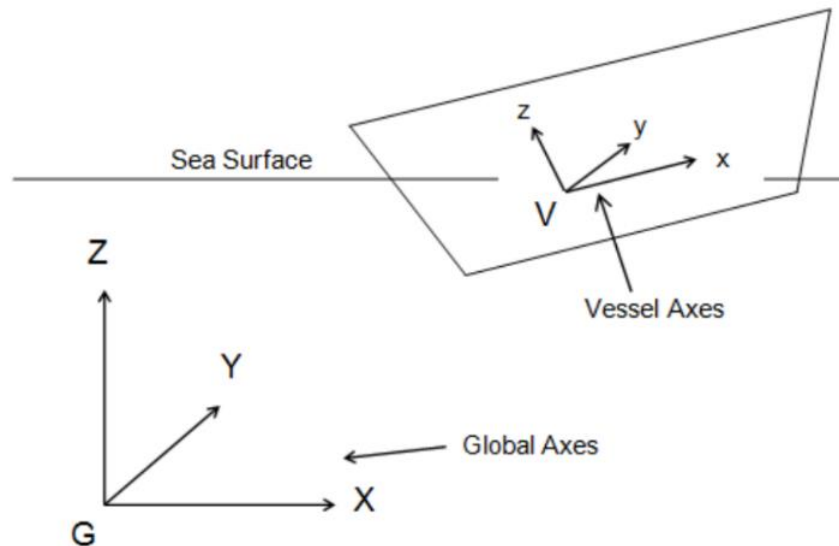


Figure 4.1 Coordinate system in OrcaFlex [28]

4.2. Direction convention

As illustrated in Figure 4.2 OrcaFlex determines direction and headings by getting azimuth and declination angle as an input. All angles are defined in degrees and positive angle starts from X-axis and clockwise rotation toward Y-axis. Loads directions are defined with respect to global coordinate system and directions of environmental loads such as waves, wind, and currents are defined based on their propagation direction.

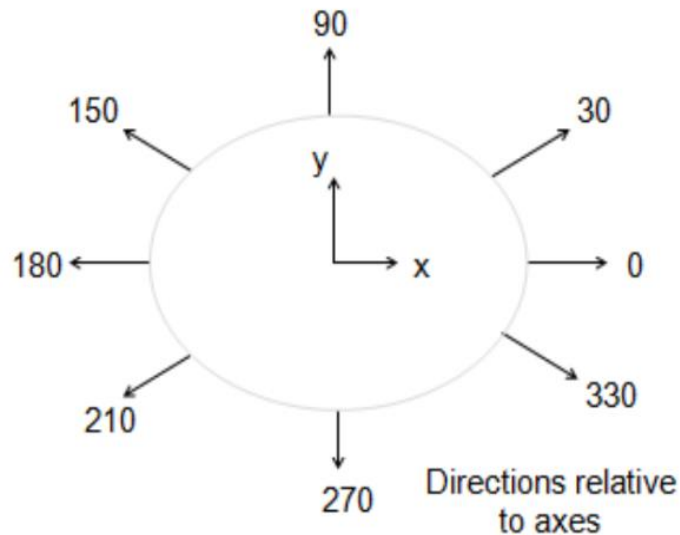


Figure 4.2 Direction and Headings [28]

4.3. 6D buoys

OrcaFlex provides 6D buoy object which has all six degrees of freedom, and their translational and rotational motions are calculated during the simulation. 6D buoys consist of three different categories called lumped buoys, spar buoys, and towed fish buoys to model various marine objects. Although these objects are called buoys, they are not necessarily buoyant. The object density can be defined so that they model any rigid body for simulation.

Buoys wave kinematic is calculated by defining the method. It can be specified by defining parameters in environment form or selecting a tailored method for a specific buoy. It is also possible to consider the effect of vessel on the buoy via defining vessel disturbance effect. Each 6D buoy can be fixed, free, anchored, or connected to another object. The buoys origin's location

in global coordinate system is defined by specifying x, y, and z and the buoy orientation is defined by specifying angles of rotation 1, rotation 2, and rotation 3 which are rotation angle around x, y, z axis in global coordinate system respectively. For static analysis, it is possible to restrict the buoy to certain degrees of freedom which can be all 6 degrees or only translational degrees. The OrcaFlex user can define the mass of the object and its mass moment of inertia about local coordinate axis of the object. Object center of mass and its bulk module can be defined to simulate bodies with eccentric mass distribution and compressible structure.

4.4. Static analysis

The first stage of simulation is static analysis. An analysis is considered static when the external forces are zero. In case of external load being applied, the analysis is called steady state analysis. The purpose of static analysis is to find the static equilibrium of the model before initiating dynamic analysis. Using an iterative procedure, this analysis calculates or determines the system balance given applied load. This static study simply considers the structural models' own weight, hydrodynamic drag from wind and current and buoyancy. Later, the configuration of the 6D buoy model is determined once the equilibrium calculation is performed.

4.5. Dynamic analysis

The second stage of the simulation is dynamic analysis. Once the static analysis is completed, time-based dynamic analysis is performed for the model's motion over a certain period. The main purpose of the dynamic analysis is to determine the structural response as result of interaction of wind, wave, and current load, and other design elements. The simulation period is represented by a series of sequential phases in the dynamic analysis, see Figure 4.3. As shown in the Figure 4.3, the initial stage is build-up stage. This stage allows waves and structure moment build up to their full amplitude from zero. This step also shortens the transition simulation time from static to full dynamic motion.

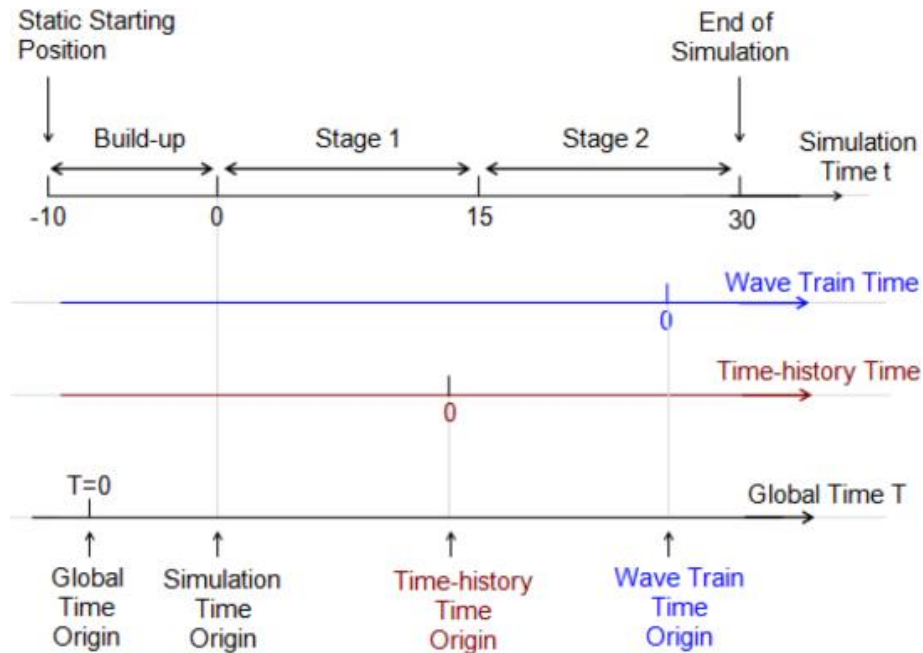


Figure 4.3 Simulation stages and time in dynamic analysis [28]

The equation of motion is solved by utilizing Explicit and Implicit dynamic integration scheme in OrcaFlex software, see Eq.[4.1]. All the geometric non-linearities including large variation of contact and wave stresses are considered in the simulation. This is because the system geometry is recomputed at each time step using both the last-mentioned schemes. The explicit approach is Forward Euler with a fixed time step. The static analysis determines the orientation and starting location of the object in the model, at the start of the time simulation. The software utilize the Generalized- α integration approach introduced by Chung and Hulbert [29]. The forces, damping and moment are computed in the same manner as the explicit approach. At the completion of each time step, the equation of motion for the system is solved.

$$M(p, a) + C(p, v) + K(p) = F(p, v, t) \quad [4.1]$$

4.6. Hydrodynamic loads

To calculate wave and current loads on fixed cylindrical objects, Morrison's equation is the main formula. The formula consists of two parts which are inertia forces and drag forces. Acceleration of water particles constitutes the inertia force while velocity of the water particles generates the drag force. For calculating the forces on moving bodies, the same principle is applicable,

however, modification of the formula is required to include the motion of the object. OrcaFlex uses an expanded variant of Morrison's equation to compute hydrodynamic stresses on 6D buoys. Morrison's equation, in its expanded version is employed in OrcaFlex as follow:

$$F_w = (\Delta \cdot a_w + C_a \cdot \Delta \cdot a_r) + \frac{1}{2} \cdot \rho \cdot V_r \cdot |V_r| \cdot C_d \cdot A \quad [4.2]$$

Chapter 5: Numerical validation of small-scale model

Since the majority of objects offshore have cylindrical geometry, a drilling pipe is selected as dropped object in this thesis. The specifications of the selected drilling pipe are based on a model from Aanesland et al. (1987). Details of the selected drilling pipe are listed in Table 5.1.

Table 5.1 Drilling pipe properties

Parameters	Symbol	Full scale	Model scale (1:20.32)
Length (m)	L	9.95	0.45
Mass (kg)	m	2238	0.2466
Outer Diameter(m)	D_{out}	0.203	0.01

A set of parameters and their effects on spatial dynamic motion of the drilling pipe are studied. A list of the selected parameters is presented in Table 5.2. The case study was performed by Aanesland et al. (1987). The initial location of the object was placed so that the pipe is fully submerged, and the water is undisturbed. The initial velocity of the object is equal to zero. Trajectory of the object is studied for drop angle (β) equal to 0° , 30° , 45° , 60° and 90° . Figure 5.1 illustrates the numerical and experimental model setup used by Aanesland et al. (1987).

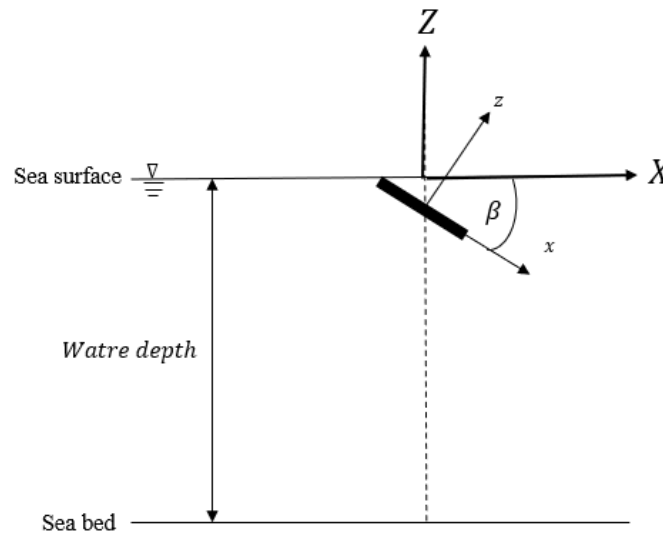


Figure 5.1 Model setup for dropped drilling pipe [4]

Aanesland et al. (1978) defined constant drag coefficients for calculating the normal and axial drag force on the cylinder. However, the drag coefficient is a function of Reynolds number, and it changes as the velocity of the object changes during excursion. In this work, OrcaFlex was used to define variable drag force coefficient based on the Reynolds number. The effect of drop height from water surface on terminal velocity and excursion is investigated by down scaling the drop height of 30 m to 1.48 m for small scale model simulation. The slender body theory is based on assuming smooth change of geometry. Based on this theory, the cylinder's ends should be pointed, while these ends are different for drilling pipe. To implement the effect of this abrupt change in slender body theory, Aanesland et al. (1987) introduced an effective trailing edge (X_t) as percentage of drilling pipe length (L). They investigated the effect of trailing edge length (from 0.3 to 0.5) on the motion of the drilling pipe. Based on their results it can be concluded that different effective trailing edge lengths will provide different pipe trajectories and consequently different landing points. Due to limitations in OrcaFlex software, trailing edge is not investigated in this work. However, the effect of different Munk moment coefficients is studied. Zheng et al. (2022) performed a series of investigations on the effect of Munk moment on towed cables under water during transport to provide a theoretical foundation for optimum towed body design. By considering some initial assumptions their study has compared the expression of Munk moment defined in OrcaFlex and classical towed body kinematics and developed a relation between the two forms of Munk moment expressions. They used 6 degree of freedom body to simulate the towed cables and investigated the effect of different Munk moment coefficients ranging from 0 to 3 [30]. In this work, the same range of Munk moment coefficients are studied for the dropped object of the drilling pipe. To make the simulations as close as possible to real life event, variable drag force coefficient was defined in the present work. The coefficients are defined so that it changes according to instantaneous Reynolds number.

Table 5.2 List of investigated parameters

Influencing Factors (unit)	Symbol	Range
Drop angle (deg)	β	0 - 90
Drop height (m)	h	0 - 1.48
Munk moment coefficient	C_{mm}	0 - 3
Drag moment coefficient	$C_{d,moment}$	0.9 - 1.2

5.1. Model setup

A 6D buoy object (Type: towed fish) from OrcaFlex is selected for modeling the drilling pipe. Based on the information provided in Table 5.2, the input data for simulating the model scale of drilling pipe in OrcaFlex is calculated. The mass moments of inertia for the model are calculated by the following formulae.

$$M_{44} = \frac{m}{2} \cdot (r_o^2 + r_i^2) \quad [5.1]$$

$$M_{66} = M_{55} = \frac{m}{12} \cdot (3 \cdot (r_o^2 + r_i^2) + L^2) \quad [5.2]$$

Drag force on cylinder is divided into two components, normal and axial. Illustration of normal and axial drag areas for simulation of dropped object in OrcaFlex is presented in Figure 5.2.

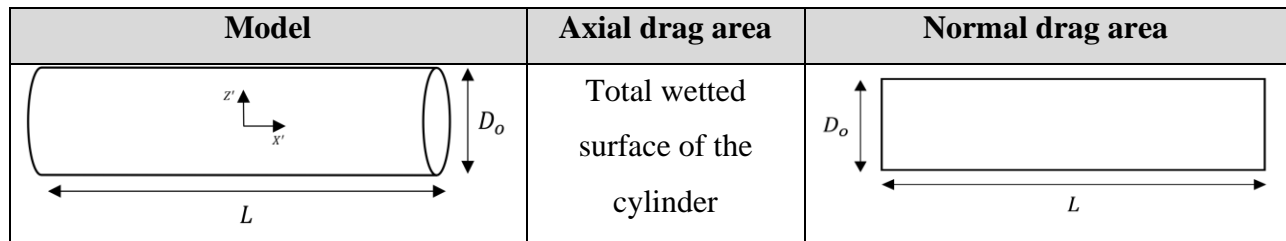


Figure 5.2 Illustration of drag areas

Variable drag coefficients for normal and axial direction are defined by introducing Morrison elements to the model. However, OrcaFlex only allows variable drag coefficient in normal direction of Morrison element. This is while the drag coefficient also changes in axial direction. To overcome this limitation, the author has defined a Morrison element which has an axis normal to cylinder axis. Figure 5.3 illustrates the model and location of Morrison elements in OrcaFlex.

The drag area for axial Morrison element is corrected by defining a modified drag diameter in OrcaFlex. It is defined so that the drag area is equal to the total wet surface of the pipe.

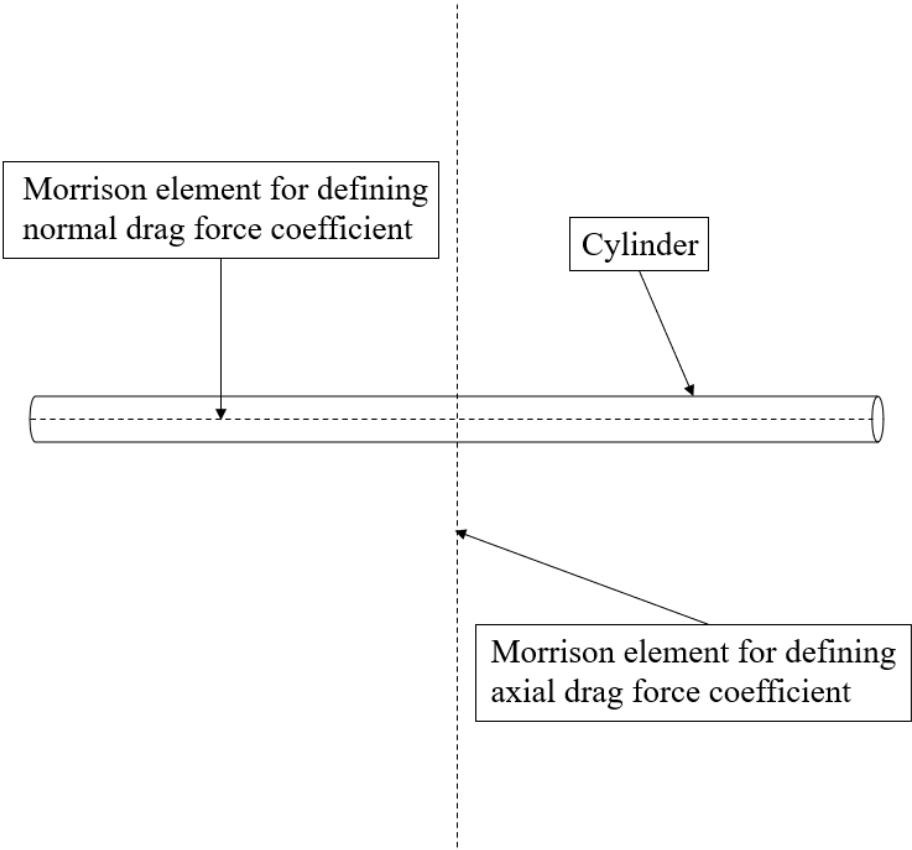


Figure 5.3 Location of Morrison elements on the cylinder

Figure 5.4 illustrates the experimental data in combination with laminar theory results for variation in drag coefficient of cylinder in normal flow with respect to Reynolds number.

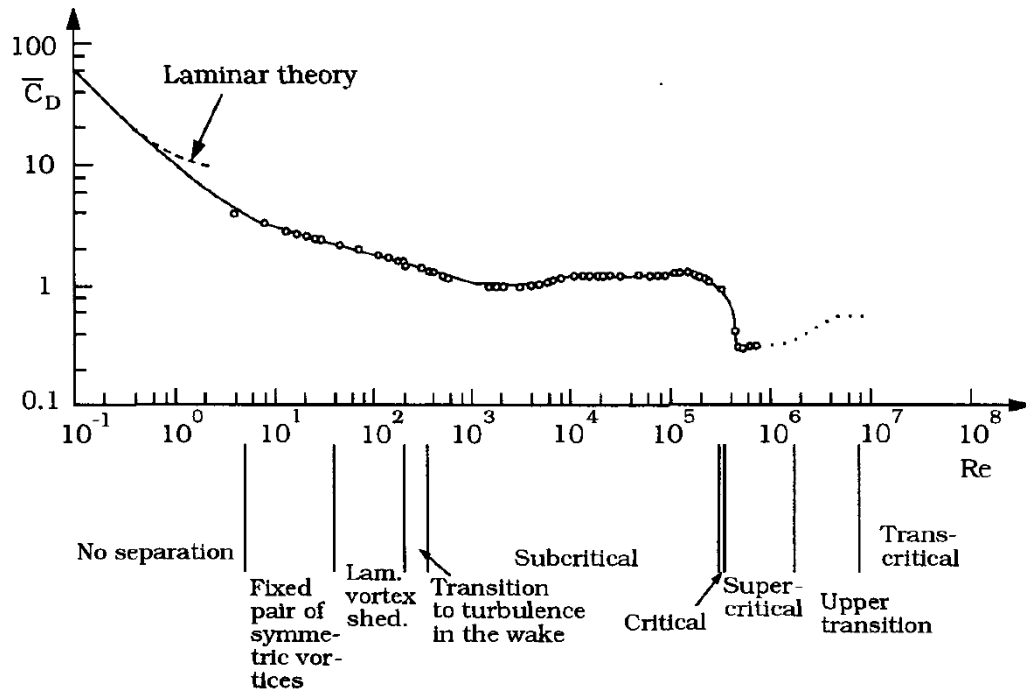


Figure 5.4 Drag coefficient in axial flow for smooth cylinder as a function of Reynolds number

[31]

In axial direction, the projected surface of the cylinder is very small and leads to negligible pressure drag force in that direction. Considering this, the skin friction force is dominant in the axial direction. The author used friction drag coefficient (C_f) and wetted area of the cylinder instead of the drag coefficient and axial drag area respectively in simulation. Stephen A. Jordan (2013) formulated a model for axisymmetric skin friction coefficient (C_f) on a long thin cylinder. Figure 5.5 illustrates the variation of friction drag coefficient with respect to Reynolds numbers Re_x (Reynolds number based on surface length) and Re_a (Reynolds number based on diameter) for a cylinder in axial flow according to Stephen A. Jordan (2013). In this work the skin friction coefficient of empirical model from Stephen A. Jordan (2013) is used. Figure 5.6 provides theoretical value for skin friction coefficient in different flow regimes and different plate roughness.

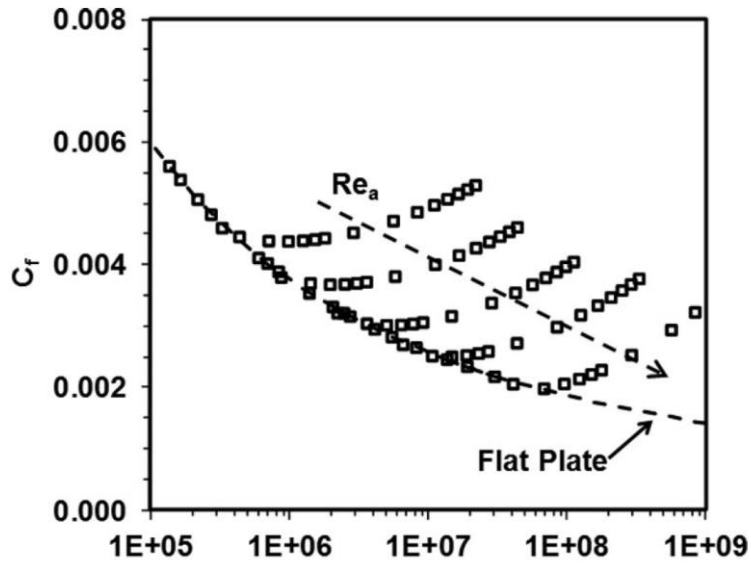


Figure 5.5 Skin friction streamwise behavior along the thin cylinder in terms of Reynolds numbers Re_x and Re_a with comparison to flat plate empirical model [32]

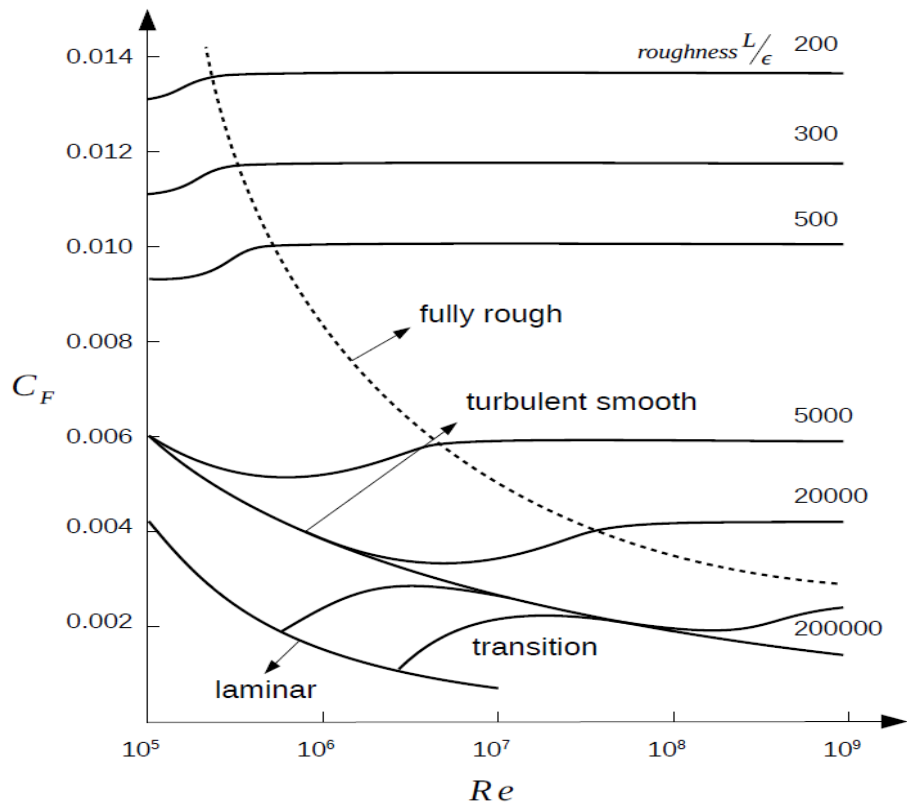


Figure 5.6 Plots of skin friction coefficient for smooth and rough flat plate at laminar, transition, and turbulent flow regimes [33]

To calculate the drag moment, OrcaFlex follows the same procedure for calculating the drag forces in normal and axial directions. But drag reference area is replaced by third moment of area and multiplied by drag coefficient in drag formula. So, the same drag coefficient as drag force can be used for drag moment coefficient. However, the Morrison elements defined in OrcaFlex are not facilitating options for variable drag moment coefficient. So, the author has decided to estimate the Reynolds number for the cylinder and plug in a constant drag moment coefficient. Formula for calculating the third moment of area for simple cylinder is presented below [28].

$$I_n = \frac{D_o \cdot L^4}{23} \quad [5.3]$$

$$I_a = \frac{D_o^5 - D_i^5}{60} \quad [5.4]$$

Since the effect of slam force is not investigated in this work the slam force data is selected to be zero. Calculation of added mass in normal direction is performed based on DNV-RP-C205 [34] and added mass in axial direction is assumed to be same as circular plate. A summary of the coefficients and values for the downscaled model in OrcaFlex is provided in Table 5.3 to Table 5.7. In

Table 5.5 the unit damping force and unit damping moment is considered zero since the motion is not an oscillatory motion.

Table 5.3 Geometry setting, and coefficient used in OrcaFlex

Parameter	Unit	X	Y	Z
Mass	<i>te</i>	247E-06	-	-
Mass moment of inertia	<i>te · m²</i>	3.42E-09	4.16E-09	4.16E-09
Centre of mass	<i>m</i>	0	0	0
Stack base center	<i>m</i>	-0.225	0	0
Length	<i>m</i>	0.45	-	-
Inner diameter	<i>m</i>	0	-	-
Outer diameter	<i>m</i>	0.01	-	-

Table 5.4 Drag and slam setting, and coefficient used in OrcaFlex

Drag forces				Drag moments			
Area (m^2)		Coefficients		Area moments (m^5)		Coefficients ($C_{d,moment}$)	
Normal	Axial	Normal	Axial	Normal	Axial	Normal	Axial
0.0045	0.01418	0	0	12.8E-06	1.7E-12	0.9 to 1.4	0
Slam force data							
Entry				Exit			
0				0			

Table 5.5 Added mass and damping setting and coefficient used in OrcaFlex.

Added mass force coefficient (C_a)		Inertia Force Coefficient (C_m)	
Normal	Axial	Normal	Axial
1.0	0.63	$C_a + 1$	$C_a + 1$
Added moment of inertia ($te \cdot m^2$)			
Normal	Axial	-	-
0	0	-	-
Unit damping force ($kN \cdot \frac{s}{m}$)		Unit damping moment ($kN \cdot m \cdot \frac{s}{rad}$)	
Normal	Axial	Normal	Axial
0	0	0	0

Table 5.6 Morison Element geometry and orientation used in OrcaFlex

Element type	Position (m)			Orientation (deg)			Length (m)
	x	y	z	Azimuth	Declination	Gamma	
Normal drag	-0.225	0	0	0	90	0	0.45
Axial friction	0	0	-0.225	0	0	0	0.45

Table 5.7 Morison elements specification used in OrcaFlex

Element name	Drag diameter		Drag coefficient		
	Normal	Axial	x	y	z
Normal drag	0.01	0.01	C_d (Variable)	C_d (Variable)	0
Axial friction	0.031	0.031	C_F (Variable)	C_F (Variable)	0

5.2. Small-scale model velocity verification

Figure 5.7 illustrates the simulation with $\beta = 0^\circ$ and $\beta = 90^\circ$ for small-scale model and Munk moment coefficient of 0 to prevent destabilizing moment on the cylinder. The object is released from fully submerged condition as illustrated in Figure 5.1. The calculated velocity for small-scale model with drop angles of 0° agrees well with experimental results of Aanesland et al. (1987). However, the calculated velocity for small-scale model with drop angles of 90° is showing slightly higher value since the model is considered as a smooth cylinder. According to Aanesland et al. (1987) experiments the terminal velocity of small-scale model for $\beta = 0^\circ$ and $\beta = 90^\circ$ are 0.96 m/s and 6.67 m/s.

Also, terminal velocity of the model is calculated in OrcaFlex for both cases when they are released from 1.48 m height above water surface. Results in Figure 5.8 show that terminal velocity of the object is not affected by release height. Although, the cylinder velocity with drop angle of 0° has reached to 4.8 (m/s) during the first phase (fall through the air), the velocity quickly reduced to 0.91 (m/s) when it has entered the water. This is while the cylinder velocity with drop angle of 90° , did not affected by the water entry and reached to its terminal velocity of 7.4 (m/s).

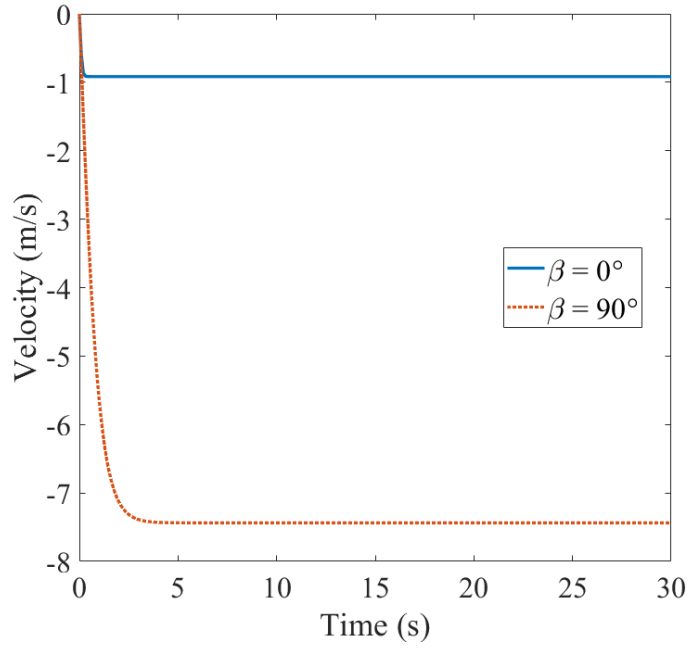


Figure 5.7 Velocity of small-scale model for $\beta = 0^\circ$ and $\beta = 90^\circ$ (fully submerged)

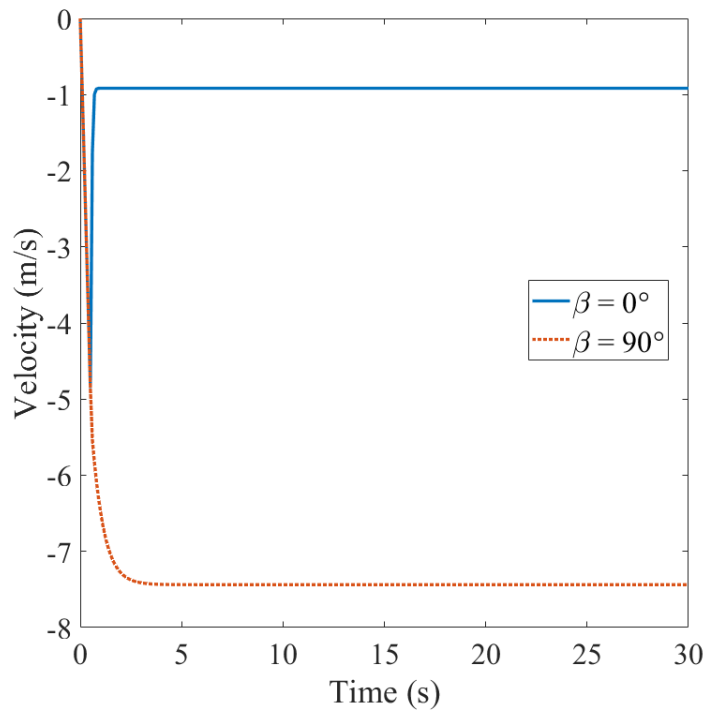


Figure 5.8 Velocity of small-scale model for $\beta=0^\circ$ and $\beta=90^\circ$ (height from surface = 1.48 m)

A series of analytical calculations are performed for estimating the terminal velocity of the scaled model using Eq.[3.10]. The analytical calculations are performed for two cases when they are released from the fully submerged condition. Table 5.8 provides a summary of the results from Aanesland et al. (1987), OrcaFlex, and analytical calculations.

Table 5.8 Terminal velocity of small-scale model for different drop cases

Drop Cases	$\beta = 0^\circ$	$\beta = 90^\circ$
Aanesland et al.	$0.96 \left(\frac{m}{s}\right)$	$6.67 \left(\frac{m}{s}\right)$
OrcaFlex	$0.91 \left(\frac{m}{s}\right)$	$7.4 \left(\frac{m}{s}\right)$
Analytical calculation (Drag force coefficient in normal direction = 1) (Skin friction coefficient in axial direction = 0.005)	$0.96 \left(\frac{m}{s}\right)$	$7.6 \left(\frac{m}{s}\right)$

Based on the results given in Table 5.8, estimated terminal velocity for pure lateral motion of scaled model (when $\beta = 0^\circ$) is very close to each other. This is while terminal velocities of the scaled model in pure axial motion (when $\beta = 90^\circ$) for analytical calculations and OrcaFlex are higher than results from Aanesland et al. (1987). This difference is because models are considered as a smooth cylinder in turbulent flow.

5.3. Small-scale model excursion verification

To investigate the effect of Munk moment on the small-scale model, several simulations are performed, and different Munk moment coefficients are introduced. Model was released from fully submerged position ($z = -0.225$) and different drop angle was investigated ($\beta = 30^\circ, 45^\circ, 60^\circ$). Normal drag moment coefficient is set to one ($C_{d,moment} = 1.0$) and Munk moment coefficients of 0 to 3.0 ($C_{mm} = 0$ to $C_{mm} = 3.0$) were investigated. Figure 5.9 to Figure 5.11 are illustrating the excursion path of center of volume of dropped model for different drop angle simulated in OrcaFlex. Experimental results from Aanesland et al. (1987) are illustrated by black dash lines which provide an envelope. According to the simulations, Munk moment coefficients in range of 0.08 to 0.10 are giving the best results.

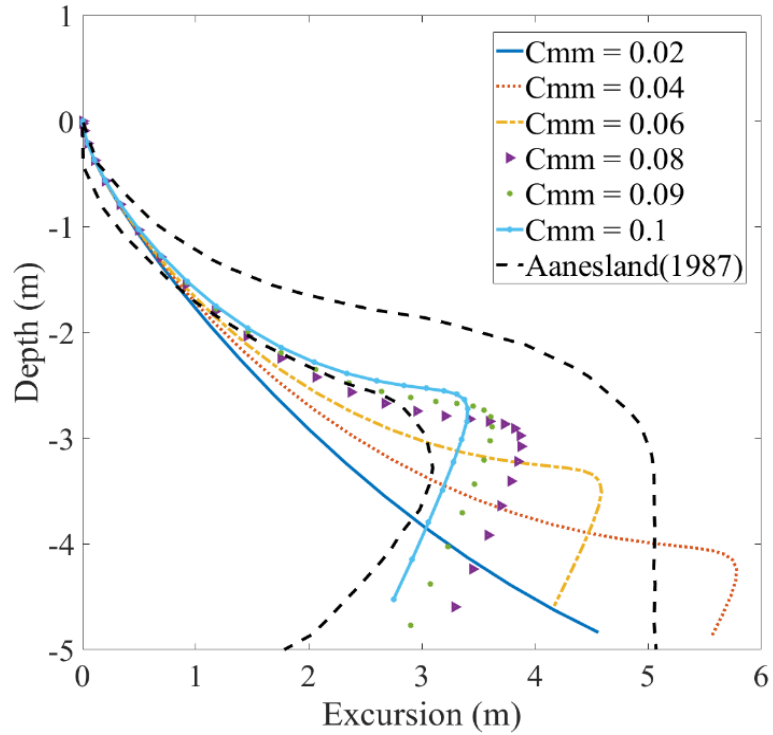


Figure 5.9 Investigation of Munk moment coefficient (C_{mm}) at $\beta = 45^\circ$ and $C_{d,moment} = 1.0$

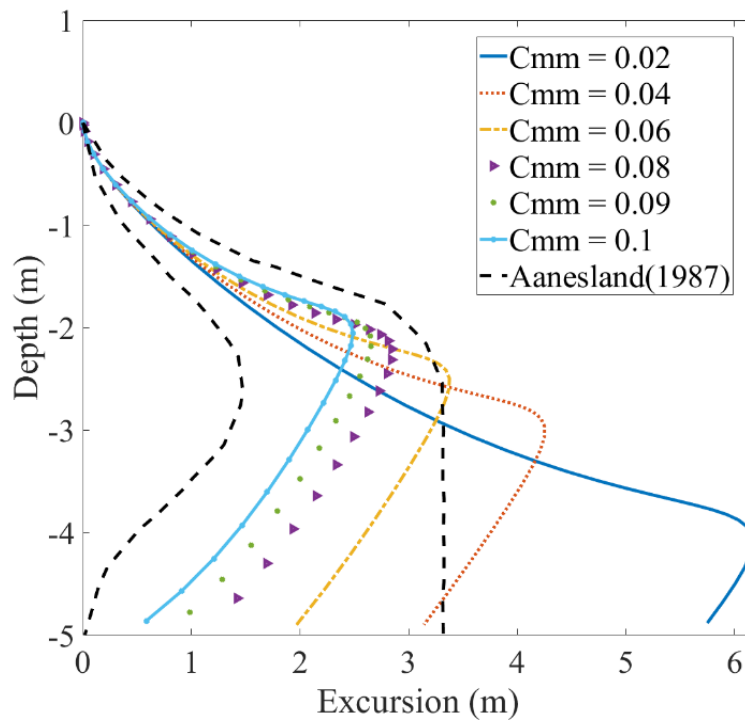


Figure 5.10 Investigation of Munk moment coefficient (C_{mm}) at $\beta = 30^\circ$ and $C_{d,moment} = 1.0$

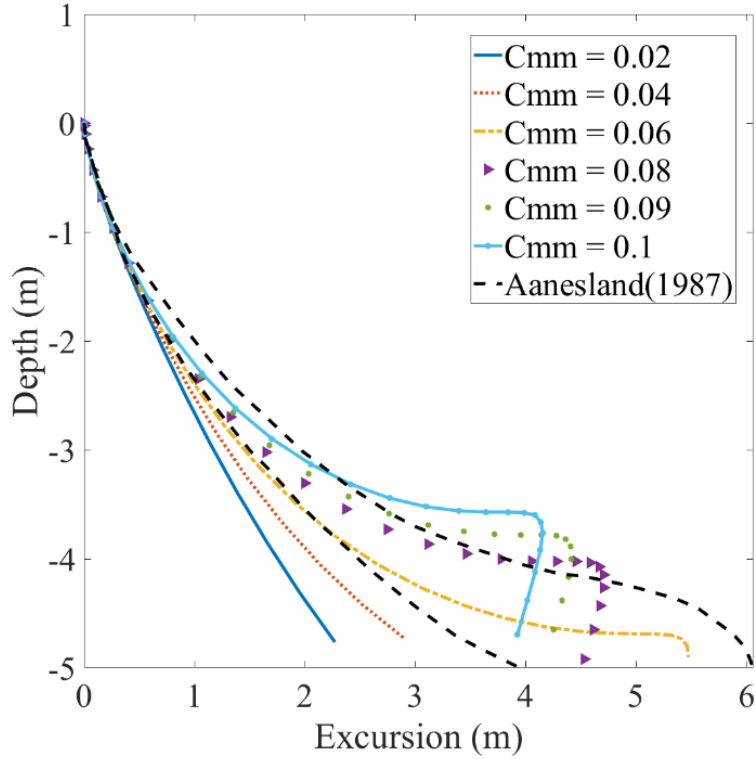


Figure 5.11 Investigation of Munk moment coefficient (C_{mm}) at $\beta = 60^\circ$ and $C_{d,moment} = 1.0$

Since OrcaFlex does not facilitate introducing variable drag moment coefficient, the author investigated the effect of drag moment coefficient on the excursion path of the cylinder. Figure 5.12 to Figure 5.14 illustrating the effect of Drag moment coefficient ($C_{d,moment}$) in range of 0.9 to 1.4 for different drop angle ($\beta = 30^\circ, 45^\circ, 60^\circ$) and Munk moment coefficient of 0.08 ($C_{mm} = 0.08$). According to the results the small-scale model with Munk moment coefficient of 0.08 ($C_{mm} = 0.08$) and drag moment coefficient of 1.4 ($C_{d,moment} = 1.4$), agrees well with experimental data from Aanesland et al. (1987).

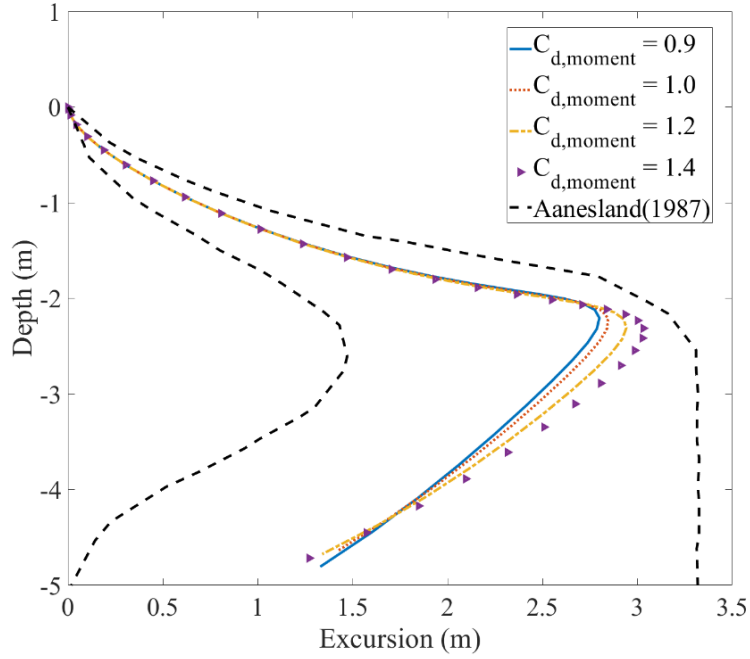


Figure 5.12 Investigation of drag moment coefficient ($C_{d,moment}$) when $\beta = 30^\circ$

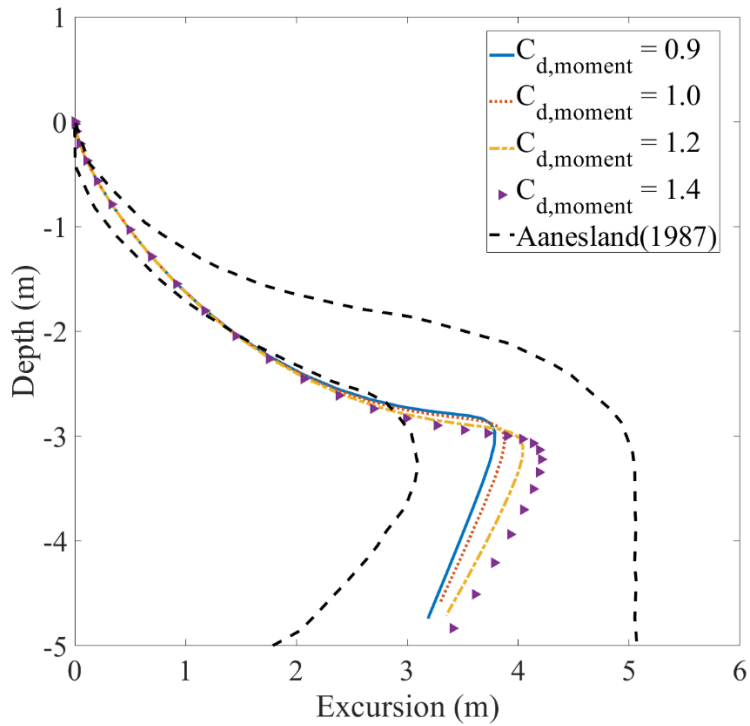


Figure 5.13 Investigation of drag moment coefficient ($C_{d,moment}$) when $\beta = 45^\circ$

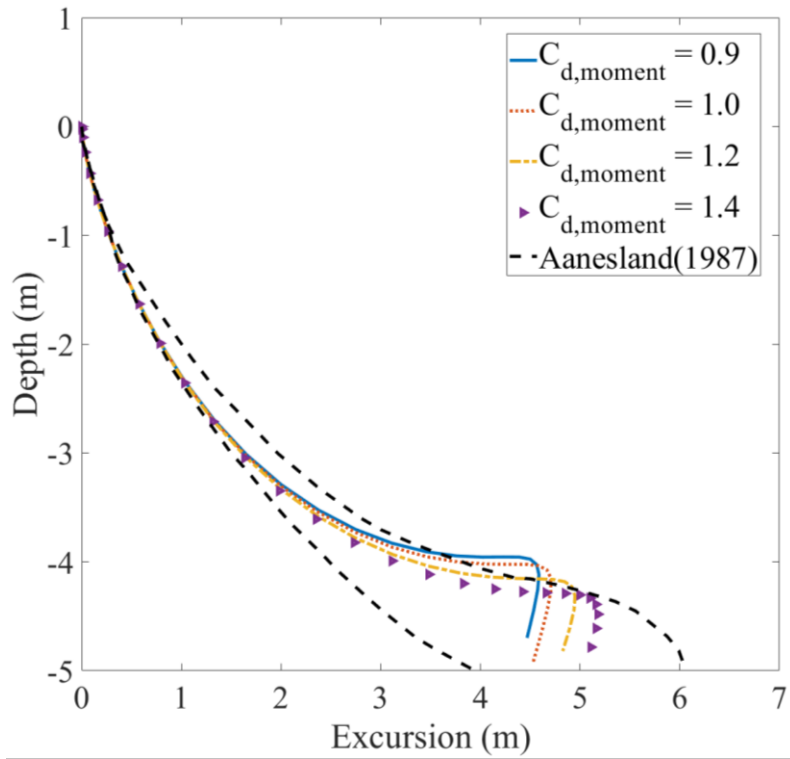


Figure 5.14 Investigation of Drag moment coefficient ($C_{d,moment}$) when $\beta = 60^\circ$

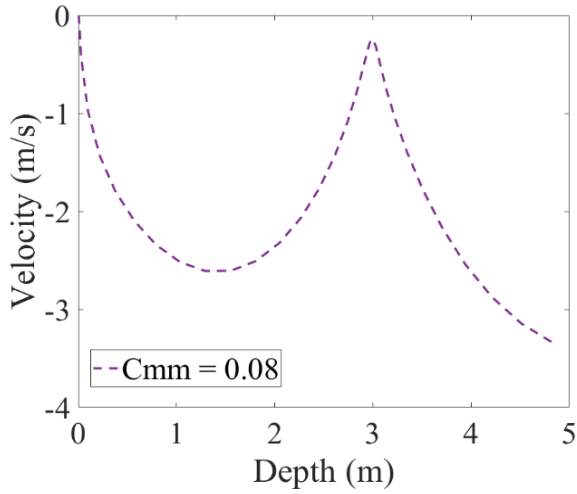
Chapter 6: Parametric study and probability calculations of drop object

6.1. Small-scale model

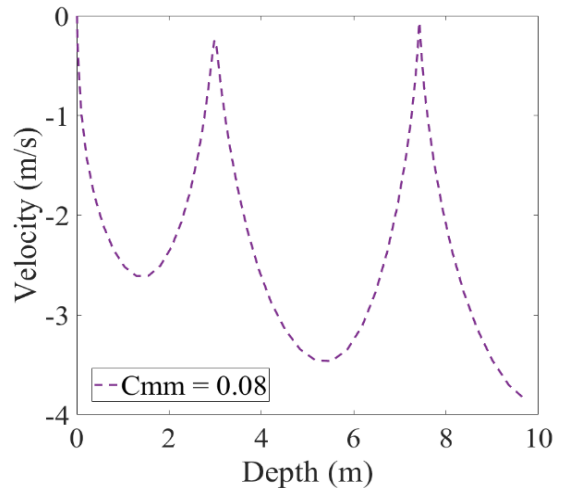
The current section presents the result from sensitivity analyses performed on small-scale model. The effect of water depth on maximum velocity of the object is investigated. In addition, the effect of Munk moment coefficient and drag moment coefficient on velocity of the cylinder is studied. Also, the influence of drop angle and drag moment coefficient in OrcaFlex on average drag force coefficient during simulation is studied.

Velocity

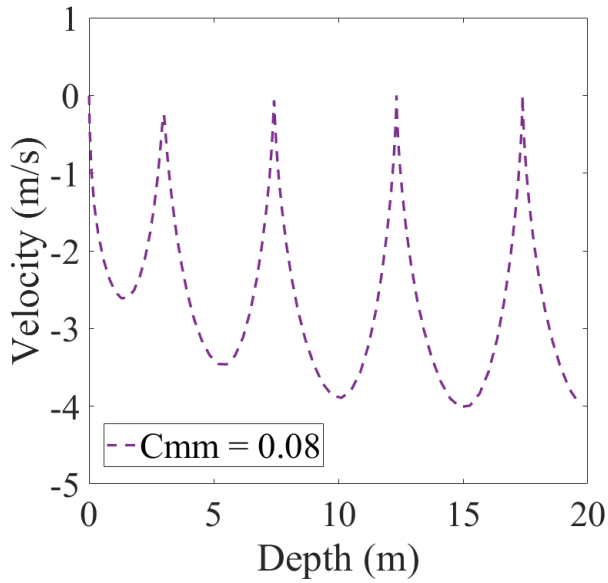
Figure 6.1 illustrates variation of velocity for small-scale model in 5 m, 10 m, 20 m, 40 m, water depths and Munk moment coefficient of 0.08 ($C_{mm} = 0.08$). According to the results, the maximum velocity that object reaches is increasing in deeper water depth. However, the maximum velocity did not increase after 20 m water depth. Figure 6.2 presents the effect of Munk moment coefficient (C_{mm}) in range of 0.02 to 0.12 on velocity of the small-scale model for 40 m water depth. The analyses are performed by applying a drag moment coefficient ($C_{d,moment} = 1.4$) and drop angle of 45 degrees ($\beta = 45^\circ$). As seen in plots, the higher Munk moment coefficient leads to higher maximum velocity. Different water depth and different drag moment coefficients in range of 0.9 to 1.4 are investigated since the estimated maximum Reynolds number is below $1E05$ and object does not experience drag crisis phenomenon. The results of the simulations are provided in Appendix I.



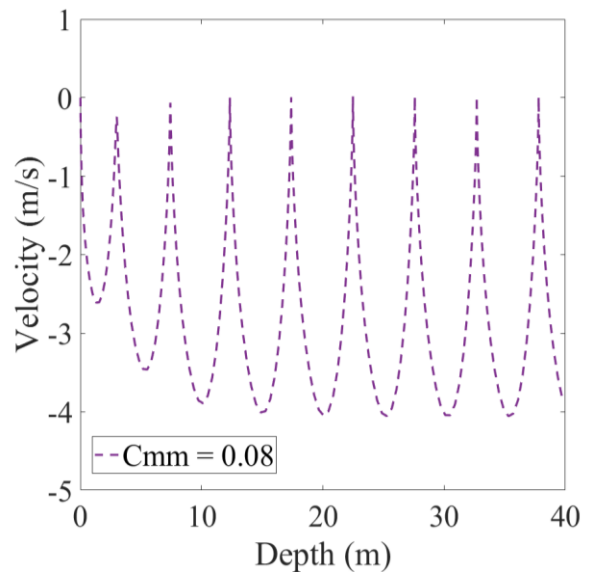
5 m water depth



10 m water depth



20 m water depth



40 m water depth

Figure 6.1 Effect of water depth on velocity of small-scale model

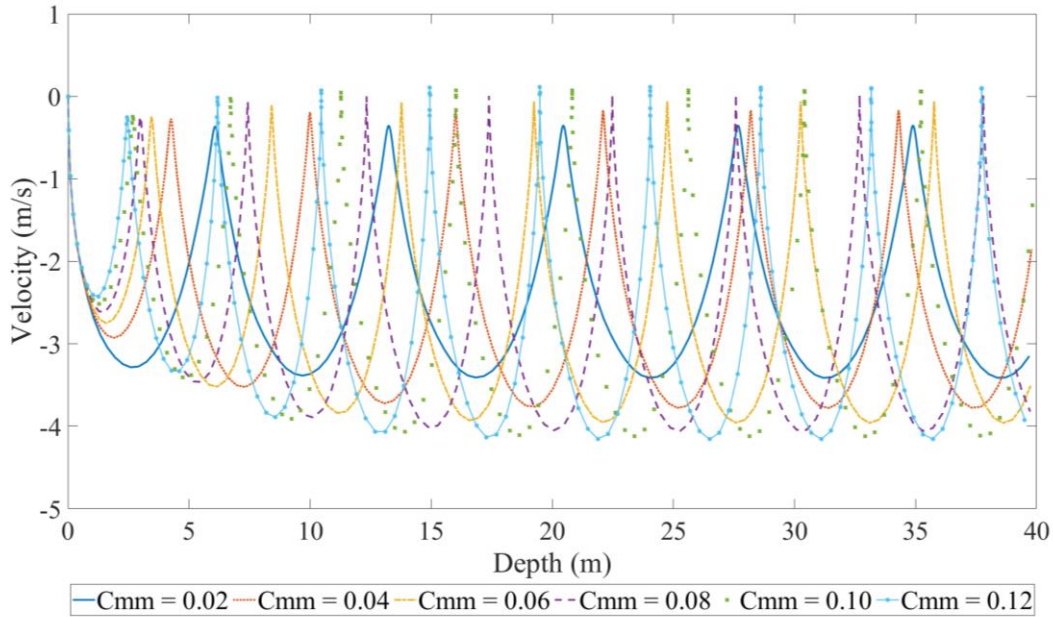


Figure 6.2 Effect of Munk moment coefficient (C_{mm}) on velocity for small-scale model in 40 m water depth

Table 6.1 to

Table 6.4 present the maximum velocity of the small-scale model in different water depths. The effect of Munk and drag moment coefficients on velocity of model is investigated and the results are summarized in Table 6.1 to

Table 6.4. All results are performed with drop angle of 45 degrees ($\beta = 45^\circ$). The results show that when water depth increases above 20 m, the maximum velocity of the object remains constant. However, the maximum velocity of the object in one hand increases as the Munk moment coefficient increases, while the rate of change is different. On the other hand, the maximum velocity of the object decreases with the increase of the drag moment coefficient.

Table 6.1 Maximum velocity of the small-scale model in 5 m water depth

	Drag moment coefficient ($C_{d,moment}$)	Munk moment coefficient					
		C_{mm} = 0.02	C_{mm} = 0.04	C_{mm} = 0.06	C_{mm} = 0.08	C_{mm} = 0.10	C_{mm} = 0.12
Maximum velocity (m/s)	$C_{d,moment} = 0.9$	-3.26	-2.91	-3.49	-4.05	-4.25	-4.42
	$C_{d,moment} = 1.0$	-3.27	-2.91	-3.57	-4.05	-4.17	-4.13
	$C_{d,moment} = 1.2$	-3.27	-2.92	-3.37	-3.54	-3.76	-3.67
	$C_{d,moment} = 1.4$	-3.28	-2.92	-2.96	-3.34	-3.40	-3.33

Table 6.2 Maximum velocity of the small-scale model in 10 m water depth

	Drag moment coefficient ($C_{d,moment}$)	Munk moment coefficient (C_{mm})					
		C_{mm} = 0.02	C_{mm} = 0.04	C_{mm} = 0.06	C_{mm} = 0.08	C_{mm} = 0.10	C_{mm} = 0.12
Maximum velocity (m/s)	$C_{d,moment} = 0.9$	-4.36	-4.67	-4.47	-4.60	-4.51	-5.17
	$C_{d,moment} = 1.0$	-4.15	-4.38	-4.37	-4.30	-4.61	-5.12
	$C_{d,moment} = 1.2$	-3.75	-3.89	-3.88	-4.04	-4.42	-4.44
	$C_{d,moment} = 1.4$	-3.38	-3.52	-3.51	-3.85	-3.90	-3.88

Table 6.3 Maximum velocity of the small-scale model in 20 m water depth

	Drag moment coefficient ($C_{d,moment}$)	Munk moment coefficient (C_{mm})					
		C_{mm} = 0.02	C_{mm} = 0.04	C_{mm} = 0.06	C_{mm} = 0.08	C_{mm} = 0.10	C_{mm} = 0.12
Maximum velocity (m/s)	$C_{d,moment} = 0.9$	-4.85	-5.33	-5.55	-5.84	-6.33	-5.85
	$C_{d,moment} = 1.0$	-4.47	-4.90	-5.16	-5.44	-5.54	-5.63
	$C_{d,moment} = 1.2$	-3.86	-4.22	-4.50	-4.60	-4.66	-4.77
	$C_{d,moment} = 1.4$	-3.40	-3.76	-3.92	-4.00	-4.10	-4.13

Table 6.4 Maximum velocity of the small-scale model in 40 m water depth

	Drag moment coefficient ($C_{d,moment}$)	Munk moment coefficient (C_{mm})					
		C_{mm} = 0.02	C_{mm} = 0.04	C_{mm} = 0.06	C_{mm} = 0.08	C_{mm} = 0.10	C_{mm} = 0.12
Maximum velocity (m/s)	$C_{d,moment} = 0.9$	-4.93	-5.52	-5.85	-6.13	-6.55	-5.91
	$C_{d,moment} = 1.0$	-4.53	-5.06	-5.33	-5.49	-5.66	-5.84
	$C_{d,moment} = 1.2$	-3.89	-4.32	-4.53	-4.67	-4.74	-4.80
	$C_{d,moment} = 1.4$	-3.41	-3.77	-3.95	-4.05	-4.12	-4.15

Figure 6.3 and Figure 6.4 illustrates the effect of axial drag moment coefficient ($C_{f,moment}$) on the velocity and spatial motion of the small-scale model. The simulation was performed in 5 m water depth. Munk moment coefficient of 0.08 ($C_{mm}=0.08$), drag moment coefficient of 1.4, and axial drag moment coefficient in range of 0.0 to 0.008 were investigated. The results indicate that the axial drag moment coefficient does not have any influence on velocity or excursion of the small-scale model.

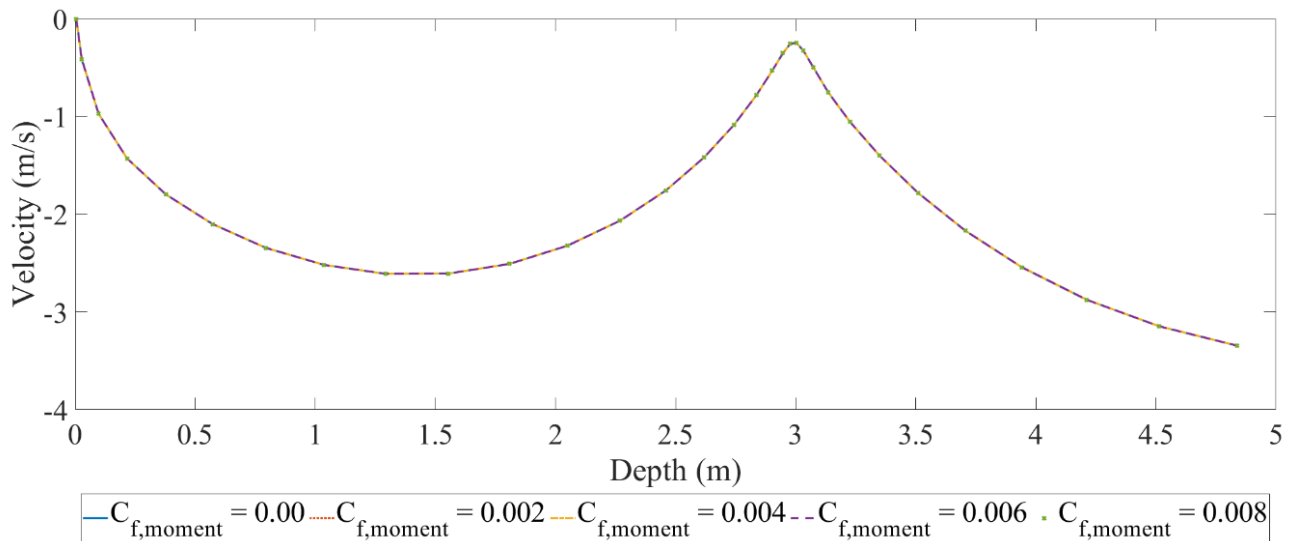


Figure 6.3 Effect of axial drag moment coefficient ($C_{f,moment}$) on velocity

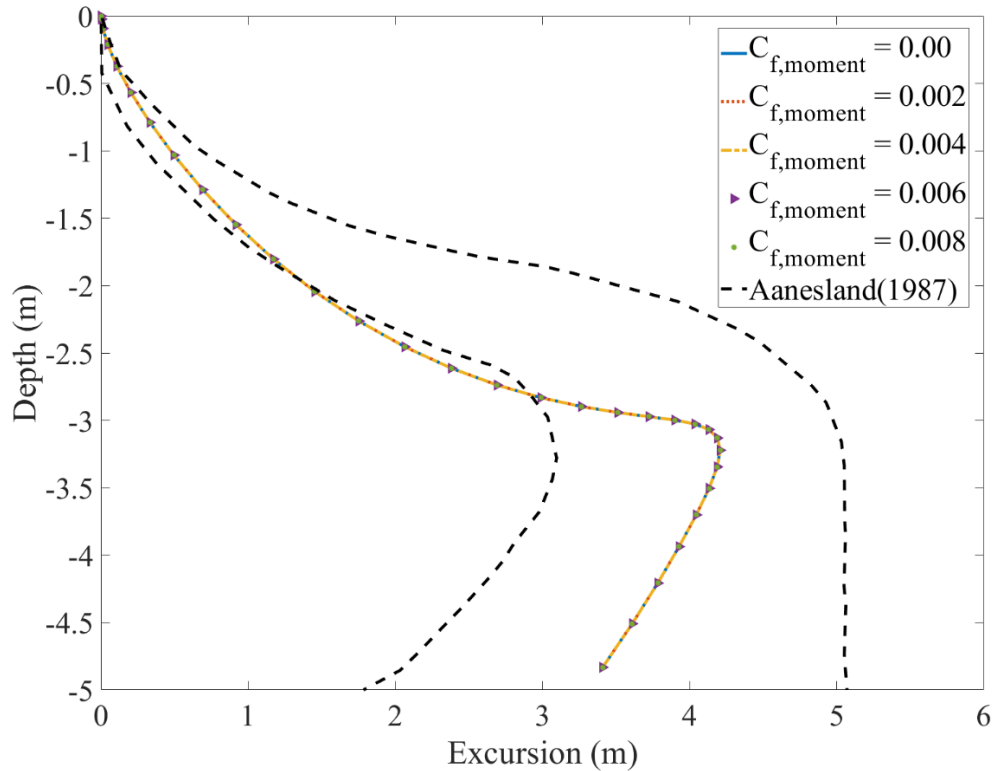


Figure 6.4 Effect of axial drag moment coefficient ($C_{f,moment}$) on excursion

OrcaFlex provides a time history of drag force coefficient (C_d) used in calculation for each time step. For the small-scale model, the drag force coefficient's time history for drop angles ($\beta = 30^\circ$, $\beta = 45^\circ$, $\beta = 60^\circ$) and drag moment coefficients ($C_{d,moment} = 0.9$, $C_{d,moment} = 1.0$, $C_{d,moment} = 1.2$, $C_{d,moment} = 1.4$) is investigated to find suitable average drag moment coefficient. Figure 6.5 illustrates the time history of drag force coefficient for small-scale model with Munk moment coefficient of 0.08 ($C_{mm} = 0.08$) and drag moment coefficient of 1.4 ($C_{d,moment} = 1.4$). Table 6.5 provides the average drag force coefficient for respective drop angles and defined drag moment coefficients. As seen in Table 6.5, increase in drag moment coefficient increases the average drag force coefficient, but, the changes are very small between $C_{d,moment} = 1.2$ and ($C_{d,moment} = 1.4$). Further, the results listed in Table 6.5 confirm that the drop angle does not affect the average drag force coefficient for a given drag moment coefficient. The results from simulations for other drag moment coefficients are provided in Appendix II.

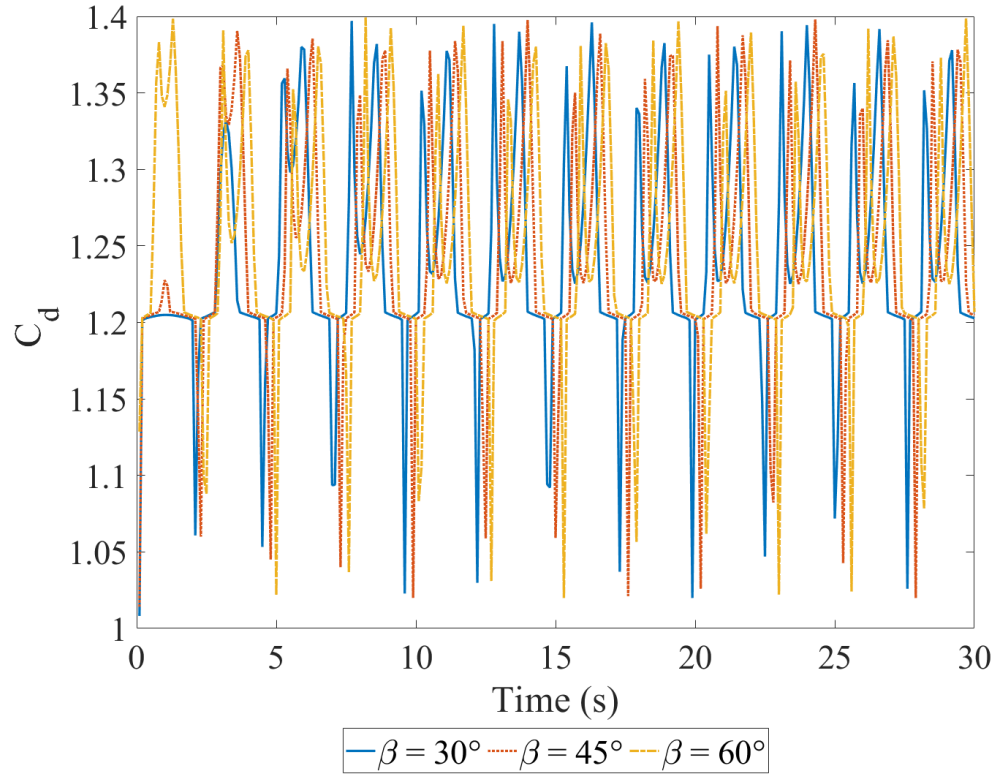


Figure 6.5 Small-scale model drag force coefficient time history for different drop angles.

Table 6.5 Effect of drop angle and drag moment coefficient on average drag force coefficient

	Drop angle (β°)	Drag moment coefficient ($C_{d,moment}$)			
		$C_{d,moment}$ = 0.9	$C_{d,moment}$ = 1.0	$C_{d,moment}$ = 1.2	$C_{d,moment}$ = 1.4
Average drag force coefficient ($C_{d,average}$)	30°	$C_{d,average}$ = 1.07	$C_{d,average}$ = 1.17	$C_{d,average}$ = 1.22	$C_{d,average}$ = 1.23
	45°	$C_{d,average}$ = 1.07	$C_{d,average}$ = 1.16	$C_{d,average}$ = 1.22	$C_{d,average}$ = 1.23
	60°	$C_{d,average}$ = 1.06	$C_{d,average}$ = 1.17	$C_{d,average}$ = 1.22	$C_{d,average}$ = 1.23

Further, effect of Munk moment coefficient on average drag force coefficient ($C_{d,average}$) of the model was investigated. Table 6.6 presents the results for range of 0.02 to 0.12 Munk moment coefficients. The results show that the average drag force coefficient remained almost constant

for different Munk moment coefficients. The results from further simulations for different Munk moment coefficient are provided in Appendix II.

Table 6.6 Effect of Munk moment coefficient on average drag force coefficient

Munk moment coefficient (C_{mm})	$C_{mm} = 0.02$	$C_{mm} = 0.04$	$C_{mm} = 0.06$	$C_{mm} = 0.08$	$C_{mm} = 0.10$	$C_{mm} = 0.12$
Average drag force coefficient ($C_{d,average}$)	1.22	1.22	1.22	1.22	1.22	1.22

The best excursion path compared to experimental data for different drop angle is illustrated in **Error! Reference source not found.** to Figure 6.8. The simulations were performed using drag moment coefficient of 1.22 ($C_{d,moment}=1.22$) and Munk moment coefficient of 0.08 ($C_{mm} = 0.08$). The excursion path fits well within the experimental data envelop for selected drop angles.

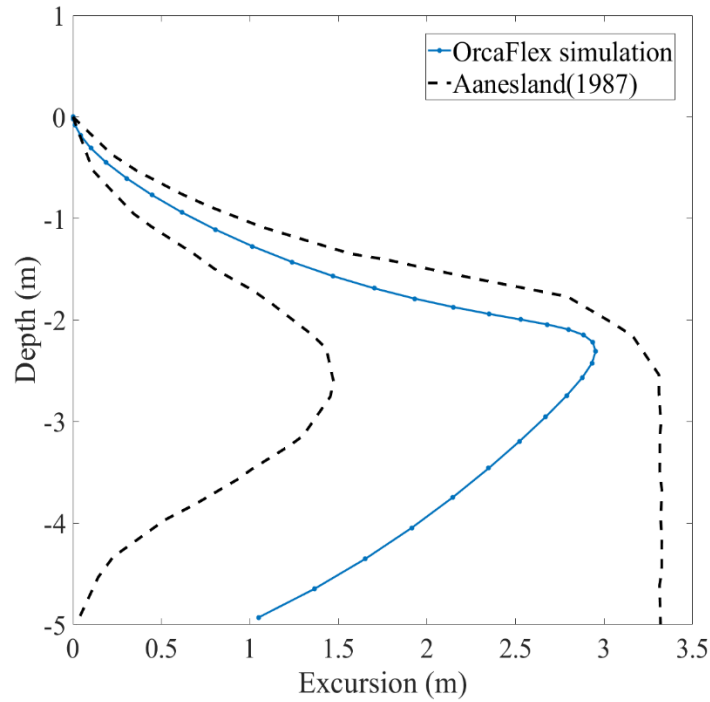


Figure 6.6 Small-scale model excursion when $\beta = 30^\circ$

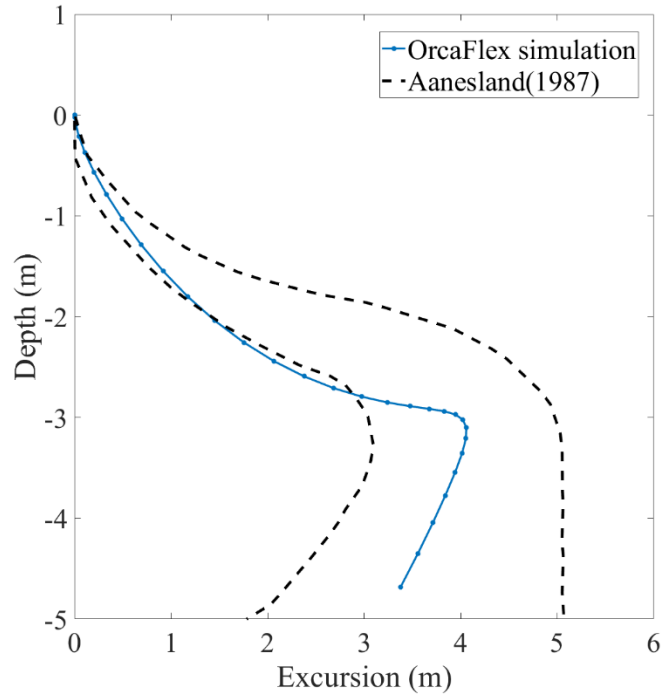


Figure 6.7 Small-scale model excursion when $\beta = 45^\circ$

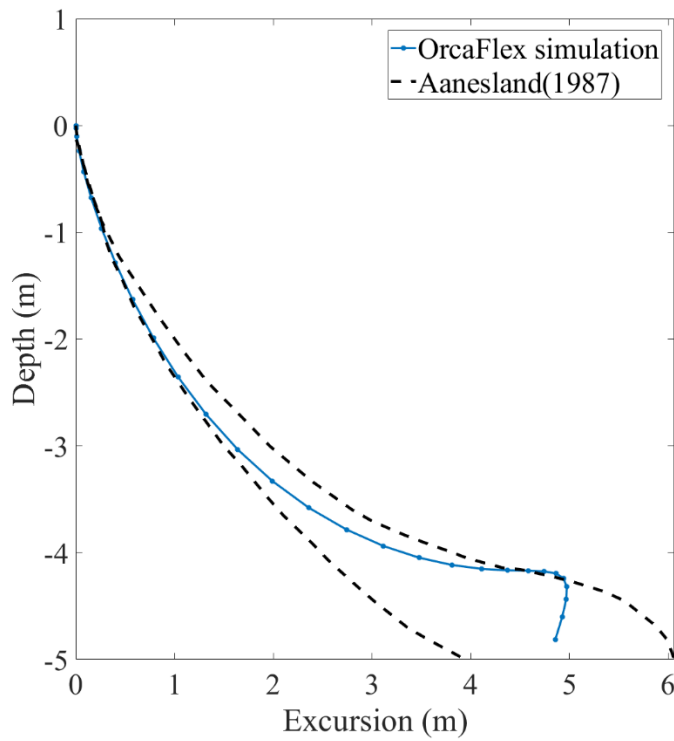


Figure 6.8 Small-scale model excursion when $\beta = 60^\circ$

6.2. Full-scale drill pipe

The analyses were performed for the dropped object of drilling. A full-scale drill pipe model was selected from Aanesland et al. (1987) and simulated using OrcaFlex software tool. To upscale the water depth, the water depths in small-scale simulations were multiplied by scaling ratio (1:20). Details of the model setup are presented in Table 6.7 to

Table 6.11.

Table 6.7 Geometry setting used in OrcaFlex

Parameter	Unit	X	Y	Z
Mass	<i>te</i>	2.2387	-	-
Mass moment of inertia	<i>te · m²</i>	0.01155	18.4752	18.4752
Centre of mass	<i>m</i>	0	0	0
Stack base center	<i>m</i>	-4.975	0	0
Length	<i>m</i>	9.95	-	-
Inner diameter	<i>m</i>	0	-	-
Outer diameter	<i>m</i>	0.2032	-	-

Table 6.8 Drag and slam setting, and coefficient used in OrcaFlex

Drag forces				Drag moments			
Area (<i>m²</i>)		Coefficients (<i>C_d</i>)		Area moments (<i>m⁵</i>)		Coefficients (<i>C_{d,moment}</i>)	
Normal	Axial	Normal	Axial	Normal	Axial	Normal	Axial
0	0	0	0	62.2395	5.77E-06	0.3 to 1.4	0
Slam force data							
Entry				Exit			
0				0			

Table 6.9 Added mass and damping setting and coefficient used in OrcaFlex.

Added mass force coefficient (C_a)		Inertia Force Coefficient (C_m)	
Normal	Axial	Normal	Axial
1.0	0.63	$C_a + 1$	$C_a + 1$
Added moment of inertia ($te \cdot m^2$)			
Normal	Axial	-	-
0	0	-	-
Unit damping force ($kN \cdot \frac{s}{m}$)		Unit damping moment ($kN \cdot m \cdot \frac{s}{rad}$)	
Normal	Axial	Normal	Axial
0	0	0	0

Table 6.10 Morison Element geometry and orientation used in OrcaFlex

Element type	Position (m)			Orientation (deg)			Length (m)
	x	y	z	Azimuth	Declination	Gamma	
Normal drag	-4.975	0	0	0	90	0	9.95
Axial friction	0	0	-4.975	0	0	0	9.95

Table 6.11 Morison elements specification used in OrcaFlex

Element name	Drag diameter		Drag coefficient		
	Normal	Axial	x	y	z
Normal drag	0.2032	0.2032	C_d (Variable)	C_d (Variable)	0
Axial friction	0.6382	0.6382	C_F (Variable)	C_F (Variable)	0

Table 6.12 presents the terminal velocities of the object, obtained from OrcaFlex simulation and analytical calculations for drop angle of 0° and 90° . Eq.[3.10] was used for analytical calculation of terminal velocity. For both cases the Reynolds number is estimated to be the same as the value from OrcaFlex which provides the value based on the predefined Reynolds number range and corresponding velocity. For $\beta = 0^\circ$, the drag moment coefficient ($C_{d,moment}$) is estimated to be 0.34 since in pure lateral motion, the pressure drag is the dominant force. For $\beta = 90^\circ$, $C_{f,moment}$ is estimated to be 0.002 since in pure axial motion, the skin friction is the dominant

force. Figure 6.9 illustrate the spatial motion of the dropped drilling pipe in 100 m water depth for drop angles of 0° , 30° , 45° , 60° , and 90° . This simulation is performed by using a constant drag moment coefficient ($C_{d,moment} = 1$) and Munk moment coefficient of 0.08 ($C_{mm} = 0.08$). According to Figure 6.9 the excursion path of full-scale drilling pipe is a function of drop angle.

Table 6.12 Terminal velocity of full scaled drill pipe

Drop angle	$\beta = 0^\circ$	$\beta = 90^\circ$
OrcaFlex	$7.20 \left(\frac{m}{s}\right)$	$50.42 \left(\frac{m}{s}\right)$
Analytical calculation	$7.29 \left(\frac{m}{s}\right)$	$53.61 \left(\frac{m}{s}\right)$

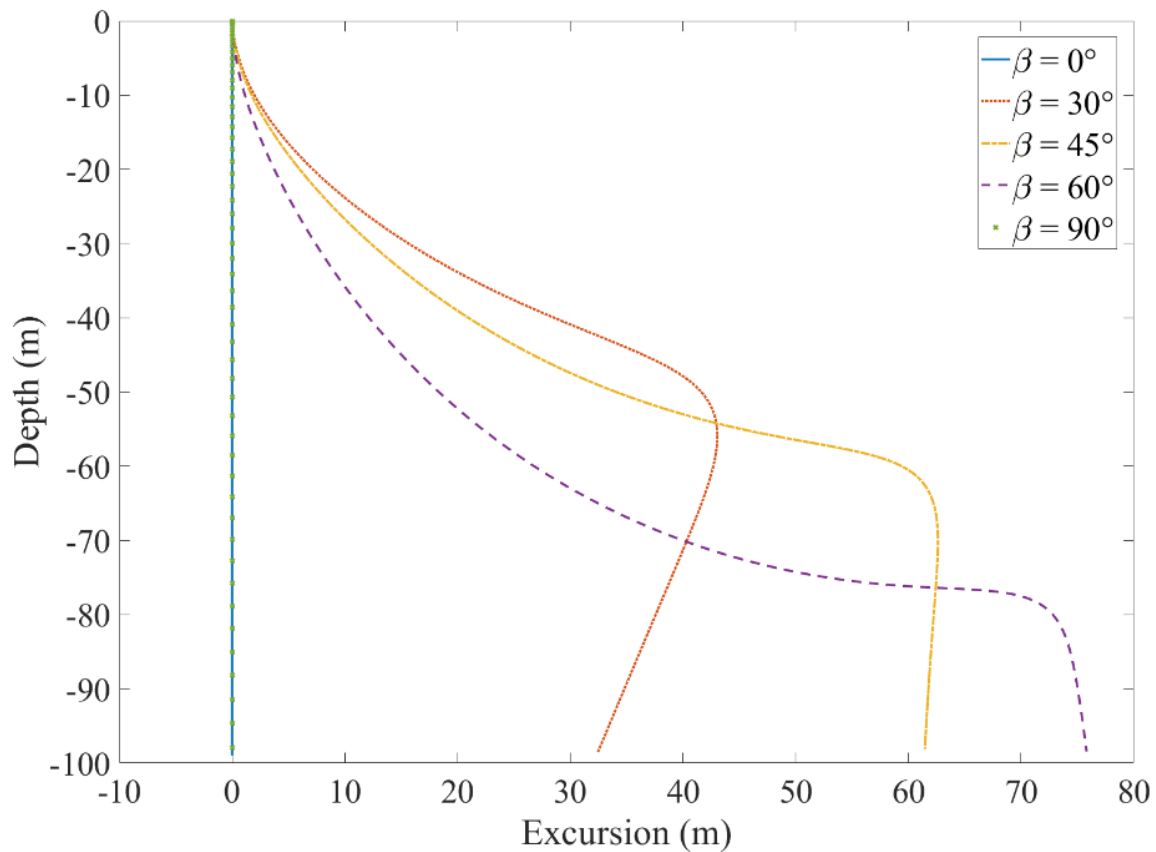


Figure 6.9 Full-scale drilling pipe excursion in 100 m water depth for different drop angle

Table 6.13 to Table 6.16 provide the maximum velocity of the full-scaled model for different Munk and drag moment coefficients with drop angle of 45° in different water depths. Since the object size and weight has increased, the order of the moments also increases. In that regard, the

Munk moment coefficient (C_{mm}) in range of 0.08 to 1.0 was investigated. Furthermore, as the estimated Reynolds number includes the drag crisis phenomenon, drag moment coefficient ($C_{d,moment}$) in range of 0.3 to 1.4 was investigated.

Unlike in the small-scale model, the results show no pattern in maximum velocity of the full-scale model for different drag and Munk moment coefficients. In small-scale model, the combination of Munk moment coefficient of 0.08 ($C_{mm} = 0.08$) and drag moment coefficient of 1.22 ($C_{d,moment} = 1.22$) showed the reasonable results when compared to experimental data. Similar combination can be valid for full-scale model. However, the results should be validated with data from experiments. No such experiments have been performed so far. Hence, it is difficult to conclude which combination is the most suitable for full scale model. Therefore, several different combinations of Munk and drag moment coefficients were performed. As seen in Table 6.13 to Table 6.16, the extreme cases happen for Munk moment coefficients in range of 0.08 to 0.2 and drag moment coefficients of 0.4 and 0.8.

Table 6.13 Maximum velocity of full-scale model in 100 m water depth

	Drag moment coefficient ($C_{d,moment}$)	Munk moment coefficient (C_{mm})						
		C_{mm} = 0.08	C_{mm} = 0.1	C_{mm} = 0.2	C_{mm} = 0.4	C_{mm} = 0.6	C_{mm} = 0.8	C_{mm} = 1.0
Maximum velocity (m/s)	$C_{d,moment} = 0.3$	-22.20	-23.83	-25.98	-23.60	-18.30	-16.61	-18.09
	$C_{d,moment} = 0.4$	-21.77	-23.05	-26.39	-19.42	-19.50	-23.02	-18.32
	$C_{d,moment} = 0.6$	-20.53	-21.81	-21.22	-15.67	-17.70	-14.73	-14.03
	$C_{d,moment} = 0.8$	-18.73	-19.86	-18.06	-15.10	-13.99	-12.01	-11.38
	$C_{d,moment} = 1.0$	-17.29	-18.27	-16.15	-14.01	-12.04	-10.71	-10.07
	$C_{d,moment} = 1.2$	-15.80	-17.04	-14.86	-12.77	-10.96	-9.96	-9.42
	$C_{d,moment} = 1.4$	-14.65	-15.85	-13.92	-11.73	-10.29	-9.58	-9.32

Table 6.14 Maximum velocity of full-scale model in 200 m water depth

	Drag moment coefficient ($C_{d,moment}$)	Munk moment coefficient (C_{mm})						
		C_{mm} = 0.08	C_{mm} = 0.1	C_{mm} = 0.2	C_{mm} = 0.4	C_{mm} = 0.6	C_{mm} = 0.8	C_{mm} = 1.0
Maximum velocity (m/s)	$C_{d,moment} = 0.3$	-26.91	-26.35	-26.19	-23.60	-18.30	-16.69	-18.09
	$C_{d,moment} = 0.4$	-31.65	-31.42	-28.88	-19.62	-19.98	-24.14	-19.73
	$C_{d,moment} = 0.6$	-29.60	-27.58	-23.95	-23.63	-21.05	-17.75	-15.31
	$C_{d,moment} = 0.8$	-24.43	-22.92	-25.68	-20.09	-16.17	-13.57	-11.84
	$C_{d,moment} = 1.0$	-21.43	-22.03	-20.68	-16.25	-13.21	-11.29	-10.20
	$C_{d,moment} = 1.2$	-19.39	-21.30	-17.89	-14.31	-11.56	-10.10	-9.42
	$C_{d,moment} = 1.4$	-17.91	-19.72	-16.03	-12.77	-10.45	-9.58	-9.32

Table 6.15 Maximum velocity of full-scale model in 400 m water depth

	Drag moment coefficient ($C_{d,moment}$)	Munk moment coefficient (C_{mm})						
		C_{mm} = 0.08	C_{mm} = 0.1	C_{mm} = 0.2	C_{mm} = 0.4	C_{mm} = 0.6	C_{mm} = 0.8	C_{mm} = 1.0
Maximum velocity (m/s)	$C_{d,moment} = 0.3$	-26.91	-26.35	-26.19	-23.60	-18.30	-16.69	-18.09
	$C_{d,moment} = 0.4$	-31.65	-31.42	-28.88	-19.62	-19.98	-24.4	-19.73
	$C_{d,moment} = 0.6$	-29.60	-27.58	-23.95	-23.63	-24.08	-18.61	-15.53
	$C_{d,moment} = 0.8$	-36.78	-43.06	-28.80	-22.68	-16.75	-13.75	-11.92
	$C_{d,moment} = 1.0$	-29.69	-30.71	-25.04	-17.61	-13.66	-11.41	-10.22
	$C_{d,moment} = 1.2$	-26.19	-24.91	-20.99	-14.95	-11.72	-10.12	-9.42
	$C_{d,moment} = 1.4$	-22.64	-21.57	-18.15	-13.14	-10.50	-9.58	-9.32

Table 6.16 Maximum velocity of full-scale model in 800 m water depth

	Drag moment coefficient ($C_{d,moment}$)	Munk moment coefficient (C_{mm})						
		C_{mm} = 0.08	C_{mm} = 0.1	C_{mm} = 0.2	C_{mm} = 0.4	C_{mm} = 0.6	C_{mm} = 0.8	C_{mm} = 1.0
Maximum velocity (m/s)	$C_{d,moment} = 0.3$	-26.91	-26.35	-26.19	-23.60	-18.30	-16.69	-18.09
	$C_{d,moment} = 0.4$	-31.65	-31.42	-28.88	-19.62	-19.98	-24.14	-19.73
	$C_{d,moment} = 0.6$	-29.60	-27.58	-23.95	-23.63	-27.48	-18.66	-15.55
	$C_{d,moment} = 0.8$	-36.78	-43.34	-29.70	-23.35	-16.77	-13.77	-11.92
	$C_{d,moment} = 1.0$	-35.98	-35.26	-27.18	-17.67	-13.68	-11.41	-10.22
	$C_{d,moment} = 1.2$	-27.81	-26.67	-21.36	-15.02	-11.74	-10.12	-9.42
	$C_{d,moment} = 1.4$	-23.72	-22.79	-18.44	-13.17	-10.80	-9.58	-9.32

Table 6.17 to Table 6.20 present the velocity of the full-scale model at the moment of landing on seabed for different for different Munk and drag moment coefficients with drop angle of 45° in different water depths. Based on the result from Table 6.17 to Table 6.20, no pattern is observed in landing velocity of the full-scale model for different drag and Munk moment coefficients. However, the results indicate that small changes in water depth will lead to drastic variation in velocity. So, the Impact energy of the full-scale model is calculated using maximum velocity table as the input. Impact energy of the full-scale model is computed using Eq.[3.70] and Eq.[3.71]. The added mass coefficient of 1 is selected based on DNV-RP-C205.

Table 6.17 Landing velocity of full-scale model in 100 m water depth

	Drag moment coefficient ($C_{d,moment}$)	Munk moment coefficient (C_{mm})						
		C_{mm} = 0.08	C_{mm} = 0.1	C_{mm} = 0.2	C_{mm} = 0.4	C_{mm} = 0.6	C_{mm} = 0.8	C_{mm} = 1.0
Landing velocity (m/s)	$C_{d,moment} = 0.3$	-22.20	-23.83	-25.98	-12.09	-14.05	-6.9	-10.56
	$C_{d,moment} = 0.4$	-21.77	-23.05	-26.39	-11.42	-19.50	-23.02	-8.95
	$C_{d,moment} = 0.6$	-20.53	-21.81	-20.74	-15.09	-17.24	-8.56	-14.03
	$C_{d,moment} = 0.8$	-18.73	-19.86	-15.31	-15.10	-8.87	-10.70	-10.36
	$C_{d,moment} = 1.0$	-17.29	-18.27	-12.15	-14.01	-5.90	-10.16	-8.43
	$C_{d,moment} = 1.2$	-15.80	-17.04	-10.05	-12.77	-5.81	-9.67	-7.79
	$C_{d,moment} = 1.4$	-14.65	-15.85	-8.58	-11.73	-6.04	-9.15	-7.65

Table 6.18 Landing velocity of full-scale model in 200 m water depth

	Drag moment coefficient ($C_{d,moment}$)	Munk moment coefficient (C_{mm})						
		C_{mm} = 0.08	C_{mm} = 0.1	C_{mm} = 0.2	C_{mm} = 0.4	C_{mm} = 0.6	C_{mm} = 0.8	C_{mm} = 1.0
Landing velocity (m/s)	$C_{d,moment} = 0.3$	-16.64	-13.26	-18.53	-11.90	-12.17	-14.84	-8.63
	$C_{d,moment} = 0.4$	-24.13	-9.33	-4.64	-10.34	-18.85	-20.44	-16.24
	$C_{d,moment} = 0.6$	-20.29	-13.83	-15.05	-21.84	-18.32	-14.36	-10.94
	$C_{d,moment} = 0.8$	-12.95	-20.84	-21.37	-2.99	-6.17	-6.14	-6.29
	$C_{d,moment} = 1.0$	-16.27	-22.03	-9.56	-13.52	-12.76	-10.92	-9.60
	$C_{d,moment} = 1.2$	-17.32	-21.30	-13.64	-14.31	-11.11	-9.62	-9.33
	$C_{d,moment} = 1.4$	-16.95	-19.72	-14.30	-12.48	-8.80	-8.29	-8.59

Table 6.19 Landing velocity of full-scale model in 400 m water depth

	Drag moment coefficient ($C_{d,moment}$)	Munk moment coefficient (C_{mm})						
		C_{mm} = 0.08	C_{mm} = 0.1	C_{mm} = 0.2	C_{mm} = 0.4	C_{mm} = 0.6	C_{mm} = 0.8	C_{mm} = 1.0
Landing velocity (m/s)	$C_{d,moment} = 0.3$	-8.94	-21.12	-5.27	-13.71	-13.33	-11.85	-10.91
	$C_{d,moment} = 0.4$	-9.07	-18.92	-18.44	-4.75	-6.17	-12.11	-6.67
	$C_{d,moment} = 0.6$	-28.28	-3.61	-18.34	-21.45	-16.07	-17.53	-15.50
	$C_{d,moment} = 0.8$	-0.82	-43.06	-25.21	-20.11	-11.48	-12.79	-11.70
	$C_{d,moment} = 1.0$	-29.69	-29.60	-14.81	-13.54	-9.74	-11.24	-10.15
	$C_{d,moment} = 1.2$	-23.14	-13.64	-20.43	-13.80	-7.01	-6.94	-6.83
	$C_{d,moment} = 1.4$	-2.31	-20.33	-3.88	-9.45	-9.30	-9.35	-8.38

Table 6.20 Landing velocity of full-scale model in 800 m water depth

	Drag moment coefficient ($C_{d,moment}$)	Munk moment coefficient (C_{mm})						
		C_{mm} = 0.08	C_{mm} = 0.1	C_{mm} = 0.2	C_{mm} = 0.4	C_{mm} = 0.6	C_{mm} = 0.8	C_{mm} = 1.0
Landing velocity (m/s)	$C_{d,moment} = 0.3$	-12.74	-10.45	-10.72	-14.18	-15.20	-7.99	-12.51
	$C_{d,moment} = 0.4$	-21.98	-19.16	-9.20	-17.53	-17.65	-13.51	-15.56
	$C_{d,moment} = 0.6$	-7.43	-24.63	-12.62	-16.15	-5.94	-16.45	-10.46
	$C_{d,moment} = 0.8$	-29.04	-25.53	-21.11	-8.72	-16.52	-7.63	-11.22
	$C_{d,moment} = 1.0$	-32.55	-22.73	-20.47	-16.78	-10.21	-11.41	-8.84
	$C_{d,moment} = 1.2$	-27.81	-19.28	-19.12	-7.66	-10.45	-6.40	-6.77
	$C_{d,moment} = 1.4$	-17.40	-6.54	-15.22	-7.06	-10.06	-6.67	-7.64

Table 6.21 to Table 6.24, present the result for effective energy of full-scale model for different drag and Munk moment coefficient in selected water depths 100 m, 200 m, 400 m, and 800 m. The highest effective energy in 100 m water depth belongs to case with Munk moment coefficient of 0.2 and drag moment coefficient of 0.4. In 200 m water depth maximum effective energy is resulted from Munk moment coefficient of 0.08 and drag moment coefficient of 0.4.

For 400 m and 800 m water depths, the maximum effective energy is resulted from combination of Munk moment coefficient of 0.1 and drag moment coefficient of 0.8. Based on the results, the maximum effective energy of the full-scale model remains constant in water depth above 400 m.

Table 6.21 Effective energy of full-scale model in 100 m water depth

	Drag moment coefficient ($C_{d,moment}$)	Munk moment coefficient (C_{mm})						
		C_{mm} = 0.08	C_{mm} = 0.1	C_{mm} = 0.2	C_{mm} = 0.4	C_{mm} = 0.6	C_{mm} = 0.8	C_{mm} = 1.0
Effective energy (kJ)	$C_{d,moment} = 0.3$	633.17	729.57	867.15	715.55	430.25	354.45	420.43
	$C_{d,moment} = 0.4$	608.88	682.59	894.74	484.52	488.52	680.81	431.19
	$C_{d,moment} = 0.6$	541.49	611.12	578.51	315.47	402.50	278.75	252.89
	$C_{d,moment} = 0.8$	450.70	506.73	419.04	292.93	251.45	185.31	166.38
	$C_{d,moment} = 1.0$	384.07	428.84	335.09	252.17	186.24	147.37	130.28
	$C_{d,moment} = 1.2$	320.72	373.04	283.70	209.51	154.33	127.45	114.00
	$C_{d,moment} = 1.4$	275.73	322.76	248.94	176.77	136.03	117.91	111.60

Table 6.22 Effective energy of full-scale model in 200 m water depth

	Drag moment coefficient ($C_{d,moment}$)	Munk moment coefficient (C_{mm})						
		C_{mm} = 0.08	C_{mm} = 0.1	C_{mm} = 0.2	C_{mm} = 0.4	C_{mm} = 0.6	C_{mm} = 0.8	C_{mm} = 1.0
Effective energy (kJ)	$C_{d,moment} = 0.3$	930.34	892.03	881.23	715.55	430.25	357.87	420.43
	$C_{d,moment} = 0.4$	1286.96	1268.32	1071.55	494.55	512.87	748.67	500.12
	$C_{d,moment} = 0.6$	1125.64	977.25	736.93	717.37	569.27	404.77	301.14
	$C_{d,moment} = 0.8$	766.77	674.91	847.24	518.53	335.92	236.58	180.10
	$C_{d,moment} = 1.0$	590.01	623.51	549.44	339.25	224.19	163.76	133.66
	$C_{d,moment} = 1.2$	483.03	582.88	411.18	263.08	171.68	131.06	114.00
	$C_{d,moment} = 1.4$	412.10	499.61	330.13	209.51	140.30	117.91	111.60

Table 6.23 Effective energy of full-scale model in 400 m water depth

	Drag moment coefficient ($C_{d,moment}$)	Munk moment coefficient (C_{mm})						
		C_{mm} = 0.08	C_{mm} = 0.1	C_{mm} = 0.2	C_{mm} = 0.4	C_{mm} = 0.6	C_{mm} = 0.8	C_{mm} = 1.0
Effective energy (kJ)	$C_{d,moment} = 0.3$	930.34	892.03	881.23	715.55	430.25	357.87	420.43
	$C_{d,moment} = 0.4$	1286.96	1268.32	1071.55	494.55	512.87	764.88	500.12
	$C_{d,moment} = 0.6$	1125.64	977.25	736.93	717.37	744.95	444.95	309.86
	$C_{d,moment} = 0.8$	1737.96	2382.12	1065.62	660.85	360.45	242.90	182.54
	$C_{d,moment} = 1.0$	1132.50	1211.65	805.54	398.41	239.73	167.26	134.19
	$C_{d,moment} = 1.2$	881.23	797.19	566.03	287.14	176.47	131.58	114.00
	$C_{d,moment} = 1.4$	658.52	597.75	423.22	221.82	141.64	117.91	111.60

Table 6.24 Effective energy of full-scale model in 800 m water depth

	Drag moment coefficient ($C_{d,moment}$)	Munk moment coefficient (C_{mm})						
		C_{mm} = 0.08	C_{mm} = 0.1	C_{mm} = 0.2	C_{mm} = 0.4	C_{mm} = 0.6	C_{mm} = 0.8	C_{mm} = 1.0
Effective energy (kJ)	$C_{d,moment} = 0.3$	930.34	892.02	881.22	715.55	430.24	357.87	420.43
	$C_{d,moment} = 0.4$	1286.95	1268.32	1071.54	494.55	512.87	748.67	500.11
	$C_{d,moment} = 0.6$	1125.64	977.24	736.93	717.37	970.17	447.34	310.65
	$C_{d,moment} = 0.8$	1737.96	2413.20	1133.25	700.47	361.31	243.60	182.54
	$C_{d,moment} = 1.0$	1663.17	1597.28	949.10	401.13	240.43	167.25	134.18
	$C_{d,moment} = 1.2$	993.61	913.82	586.16	289.83	177.07	131.57	114.00
	$C_{d,moment} = 1.4$	722.84	667.27	436.85	222.83	149.85	117.90	111.59

To find out average drag force coefficient throughout the excursion, several simulations were carried out for different drag moment coefficients ($C_{d,moment}$). The range of drag moment coefficient is decided based on the estimated Reynolds number from simulations for drop angle 0° and 90° . The velocity of the drilling pipe is at minimum when the motion is pure lateral and at maximum when the motion is pure axial. According to OrcaFlex simulations, the expected

Reynolds number corresponding to object's maximum velocity is 7.27E06 which is above the drag crisis range. Drag crisis causes sudden drop in drag coefficient for Reynolds number between 1E05 to 1E06. To encompass the effect of drag crisis in simulations, drag moment coefficients in range of 0.3 to 1.4 is selected as the inputs. Table 6.25 provides the average drag force coefficient throughout the simulation for different drag moment coefficients and Munk moment coefficient of 0.08 for full-scale model. According to the results obtained, the average drag force coefficient is approximately 0.54.

Table 6.25 Effect of drag moment coefficient on Average drag force coefficient

Drag Moment coefficient ($C_{d,moment}$)	0.3	0.4	0.5	0.6	0.7	0.8	0.9	1.0	1.1	1.2	1.3	1.4
Average drag force coefficient (C_d)	0.52	0.53	0.53	0.53	0.53	0.54	0.54	0.54	0.54	0.55	0.55	0.55

Probability analysis

DNV-RP-F107 [5] provides a method for calculating the probability of landing of dropped object in a certain radius from dropped point. Based on Table 3.1 from DNV-RP-F107, the model is considered as a round shape object with weight of 2.23 tone and angular deviation of 5 ($\alpha = 5$). Figure 6.10 and Figure 6.11 present the probability of exceedance for full-scale model for different water depths. Results from DNV-RP-F107 are presented in Figure 6.10 and results from OrcaFlex simulations are provided in Figure 6.11. In the figures, the probability of exceedance increases by increasing the water depth and it reduces as the horizontal distance from drop location increases. Appendix III provides details for comparison of probability of exceedance between DNV guidelines and OrcaFlex simulations. Figure 6.12 compares the probability of impact of the full-scale model to 20-inch subsea pipeline for 100 m water depth. In Table 6.26 to Table 6.29, probability of impact of the full-scale model to a 20-inch subsea pipeline is computed for different horizontal radius from drop location and different water depths. As seen in Table 6.26, DNV (RP) estimates zero probability of impact at 80 m horizontal distance from drop point, while the OrcaFlex simulations predict 2.27E-04 percent probability for impact

between dropped full-scale model and the subsea pipeline at 80 m horizontal distance from drop point. In Table 6.27, DNV (RP) estimates zero probability of impact between dropped full-scale model and the subsea pipeline at 160 m horizontal distance from drop point, while the OrcaFlex simulations suggest that there is 4.04E-05 percent probability of impact between dropped full-scale model and the subsea pipeline at 160 m horizontal distance from drop point. A similar pattern has been observed for probability of impact at 400 m and 800 m water depth. The DNV guideline shows a lower probability of impact in far location from drop point in comparison to OrcaFlex simulations. Though, DNV estimation for probability of impact at short distances from drop points is higher than OrcaFlex simulations. This implies that DNV recommendation is conservative for far horizontal distances from drop points.

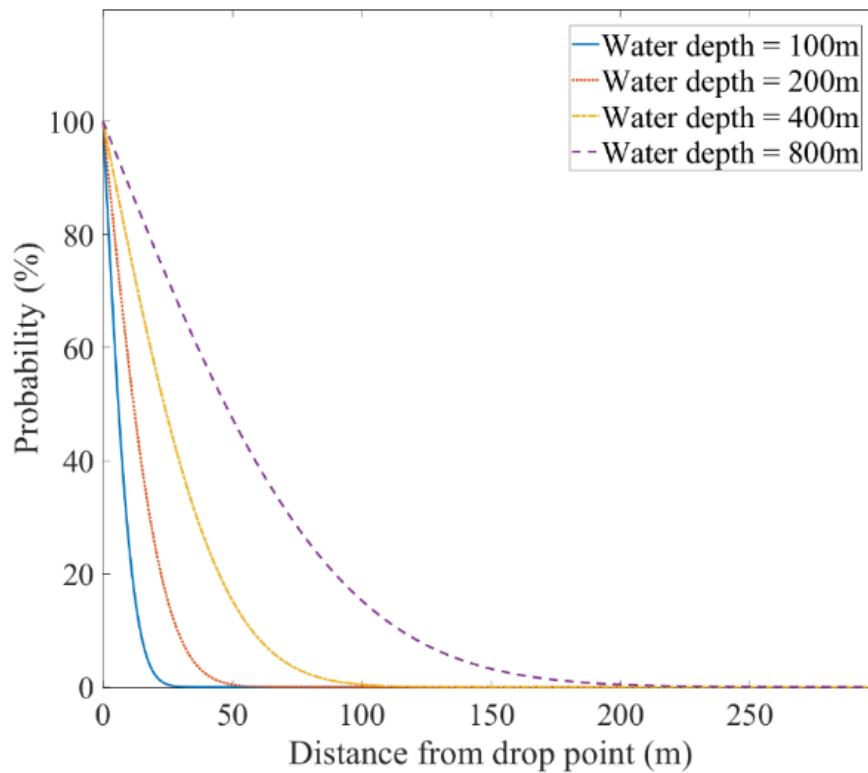


Figure 6.10 Probability of exceedance for different water depth according to DNV (RP)

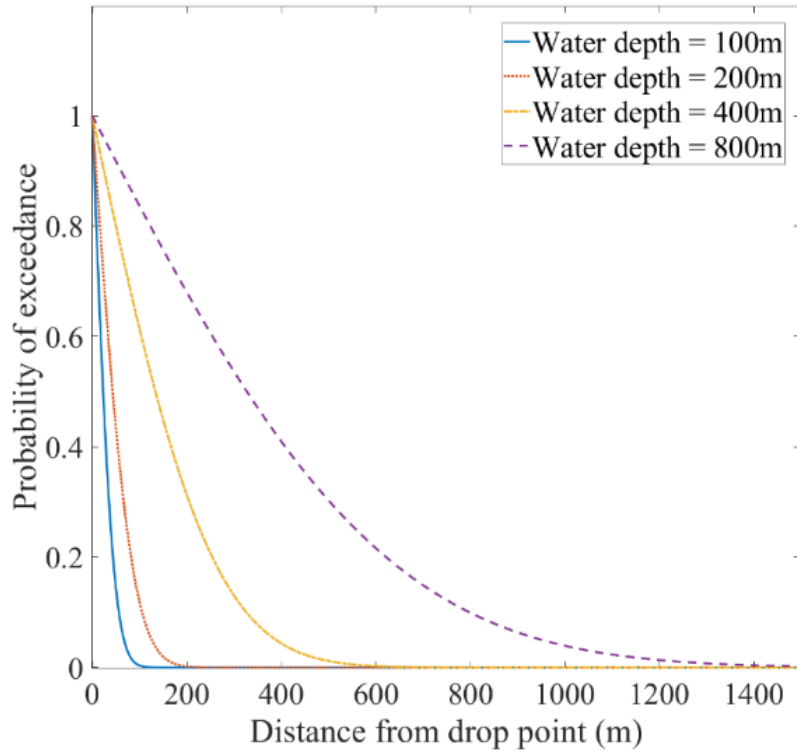


Figure 6.11 Probability of exceedance different water depth according to OrcaFlex simulation

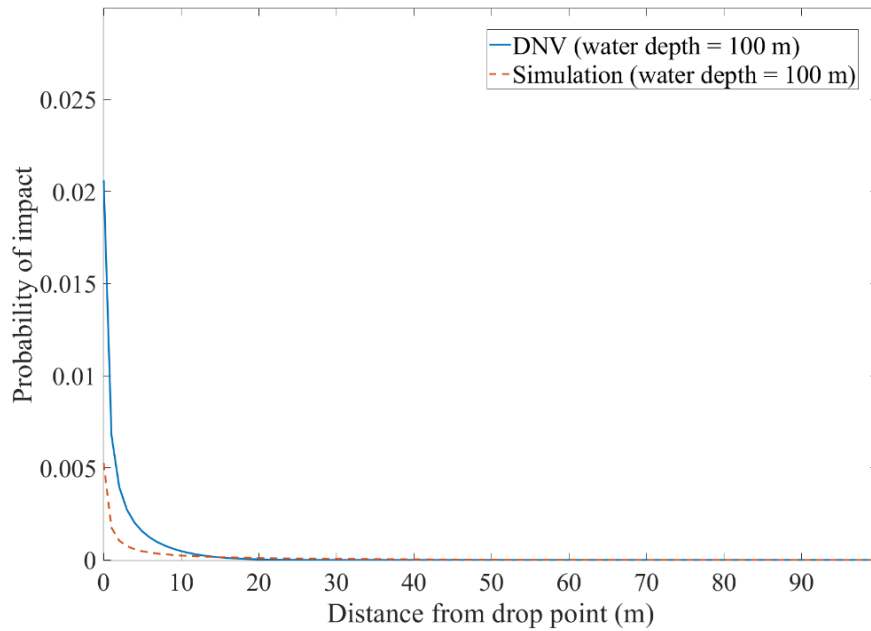


Figure 6.12 Comparison of probability of hit in 100 m water depth

Table 6.26 Comparison of probability of impact in 100 m water depth for different locations from drop point

Distance from drop point (m)	$P_{hit,sl,r}(DNV)(\%)$	$P_{hit,sl,r}(Simulations)(\%)$
10	6.03E-02	2.66E-02
20	4.43E-03	1.15E-02
40	9.90E-07	3.44E-03
80	0	2.27E-04
160	0	3.43E-08
320	0	0
640	0	0
1280	0	0

Table 6.27 Comparison of probability of impact in 200 m water depth for different locations from drop point

Distance from drop point (m)	$P_{hit,sl,r}(DNV)(\%)$	$P_{hit,sl,r}(Simulations)(\%)$
10	4.69E-02	1.46E-02
20	1.42E-02	6.89E-03
40	1.02E-03	2.95E-03
80	2.14E-07	8.22E-04
160	0	4.04E-05
320	0	1.86E-09
640	0	0
1280	0	0

Table 6.28 Comparison of probability of impact in 400 m water depth for different locations from drop point

Distance from drop point (m)	$P_{hit,sl,r}(DNV)(\%)$	$P_{hit,sl,r}(Simulations)(\%)$
10	2.62E-02	4.79E-03
20	1.13E-02	2.33E-03
40	3.46E-03	1.13E-03
80	2.46E-04	5.29E-04
160	4.99E-08	2.07E-04
320	0	3.89E-05
640	0	3.91E-07
1280	0	0

Table 6.29 Comparison of probability of impact in 800 m water depth for different locations from drop point

Distance from drop point (m)	$P_{hit,sl,r}(DNV)(\%)$	$P_{hit,sl,r}(Simulations)(\%)$
10	1.35E-02	4.79E-03
20	6.37E-03	2.33E-03
40	2.79E-03	1.13E-03
80	8.52E-04	5.29E-04
160	6.03E-05	2.07E-04
320	1.21E-08	3.89E-05
640	0	3.91E-07
1280	0	0

Chapter 7: Conclusion and recommendation

Conclusion

The present thesis work focuses on studying the motions of unintentionally dropped cylindrical objects during various marine operations. The first part of the thesis includes the simulations of a small cylindrical model of scale 1:20.32 using numerical software “OrcaFlex” to predict trajectory of the object when dropped into sea. The results were first validated by experimental data (Aanesland et al. (1987)). The simulations of small-scale models were carried out for 4 different water depths (i.e., 5 m, 10 m, 20 m, and 40 m). All the simulations from OrcaFlex are based on 3D theory for dropped objects and a 6D buoy is selected to investigate the trajectory motion, terminal velocity, and excursion. Numerical results obtained from OrcaFlex analyses show good agreement with the experimental results. The numerical results also show that the most critical factors determining the object’s trajectories are the drop angle, normal drag moment coefficient and Munk moment coefficient. It is also observed that maximum velocity that object attained during excursion reduces as the normal drag moment coefficient increases. On the other hand, maximum velocity of the object increases as the Munk moment coefficient increases. The drop angle does not show any effect on maximum velocity. However, it determines the landing location in shallow water region. The variation of Munk moment coefficient and different drop angle does not have any effect on average drag moment coefficient throughout the excursion. When the drop angle for the cylinder is 0° , the terminal velocity shows the good agreement with experimental data and analytical results. But for 90° drop angle, the terminal velocity obtained using numerical simulation shows good agreement with analytical results and show higher values as compared to experimental data. The reason for the difference in terminal velocity for numerical and experimental results is since the cylinder is assumed to be smooth cylinder in fully turbulent flow. The maximum velocity that a small-scale cylinder attains after 20 m will be constant. Further, based on the numerical results of small-scale model, it can be concluded that axial drag moment coefficient has negligible effect on maximum terminal velocity and excursion.

After validating the small-scale model, the numerical simulations using OrcaFlex were carried out on full-scale model selected from Aanesland et al. (1987). The simulations were performed for 4 different water depths (i.e., 100 m, 200 m, 400 m, 800 m). Unlike small-scale model, no specific pattern for maximum velocity is observed for different combinations of normal drag and Munk moment coefficients. The maximum velocity for the full-scale model is observed for Munk moment coefficients in the range of 0.08 to 0.20 for different water depths. The highest impact energy of the full-scale model will be constant after 400 m water depth for different combination of Munk and drag moment coefficients.

The second part of the thesis includes the calculation of the probability of exceedance and probability of impact for the full-scale model with a 20-inch subsea pipeline. A combination of drag moment coefficient of 0.55 and Munk moment coefficient of 0.08 is selected to perform the simulations in different water depths. According to the predicted results, the probability of exceedance increases with the increase of water depths, while it reduces with the increase of the horizontal distance from drop location. OrcaFlex simulations show higher probability of impact between dropped object and subsea facilities at far distance locations, compared to DNV (RP). This implies that for objects that have long excursions the results from DNV (RP) are conservative. On the other hand, the DNV (RP) shows higher probability of impact for short distances from drop location compared to the probability from OrcaFlex simulations. This implies that for objects with short excursion patterns the DNV (RP) predictions are not conservative.

Future work

There are number of parameters that can be investigated in detail for providing more accurate input data to establish a model which is closer to real life event and to obtain the improved numerical calculations.

- Computing Terminal velocity and impact energy of dropped object in sea column using line object in OrcaFlex.
- Experimental investigation of terminal velocity and excursion of full-scale drilling pipe
- Dropped object behavior in splash zone and its effect on excursion.

- Wave and current effect on excursion and probability of impact of dropped object.
- Experimental investigation of Munk moment coefficient for cylindrical object in axial flow

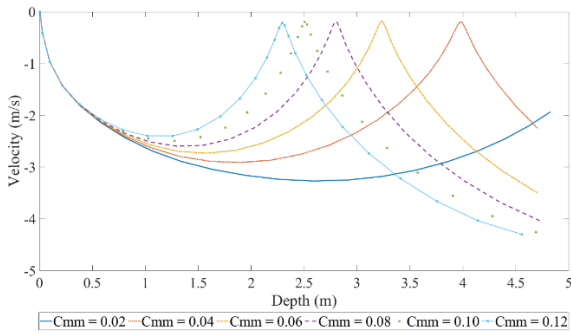
References

- [1] H. S. Håland, “Accidental Drop of Slender Cylindrical Bodies-A Numerical and Experimental Study of Velocity and Trajectory of Cylinders Falling Through Water,” Master’s Thesis, NTNU, 2018.
- [2] D. Karras, “Assessment of Marine Pipelines Subjected to Impact from Dropped Objects,” 2017.
- [3] P. Engineering, “US Navy Stockless Anchor | ABS Certificated | Pilotfits.” <https://pilotfits.com/products/us-navy-stockless-anchor/> (accessed Jan. 09, 2023).
- [4] V. Aanesland, “Numerical and experimental investigation of accidentally falling drilling pipes,” in *Offshore technology conference*, OnePetro, 1987.
- [5] D. N. Veritas, “Risk assessment of pipeline protection,” *Recomm. Pract. DNVRPF107*, 2010.
- [6] Y. Luo and J. Davis, “Motion Simulation And Hazard Assessment Of Dropped Objects,” presented at the The Second International Offshore and Polar Engineering Conference, OnePetro, Jun. 1992. Accessed: Jan. 14, 2023. [Online]. Available: <https://onepetro.org/ISOPEIOPEC/proceedings-abstract/ISOPE92/All-ISOPE92/21879>
- [7] A. D. Colwill and A. V. Ahilan, “Reliability Analysis of the Behavior of Dropped Objects,” presented at the Offshore Technology Conference, OnePetro, May 1992. doi: 10.4043/6918-MS.
- [8] A. F. Gilles, “Mine Drop Experiment,” *M Thesis Nav. Postgrad. Sch. Monterey CA*, p. 151, 2001.
- [9] G. P. Ray, “Bomb strike experiment for mine clearance operations,” NAVAL POSTGRADUATE SCHOOL MONTEREY CA, 2006.
- [10] Y. Kim, Y. Liu, and D. K. Yue, “Motion dynamics of three-dimensional bodies falling through water,” *Proc 17-Th*, 2002.
- [11] P. C. Chu and C. Fan, “Prediction of Falling Cylinder Through Air-Water-Sediment Columns,” *J. Appl. Mech.*, vol. 73, no. 2, pp. 300–314, Aug. 2005, doi: 10.1115/1.2125975.
- [12] P. C. Chu, A. Gilles, and C. Fan, “Experiment of falling cylinder through the water column,” *Exp. Therm. Fluid Sci.*, vol. 29, no. 5, pp. 555–568, Jun. 2005, doi: 10.1016/j.expthermflusci.2004.08.001.
- [13] S. Yasseri, “Experiment of free-falling cylinders in water,” *Underw. Technol.*, vol. 32, no. 3, pp. 177–191, Nov. 2014, doi: 10.3723/ut.32.177.

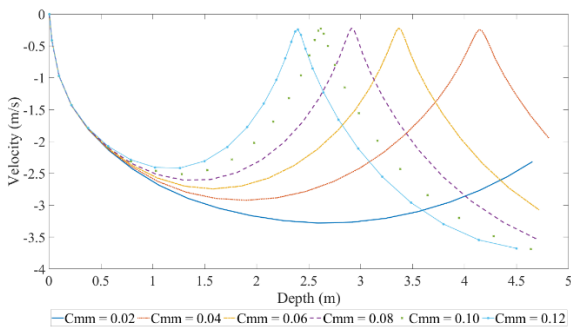
- [14] “About DROPS › DROPSOnline.” <https://www.dropsonline.org/about/> (accessed Jan. 09, 2023).
- [15] Md. R. U. Kawsar, S. A. Youssef, M. Faisal, A. Kumar, J. K. Seo, and J. K. Paik, “Assessment of dropped object risk on corroded subsea pipeline,” *Ocean Eng.*, vol. 106, pp. 329–340, Sep. 2015, doi: 10.1016/j.oceaneng.2015.06.056.
- [16] I. C. Brown and S. H. Perry, “The assessment of impact damage caused by dropped objects on concrete offshore structures,” 1989.
- [17] A. Santhakumaran, “Mathematical modeling and computational methods”.
- [18] Y. Kim, Y. Liu, and D. K. Yue, “Motion dynamics of three-dimensional bodies falling through water,” *Proc 17-Th*, 2002.
- [19] O. Faltinsen, *Sea loads on ships and offshore structures*, vol. 1. Cambridge university press, 1993.
- [20] J. N. Newman, *Marine hydrodynamics*. The MIT press, 2018.
- [21] H. Schlichting and E. Truckenbrodt, *Aerodynamics of the Airplane*. McGraw-Hill Companies, 1979.
- [22] S. F. Horner, “Fluid-Dynamic Drag, published and copyrighted by the author, 1958,” in *Library of Congress Catalog Card*,
- [23] O. T. Gudmestad and G. Moe, “Hydrodynamic coefficients for calculation of hydrodynamic loads on offshore truss structures,” *Mar. Struct.*, vol. 9, no. 8, pp. 745–758, 1996.
- [24] D. L. Parker, “An Analytic Derivation of the Relationship between the Angular Velocity Vector and the Euler Angles and their Time Derivatives,” *Am. J. Phys.*, vol. 37, no. 9, pp. 925–927, 1969.
- [25] L. I. U. Peiqing and G. U. O. Zhifei, “DERIVATION OF LIFT, DRAG AND THE KUTTA–JOUKOWSKI THEOREM FOR AIRCRAFTS 1,” *Mech. Eng.*, vol. 41, no. 6, p. 739, 2019.
- [26] R. K. Nagle, E. B. Saff, A. D. Snider, and B. West, *Fundamentals of differential equations and boundary value problems*. Addison-Wesley New York, 1996.
- [27] J. M. Schuler and F. E. Pritchard, “Six-degree-of-freedom equations of motion for a maneuvering re-entry vehicle,” CORNELL AERONAUTICAL LAB INC BUFFALO NY, 1962.
- [28] O. Ltd, “OrcaFlex User Manual Version 11.0 d.” 2020.

- [29] J. Chung and G. Hulbert, “A time integration algorithm for structural dynamics with improved numerical dissipation: the generalized- α method,” 1993.
- [30] D. Zhang, B. Zhao, and K. Zhu, “Hydrodynamic Response of Ocean-Towed Cable-Array System under Different Munk Moment Coefficients,” *Sustainability*, vol. 14, no. 3, p. 1932, 2022.
- [31] J. Fredsoe and B. M. Sumer, *Hydrodynamics around cylindrical structures (revised edition)*, vol. 26. World Scientific, 2006.
- [32] S. A. Jordan, “A skin friction model for axisymmetric turbulent boundary layers along long thin circular cylinders,” *Phys. Fluids*, vol. 25, no. 7, p. 075104, Jul. 2013, doi: 10.1063/1.4813810.
- [33] Y. A. Cengel and J. M. Cimbala, “Fundamental of Fluid Mechanics.” Tata McGraw-Hill Education, 2010.
- [34] N. Veritas, *Environmental conditions and environmental loads*. Det Norske Veritas Oslo, Norway, 2000.

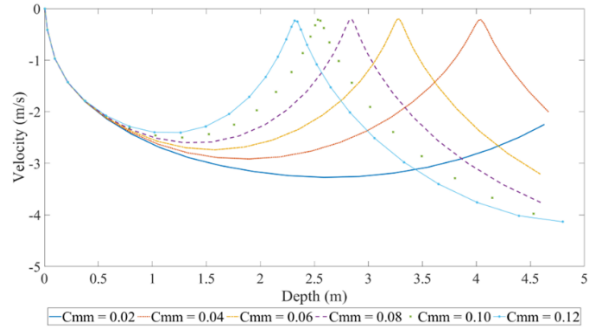
Appendix I



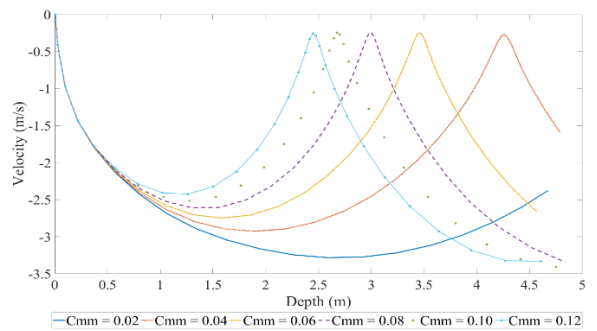
$$C_{d,moment} = 0.9$$



$$C_{d,moment} = 1.2$$

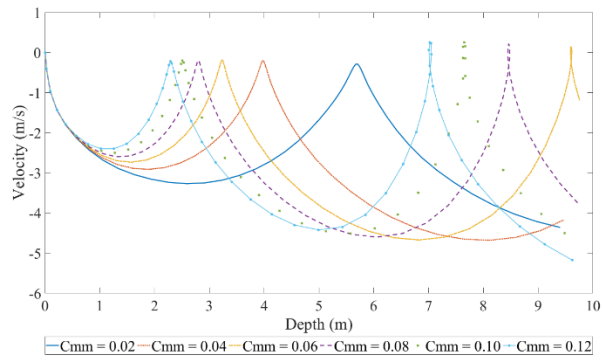


$$C_{d,moment} = 1.0$$

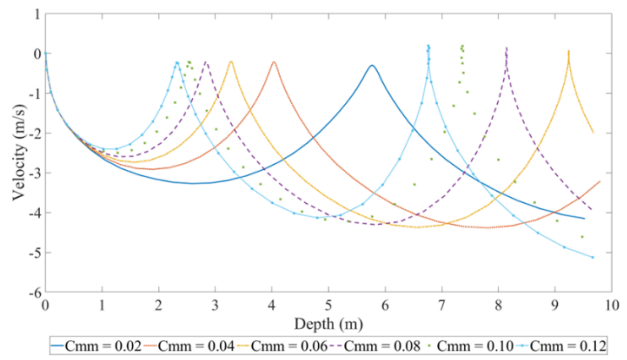


$$C_{d,moment} = 1.4$$

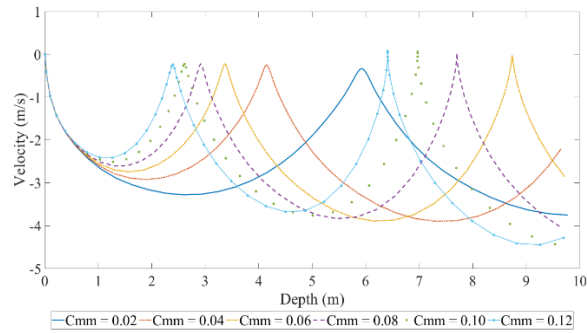
Figure 0.1 Effect of Munk moment coefficient on velocity for small-scale model with drop angle of 45° in 5 m water depth



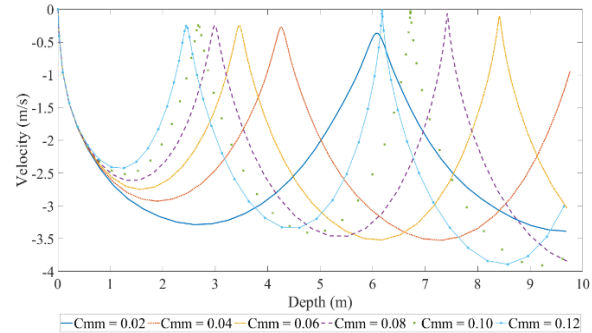
$$C_{d,moment} = 0.9$$



$$C_{d,moment} = 1.0$$



$$C_{d,moment} = 1.2$$



$$C_{d,moment} = 1.4$$

Figure 0.2 Effect of Munk moment coefficient on velocity for small scale model with drop angle of 45° in 10 m water depth

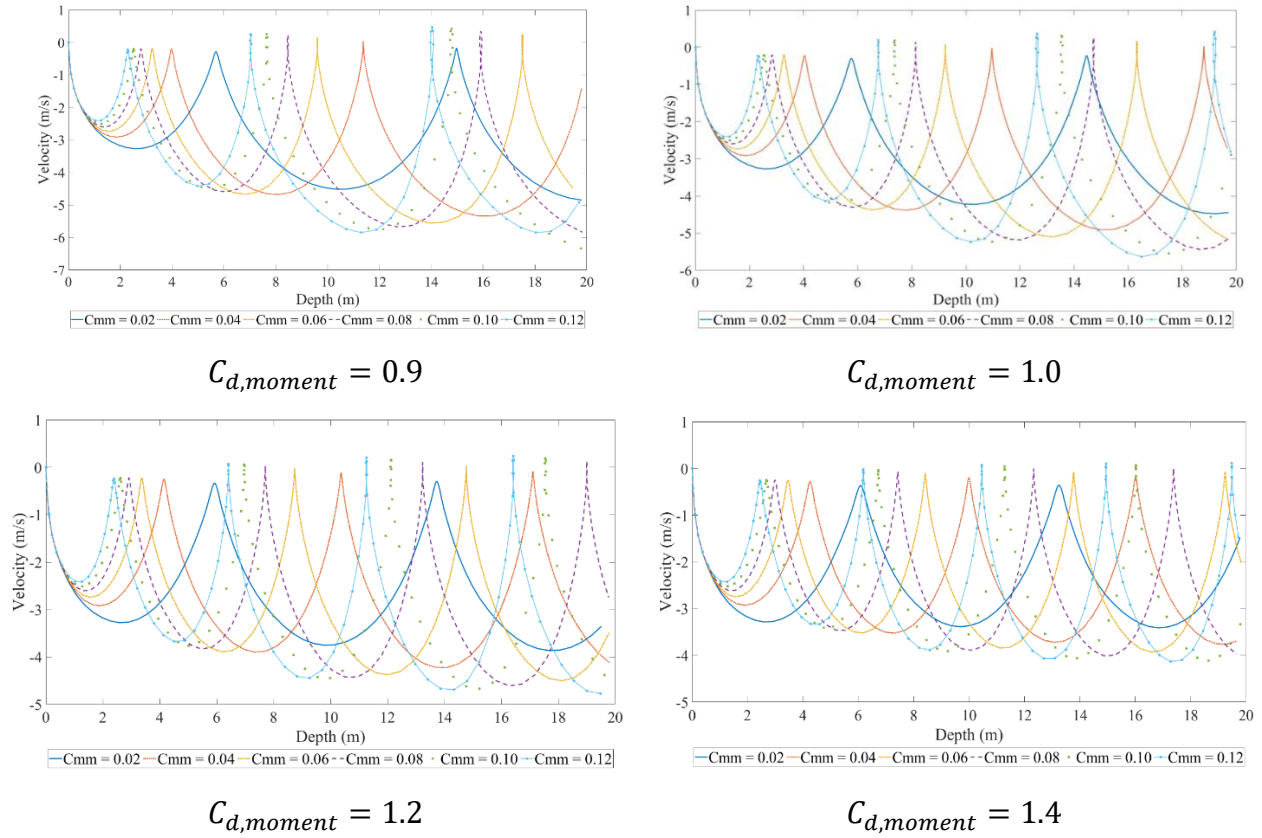
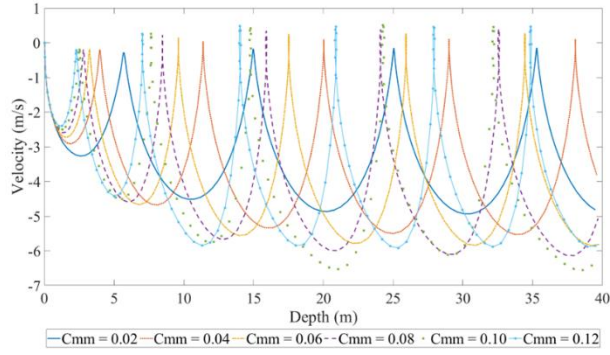
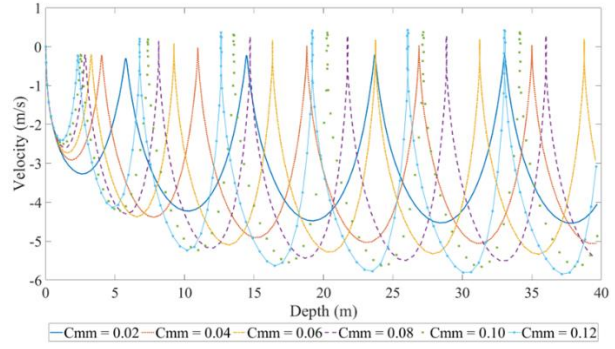


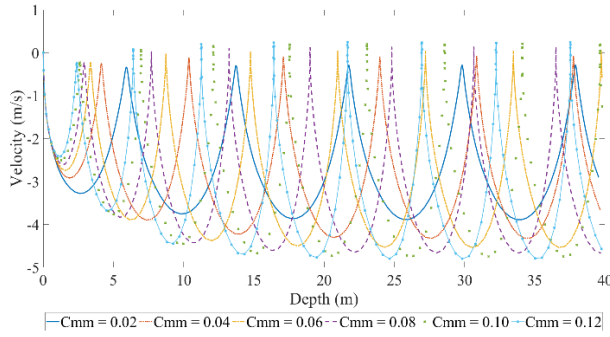
Figure 0.3 Effect of Munk moment coefficient on velocity for small scale model with drop angle of 45° in 20 m water depth



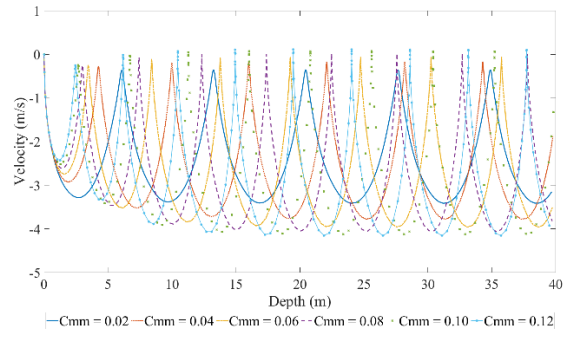
$$C_{d,moment} = 0.9$$



$$C_{d,moment} = 1.0$$



$$C_{d,moment} = 1.2$$



$$C_{d,moment} = 1.4$$

Figure 0.4 Effect of Munk moment coefficient on velocity for small scale model with drop angle of 45° in 40 m water depth

Appendix II

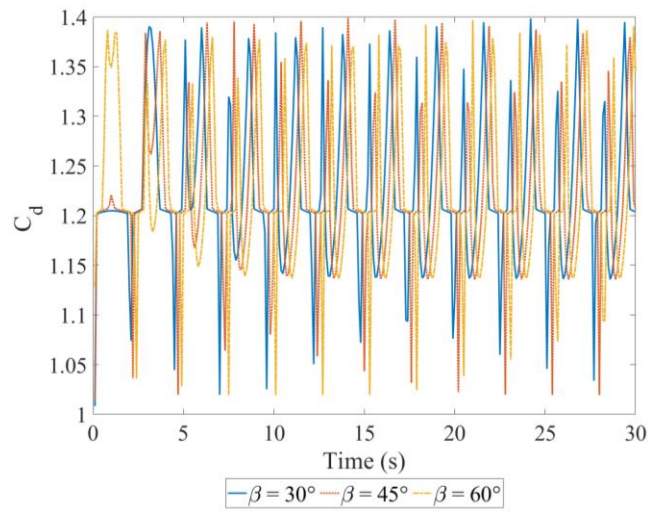
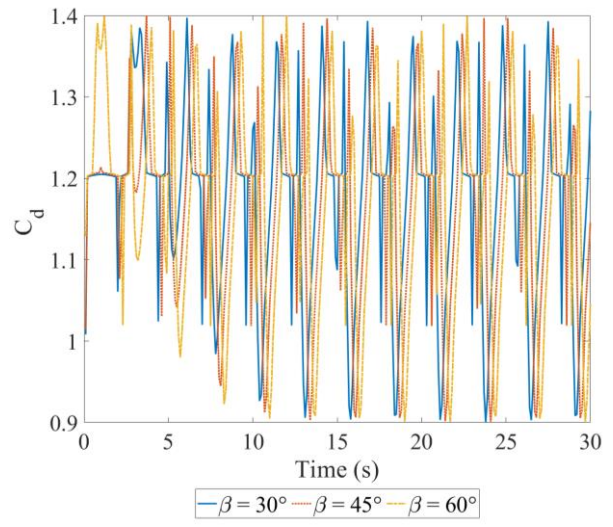
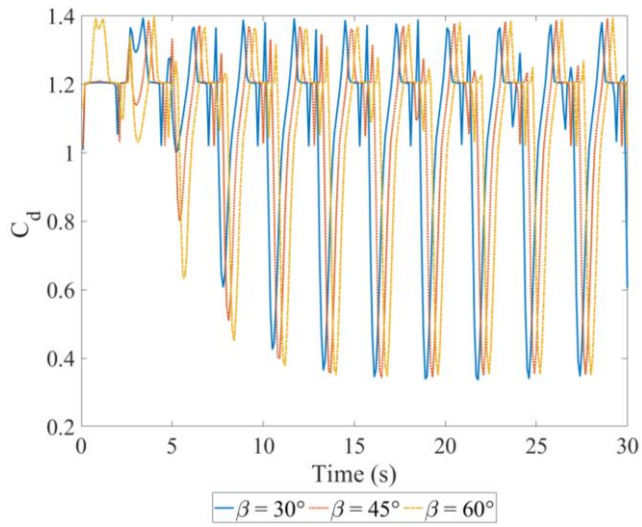
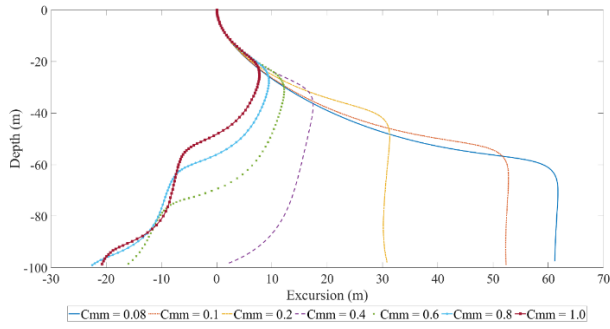
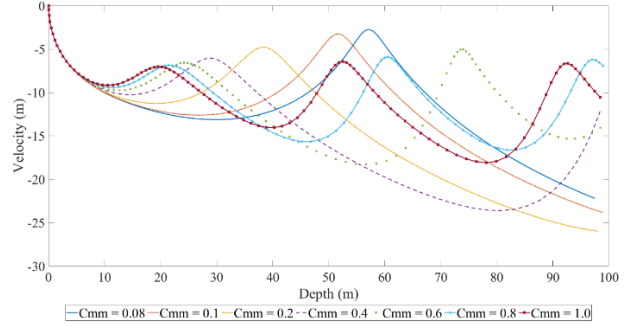


Figure 0.1 Drag force coefficient (C_d) time history for different β and $C_{mm} = 0.08$

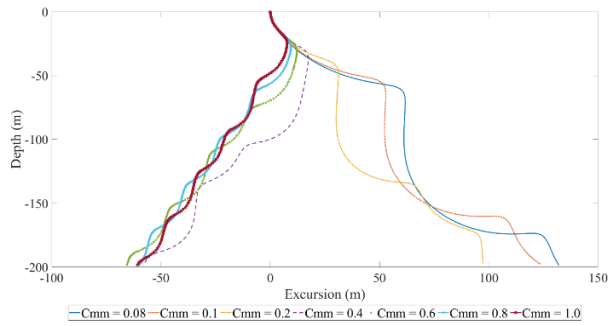
Appendix III



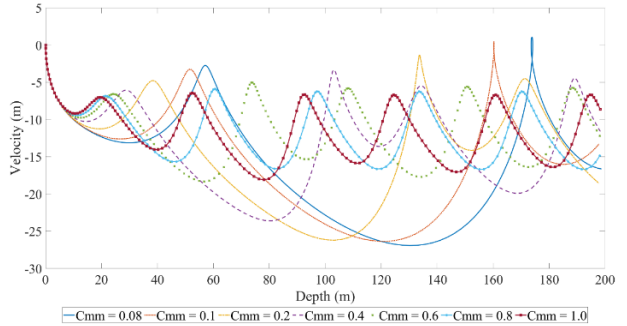
100 m water depth



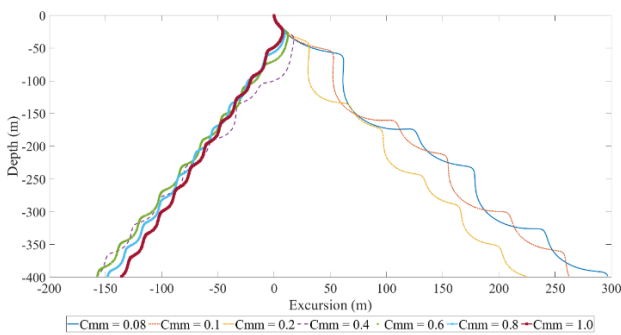
100 m water depth



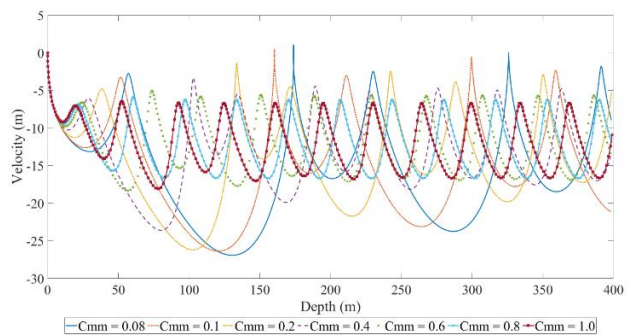
200 m water depth



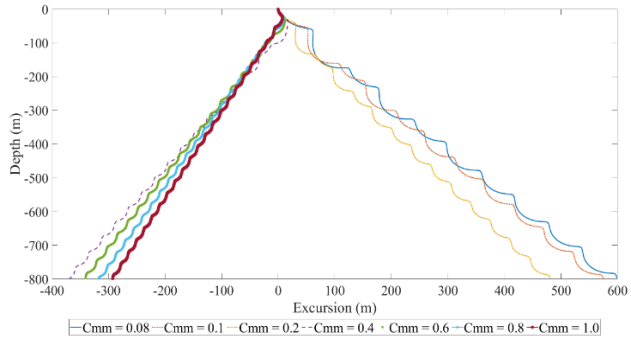
200 m water depth



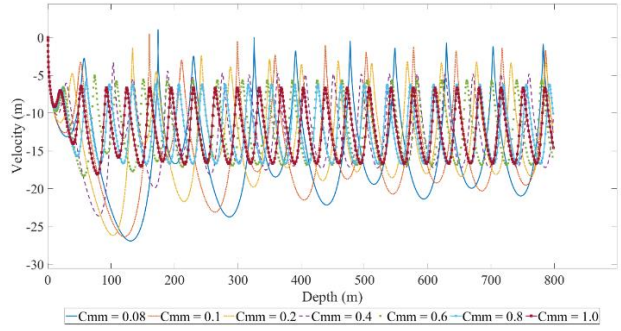
400 m water depth



400 m water depth

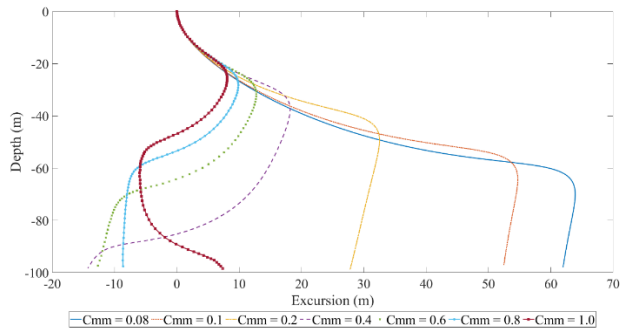


800 m water depth

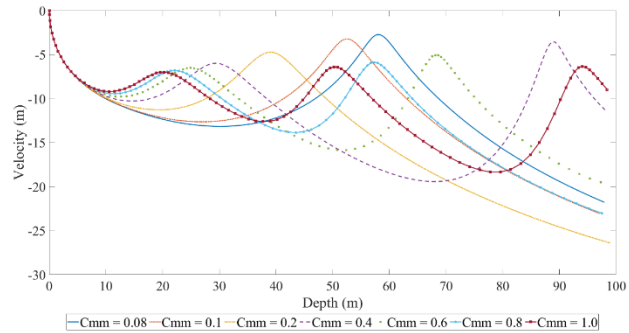


800 m water depth

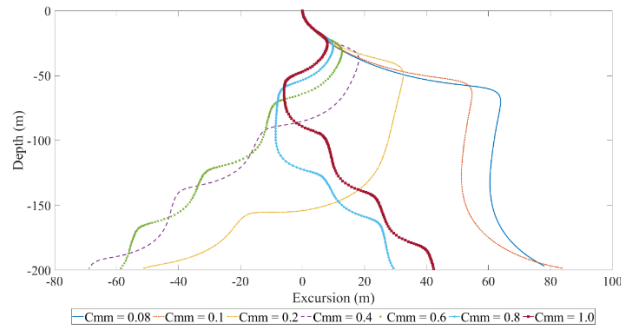
Figure 0.1 Excursion and velocity of full-scale model when $\beta = 45^\circ$ and $C_{d,moment} = 0.3$ for different Munk moment coefficient (C_{mm}) in different water depth



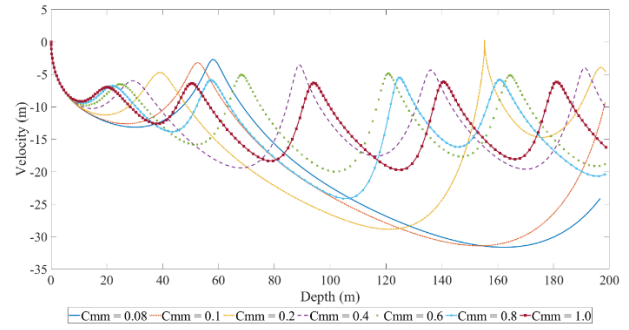
100 m water depth



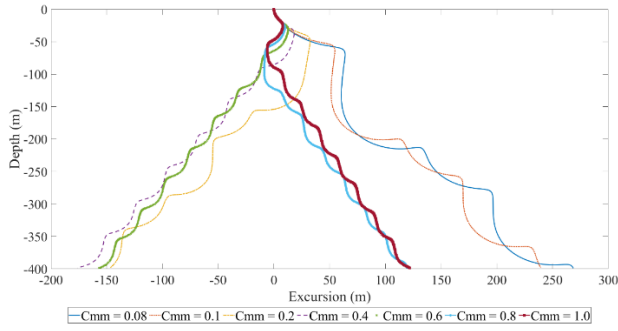
100 m water depth



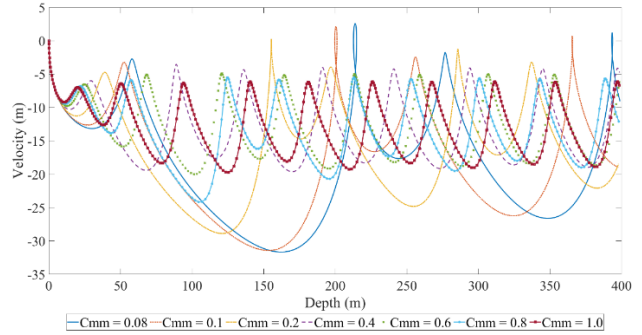
200 m water depth



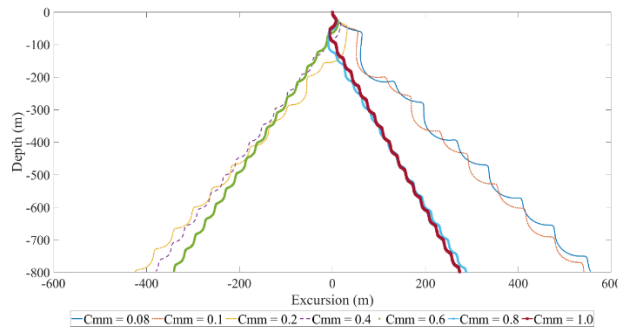
200 m water depth



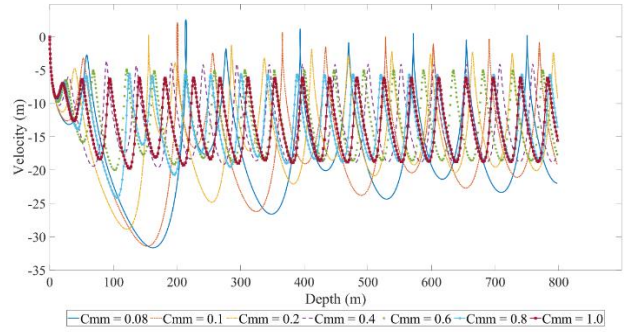
400 m water depth



400 m water depth

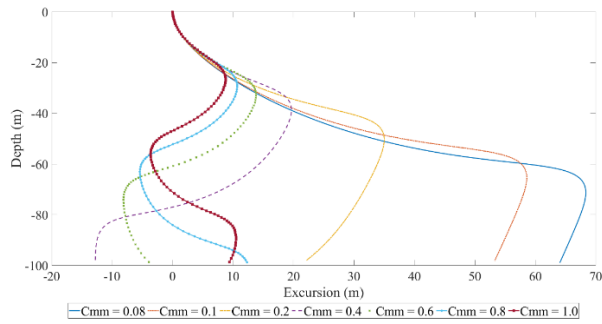


800 m water depth

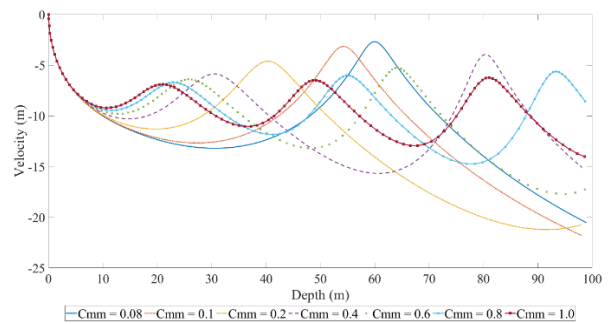


800 m water depth

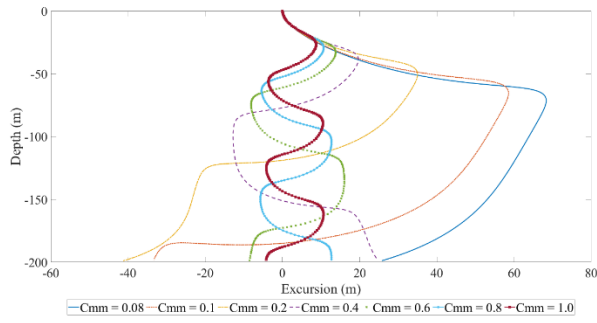
Figure 0.2 Excursion and velocity of full-scale model when $\beta = 45^\circ$ and $C_{d,moment} = 0.4$ for different Munk moment coefficient (C_{mm}) in different water depth



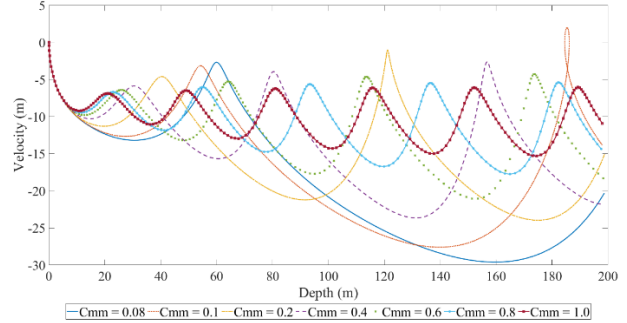
100 m water depth



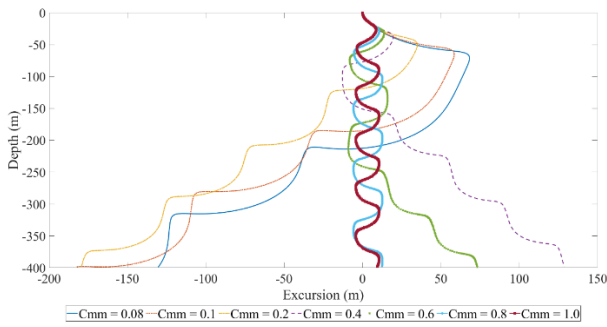
100 m water depth



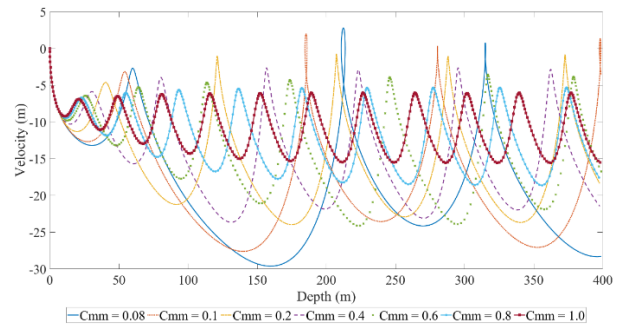
200 m water depth



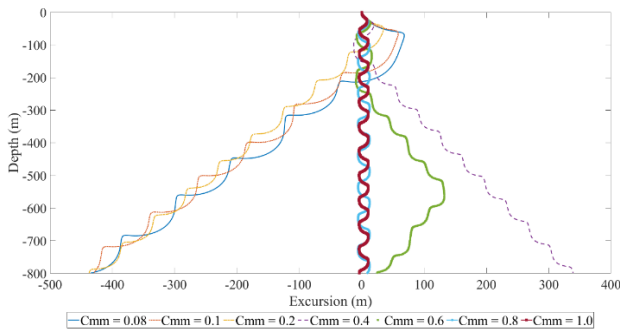
200 m water depth



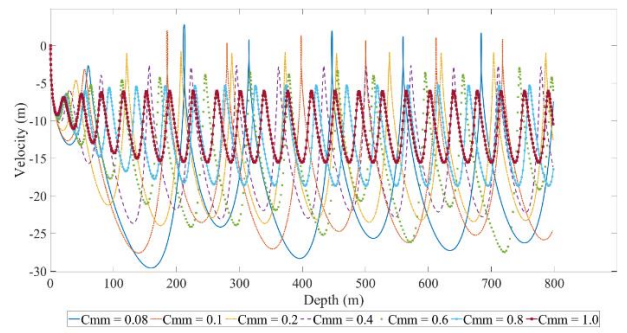
400 m water depth



400 m water depth

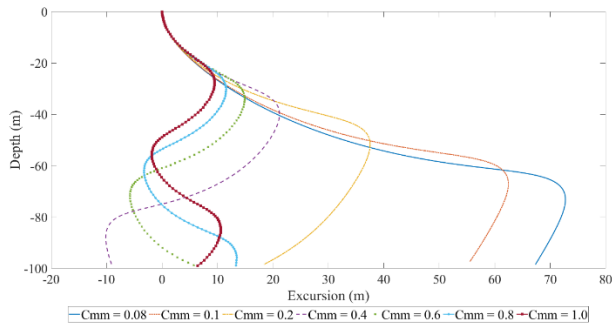


800 m water depth

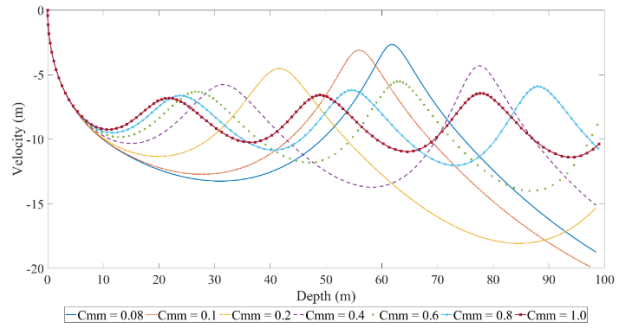


800 m water depth

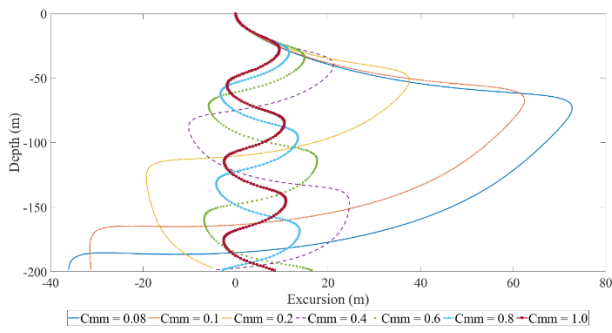
Figure 0.3 Excursion and velocity of full-scale model when $\beta = 45^\circ$ and $C_{d,moment} = 0.6$ for different Munk moment coefficient (C_{mm}) in different water depth



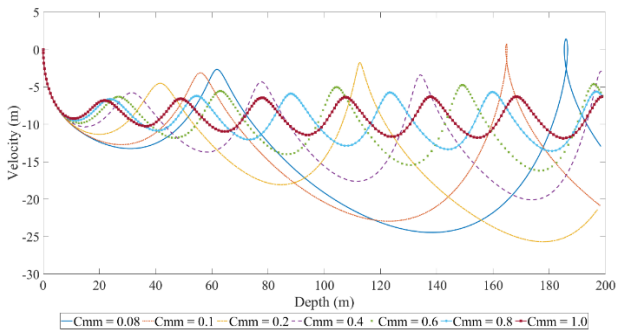
100 m water depth



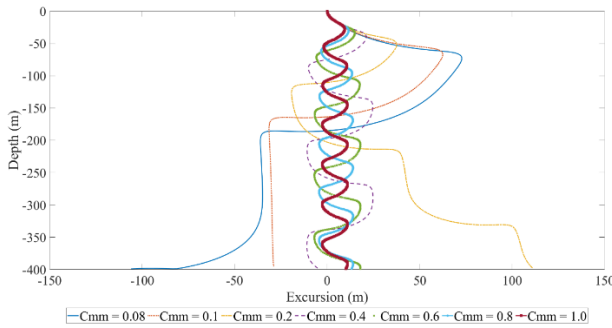
100 m water depth



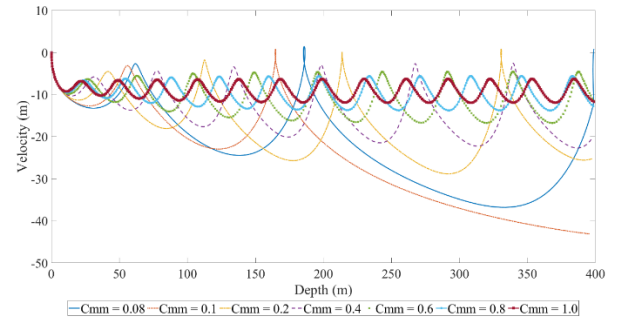
200 m water depth



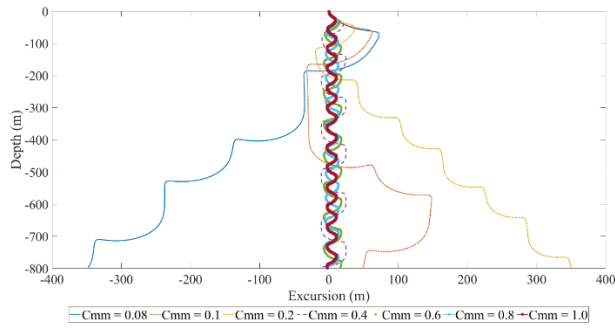
200 m water depth



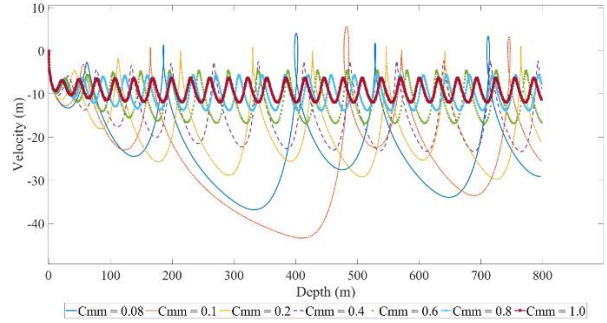
400 m water depth



400 m water depth

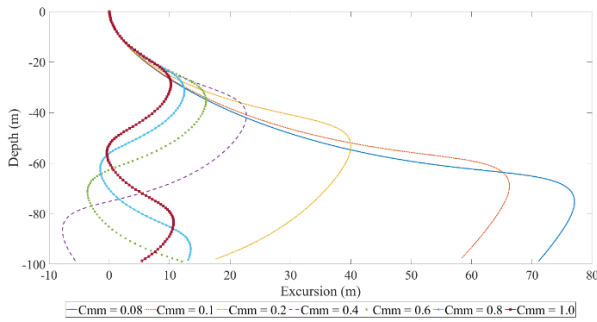


800 m water depth

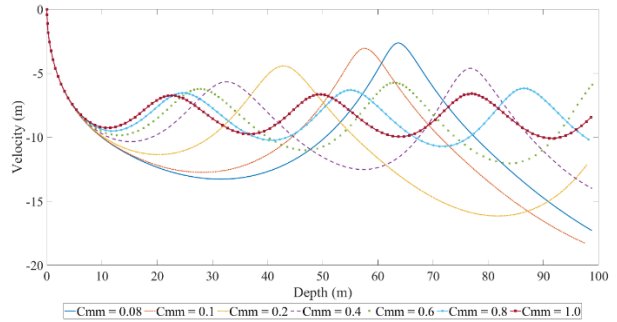


800 m water depth

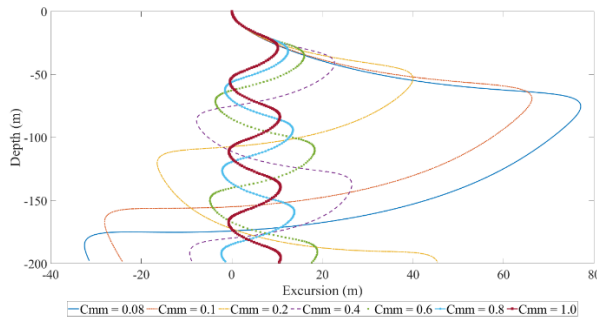
Figure 0.4 Excursion and velocity of full-scale model when $\beta = 45^\circ$ and $C_{d,moment} = 0.8$ for different Munk moment coefficient (C_{mm}) in different water depth



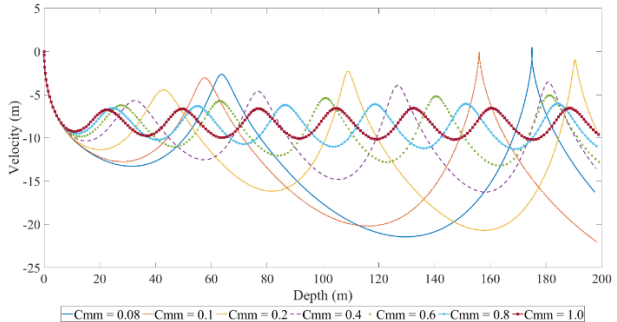
100 m water depth



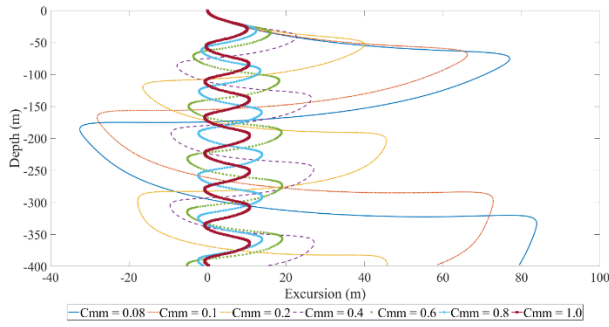
100 m water depth



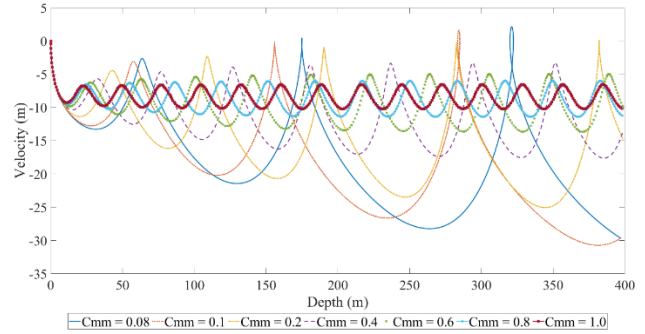
200 m water depth



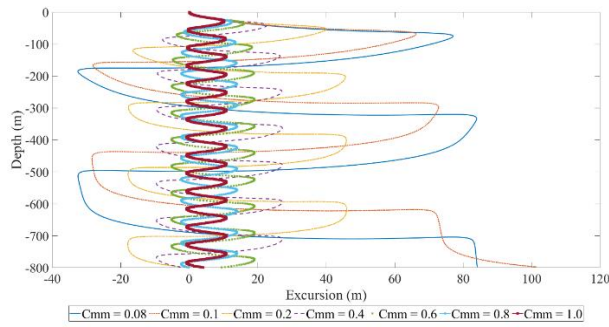
200 m water depth



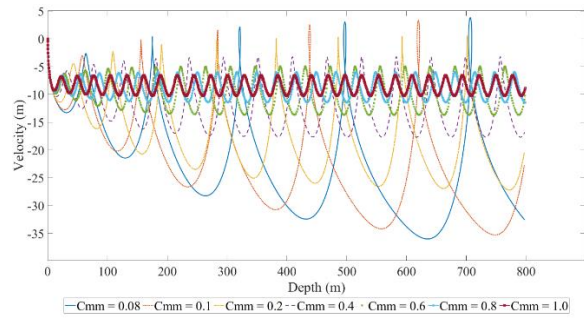
400 m water depth



400 m water depth

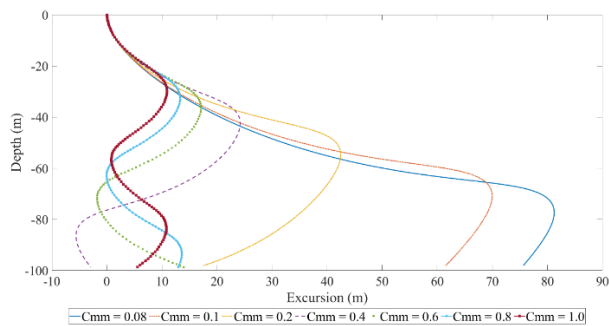


800 m water depth

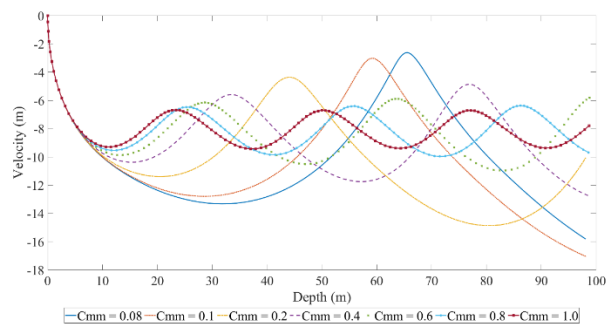


800 m water depth

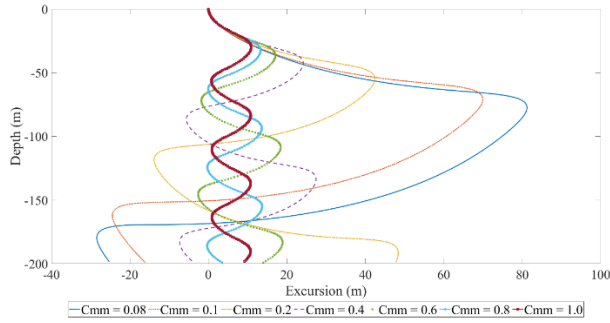
Figure 0.5 Excursion and velocity of full-scale model when $\beta = 45^\circ$ and $C_{d,moment} = 1.0$ for different Munk moment coefficient (C_{mm}) in different water depth



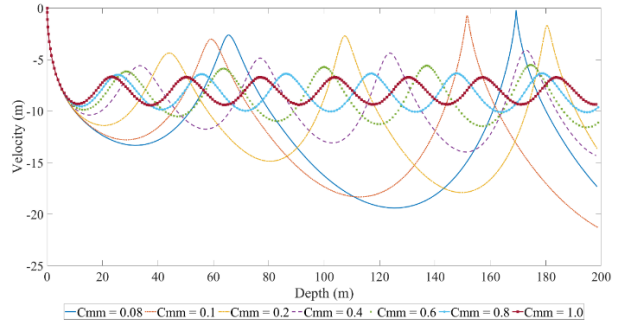
100 m water depth



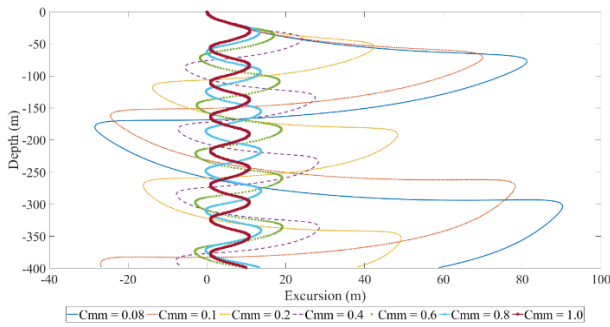
100 m water depth



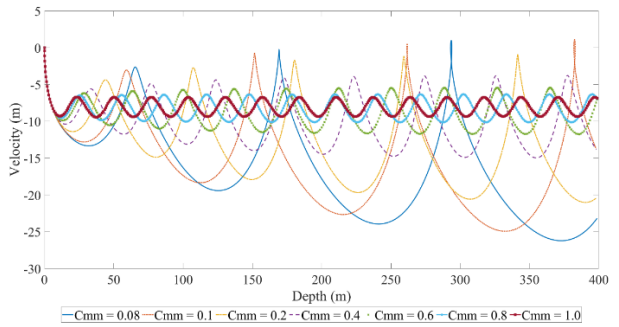
200 m water depth



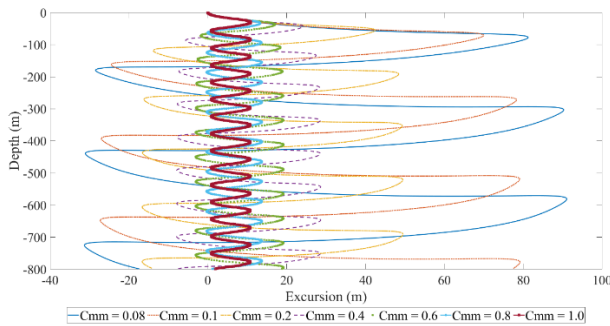
200 m water depth



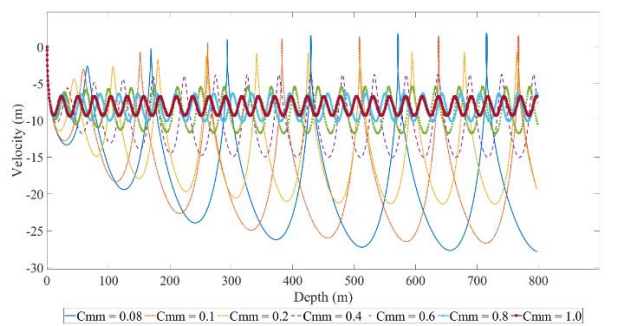
400 m water depth



400 m water depth

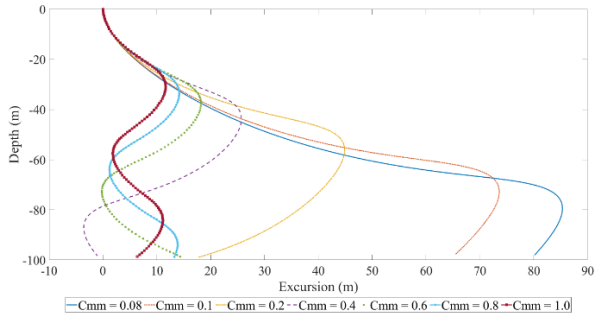


800 m water depth

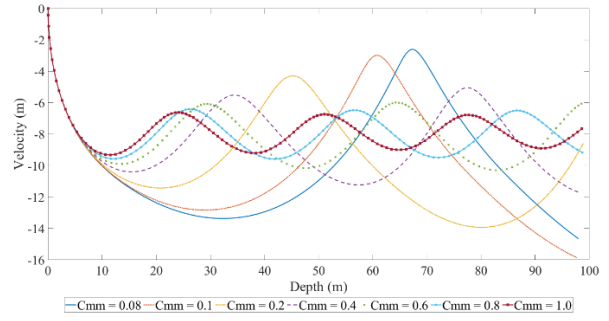


800 m water depth

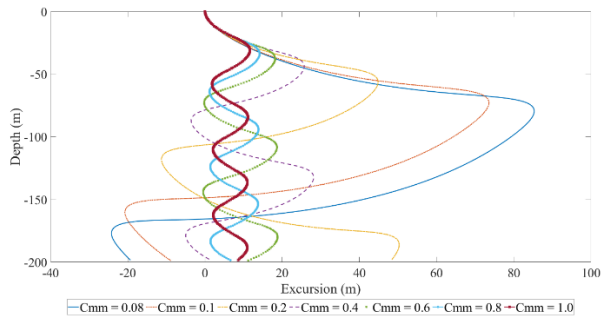
Figure 0.6 Excursion and velocity of full-scale model when $\beta = 45^\circ$ and $C_{d,moment} = 1.2$ for different Munk moment coefficient (C_{mm}) in different water depth



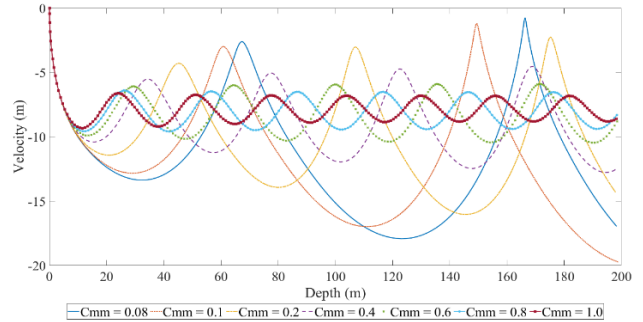
100 m water depth



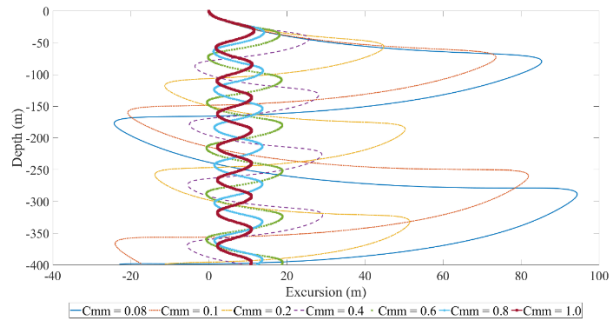
100 m water depth



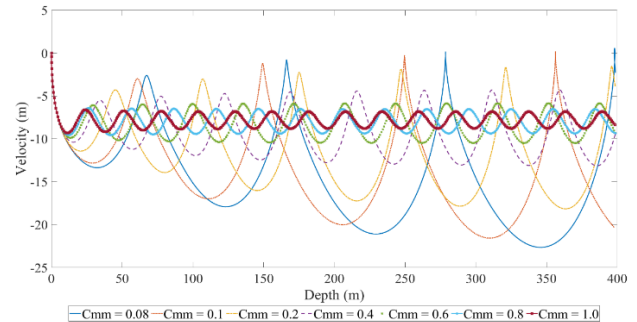
200 m water depth



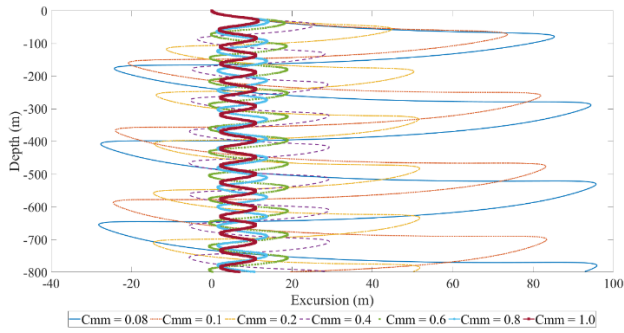
200 m water depth



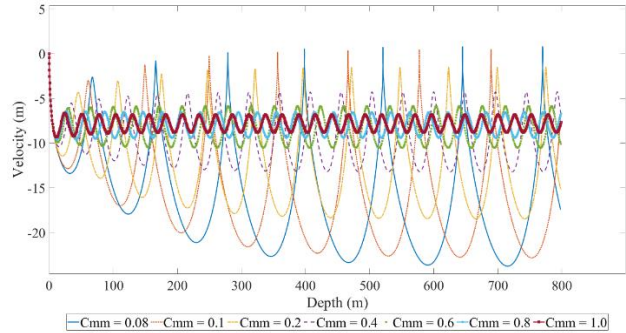
400 m water depth



400 m water depth



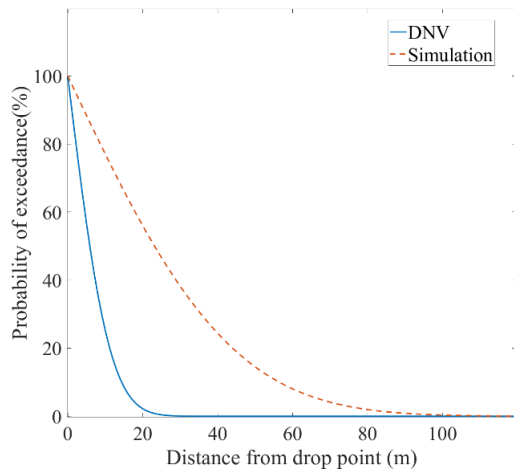
800 m water depth



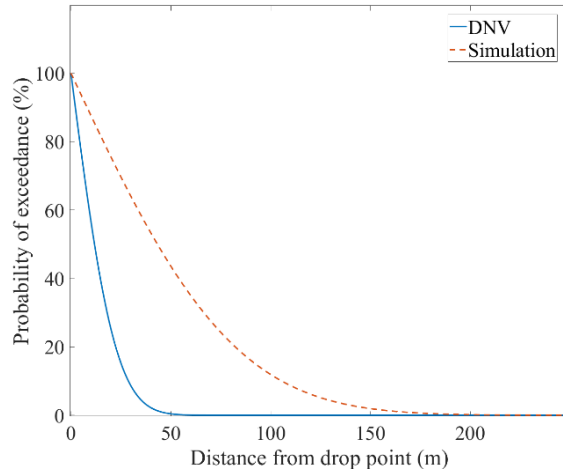
800 m water depth

Figure 0.7 Excursion and velocity of full-scale model when $\beta = 45^\circ$ and $C_{d,moment} = 1.4$ for different Munk moment coefficient (C_{mm}) in different water depth

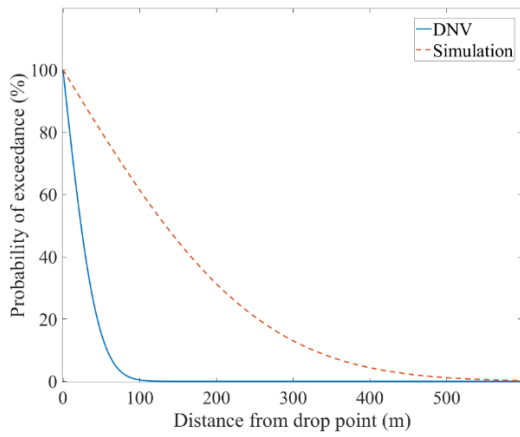
Appendix IV



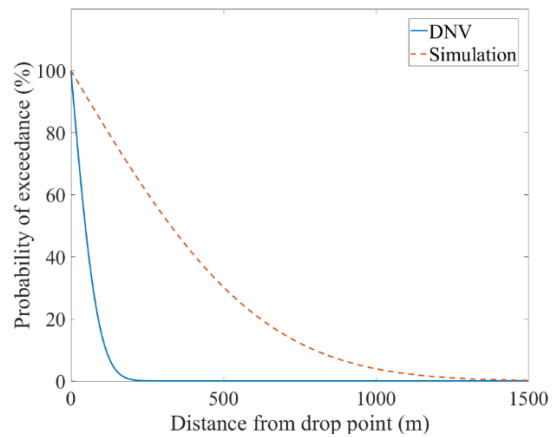
100 m water depth



200 m water depth



400 m water depth



800 m water depth

Figure 0.1 Comparison of probability of exceedance based on DNV (RP) and OrcaFlex simulations for full-scale model in different water depth

Appendix V

Detail of Analytical calculations

Small-scale model:

$$g = 0.98 \left(\frac{m}{s^2}\right)$$

$$m = 0.2466 \text{ (kg)}$$

$$\rho = 998 \left(\frac{kg}{m^3}\right)$$

$$\nabla = 3.53 \times 10^{-5} (m^3)$$

For $\beta = 0^\circ$:

$$C_d = 1.0$$

$$A = 0.01 \times 0.45 = 4.5 \times 10^{-3} (m^2)$$

$$V_T = \sqrt{2 \times 9.81 \times \left(\frac{0.2466 - 998 \times 3.53 \times 10^{-5}}{1.0 \times 4.5 \times 10^{-3} \times 998} \right)} = 0.96 \left(\frac{m}{s}\right)$$

For $\beta = 90^\circ$:

$$C_d = 0.005$$

$$A = \pi \times 0.01 \times 0.45 = 0.0142 (m^2)$$

$$V_T = \sqrt{2 \times 9.81 \times \left(\frac{0.2466 - 0.998 \times 3.53 \times 10^{-5}}{0.005 \times 4.5 \times 10^{-3} \times 0.998} \right)} = 7.6 \left(\frac{m}{s}\right)$$

Full-scale model:

$$g = 0.98 \left(\frac{m}{s^2}\right)$$

$$m = 2238.75 \text{ (kg)}$$

$$\rho = 1025 \left(\frac{kg}{m^3}\right)$$

$$\nabla = 0.3226 \text{ (m}^3\text{)}$$

For $\beta = 0^\circ$:

$$C_d = 0.34$$

$$A = 0.2032 \times 9.95 = 2.02 \text{ (m}^2\text{)}$$

$$V_T = \sqrt{2 \times 9.81 \times \left(\frac{2238.75 - 1025 \times 0.3226}{0.34 \times 2.02 \times 1025}\right)} = 7.29 \left(\frac{m}{s}\right)$$

For $\beta = 90^\circ$:

$$C_d = 0.002$$

$$A = \pi \times 0.2032 \times 9.95 = 6.351 \text{ (m}^2\text{)}$$

$$V_T = \sqrt{2 \times 9.81 \times \left(\frac{2238.75 - 1025 \times 0.3226}{0.002 \times 6.351 \times 1025}\right)} = 53.61 \left(\frac{m}{s}\right)$$

Appendix VI

```
import OrcFxAPI

import matplotlib.pyplot as plt

import pandas as pd

import math

### Calculating the cylinder data

rho = 6935 # Steel density (te/m^3)

D_o = 0.2032 # Outer diameter (m)

m_L = 225 # Mass per unit length (kg/m)

L = 9.95 # Length of the pipe (m)

D_i = 0 # Calculating the inner diameter of the

volume = math.pi*L*(D_o**2)/4 # pipe volume(m^3)

### Finding mass of the pipe

m = m_L*L/1000 # Total mass of the pipe (te)

#m = rho*volume/1000 # Total mass of the pipe (te)

### Finding mass moment of inertia

I_z = (m/12)*(3*((D_o/2)**2+(D_i/2)**2)+L**2) # Mass moment of inertia in local Z
axis(te.m^2)

I_y = (m/12)*(3*((D_o/2)**2+(D_i/2)**2)+L**2) # Mass moment of inertia in local Y
axis(te.m^2)
```

```

I_x = (m/2)*((D_o/2)**2+(D_i/2)**2)          # Mass moment of inertia in local X
axis(te.m^2)

### Find drag area

AD_n = L*D_o                                # Normal drag area (m^2)

AD_a = math.pi*(D_o+D_i)*L                  # Axial skin friction area (m^2)

print(f'Axial skin friction area of the pipe = {round(AD_a,6)} m^2')

### Find drag moment of area

MD_n = (D_o*L**4)/(32)                       # Normal drag moment of area (m^5)

MD_a = (D_o**5-D_i**5)/60                    # Axial drag moment of the area (m^5)

print(f'total mass of the pipe = {round(m,8)} te')

print(f'mass moment of inertia of the pipe (X_axis) = {round(I_x,12)} te.m^2')

print(f'mass moment of inertia of the pipe (Y_axis) = {round(I_y,8)} te.m^2')

print(f'mass moment of inertia of the pipe (Z_axis) = {round(I_z,8)} te.m^2')

print(f'Inner diameter of the pipe = {round(D_i,8)} m')

print(f'volume of the pipe = {volume} m^3')

print(f'Normal drag area of the pipe = {round(AD_n,8)} m^2')

print(f'Normal drag moment of area of the pipe = {round(MD_n,8)} m^5')

print(f'Axial drag moment of area of the pipe = {round(MD_a,8)} m^5')

```



```
### Creating variable for parametric study
```

```
x=0
```

```
a=0
```

```
b=90
```

```
i=a
```

```
drop_angle=[]
```

```
X=[]
```

```
while i<= b:
```

```
    drop_angle.append(i)
```

```
    i+=1
```

```
### Open the model
```

```
model = OrcFxAPI.Model()
```

```
# Open OF model
```

```
model.LoadData("Full_Scaled_cylinder.dat")
```

```
# Load entire simulation file
```

```
model.Reset()
```

```
# Make sure that the model is in a
```

```
reset state, this removes all simulation cache
```

```
for j in range(0, len(drop_angle)):
```

```
### Defining simulation period
```

```
model.general.StageDuration[0] = 1e-6
```

```
# First stage duration
```

```
model.general.StageDuration[1] = 180
```

```
# Drop simulation duration
```

```
### Define environmental parameters in OF model
```

```
model.environment.WaterDepth= 5000
```

```
# Define water depth (m)
```

```
model.environment.WaveHeight= 0
```

```
# Wave height (m)
```

```
model.environment.RefCurrentSpeed= 0
```

```
# Current velocity (m/s)
```

```
model.environment.Density = 1.025
```

```
# Water density (te/m3)
```

```
### Define object parameters
```

```
model.general.StartingVelocitySpeed = 0
```

```
# Initial velocity of the object
```

```
model.general.StartingVelocityDirection = 0
```

```
# Initial angle of velocity direction
```

Initial location and attitude

```
Pipe = model['buoy1']           # Selecting the object
Pipe.InitialX = 0               # Initial location of the pipe in X direction (m).
Pipe.InitialY = 0               # Initial location of the pipe in Y direction (m).
Pipe.InitialZ = -4.975         # Initial location of the pipe in Z direction (m).
Pipe.InitialRotation1 = 0      # Initial angle of inclination around X axis (degree).
Pipe.InitialRotation2 = drop_angle[j] # Initial angle of inclination around Y axis (degree).
Pipe.InitialRotation3 = 0      # Initial angle of inclination around Z axis (degree).
```

Inertia

```
Pipe.Mass = m                  # Mass of the object (te).
Pipe.MassMomentOfInertiaX = I_x # Mass moment of inertia around X axis(te.m^2).
Pipe.MassMomentOfInertiaY = I_y # Mass moment of inertia around Y axis(te.m^2).
Pipe.MassMomentOfInertiaZ = I_z # Mass moment of inertia around Z axis(te.m^2).
```

Geometry

```
Pipe.StackBaseCentreX = -L/2   # Location of stack base in X direction (m).
```

Pipe.StackBaseCentreY = 0 # Location of stack base in Y direction (m).

Pipe.StackBaseCentreZ = 0 # Location of stack base in Z direction (m).

Pipe.CylinderInnerDiameter[0] = D_i # Inner diameter of the cylinder1 (m).

Pipe.CylinderOuterDiameter[0] = D_o # Outer diameter of the cylinder1 (m).

Pipe.CylinderLength [0] = L # Length of the cylinder1 (m).

drag & Slam

Pipe.MunkMomentCoefficient = 0.08 # Munk moment coefficient

Pipe.CylinderNormalDragArea[0] = AD_n # Normal drag area (m)

Pipe.CylinderAxialDragArea[0] = AD_a # Axial skin drag area (m).

Pipe.CylinderNormalDragForceCoefficient[0] = 0 # Drag coefficient normal to cylinder longitudinal axis.

Pipe.CylinderAxialDragForceCoefficient[0] = 0 # Drag coefficient in axial direction.

Pipe.CylinderNormalDragAreaMoment[0] = MD_n # Third moment of area of the normal drag area projection (m⁵).

Pipe.CylinderAxialDragAreaMoment[0] = MD_a # Third moment of area of the axial drag area projection (m⁵).

Pipe.CylinderNormalDragMomentCoefficient[0] = 0.34 # Normal drag moment coefficient.

Pipe.CylinderAxialDragMomentCoefficient[0] = 0 # Axial drag moment coefficient.

Pipe.CylinderSlamForceDataEntry[0] = 0 # Slam force entry coefficient.

Pipe.CylinderSlamForceDataExit[0] = 0 # Slam force exit coefficient.

Added mass & damping

Ca_Normal = 1 # Normal added mass coefficient

Ca_Axial = 0.63 # Axial added mass coefficient

Pipe.CylinderNormalAddedMassForceCoefficient[0] = Ca_Normal # Normal added
mass force coefficient_Ca.

Pipe.CylinderAxialAddedMassForceCoefficient[0] = Ca_Axial # Axial added mass
force coefficient_Ca.

Pipe.CylinderNormalInertiaForceCoefficient[0] = Ca_Normal+1 # Normal inertia
force coefficient_Cm.

Pipe.CylinderAxialInertiaForceCoefficient[0] = Ca_Axial+1 # Axial inertia force
coefficient_Cm.

Pipe.CylinderNormalAddedMomentOfInertia[0] = 0 # Normal added moment of inertia
coefficient (te.m²).

Pipe.CylinderAxialAddedMomentOfInertia[0] = 0 # Axial added moment of inertia
coefficient (te.m²).

Pipe.CylinderUnitNormalDampingForce[0] = 0 # Normal unit damping force (kN/m/s).

Pipe.CylinderUnitAxialDampingForce[0] = 0 # Axial unit damping force (kN/m/s).

```
Pipe.CylinderUnitNormalDampingMoment[0] = 0    # Normal unit damping moment  
(kN.m/rad/s).
```

```
Pipe.CylinderUnitAxialDampingMoment[0] = 0    # Axial unit damping moment  
(kN.m/rad/s).
```

```
### Start simulation
```

```
model.CalculateStatics()                       # Run static analysis
```

```
model.RunSimulation()                         # Run Dynamic analysis
```

```
### save data
```

```
X = Pipe.TimeHistory('X')                    # Time history of displacement in X direction.
```

```
Z = Pipe.TimeHistory('Z')                    # Time history of displacement in Z direction.
```

```
V_x = Pipe.TimeHistory('GX velocity')        # Time history of velocity in X direction
```

```
V_z = Pipe.TimeHistory('GZ velocity')        # Time history of velocity in Z direction
```

```
V = Pipe.TimeHistory('Velocity')            # Time history for summation of velocity vectors
```

```
t = Pipe.SampleTimes()                       # Simulation duration sampling
```

```
### Create a name for the specific case
```

```

name = 'pipe'+\

'_dropAngle_'+ str(Pipe.InitialRotation2)+\

'_munk_' + str(Pipe.MunkMomentCoefficient)+\

'_Cd_'+str(Pipe.CylinderNormalDragMomentCoefficient[0])+

'_height_'+ str(Pipe.InitialZ)

model.SaveSimulation(name +'.sim')           # Save the model and simulation file

j+=1

x = x + 1                                     # Count files

df = pd.DataFrame({'time':t,'X':X,'Z':Z,'V_x':V_x,'V_z':V_z,'V':V}) # Produce a data frame
including t, X, Z

df.to_excel(name+'.xlsx',index=(False))      # Write the data frame to excel and removing
index

### Plot the data

plt.plot(X,Z)

plt.xlabel('Excursion')

plt.ylabel('Depth')

plt.legend(['0', '30', '45','60','90'],title = 'Munk')

```

```

plt.title('h='+str(Pipe.InitialZ)+'-Munk moment coefficient =
'+str(Pipe.MunkMomentCoefficient)+'_Cd_' +
str(Pipe.CylinderNormalDragMomentCoefficient[0]))

print(x)

```

```

df1 = pd.DataFrame()          # Create an empty DataFrame to store the extracted data

df2 = pd.DataFrame()

df3 = pd.DataFrame()

df4 = pd.DataFrame()

df5 = pd.DataFrame()

df6 = pd.DataFrame()

file_name = 'pipe_dropAngle'

for file in glob.glob(file_name+'*.xlsx'):      # Loop through all Excel files in a directory

    column_name = file.split('.')[0]          # Extract the file name without the extension

    X_data = pd.read_excel(file, usecols=['X']) # Read the Excel file and extract the desired
column

    df1[column_name] = X_data                  # Add the extracted column to the DataFrame
with the file name as the column name

    Z_data = pd.read_excel(file, usecols=['Z']) # Extracting Z data from last excel file

    df2[column_name] = Z_data

```



```

V_x_data = pd.read_excel(file, usecols=['V_x']) # Extracting Velocity in X direction data

df3[column_name] = V_x_data

V_z_data = pd.read_excel(file, usecols=['V_z']) # Extracting Velocity in Z direction data

df4[column_name] = V_z_data

time_data = pd.read_excel(file, usecols=['time']) # Extracting Velocity in Z direction data

df5[column_name] = time_data

V_data = pd.read_excel(file, usecols=['V']) # Extracting Velocity in Z direction data

df6[column_name] = V_data

### Create a file name

name1 = 'excursion_'+ file_name

name2 = 'depth_'+ file_name

name3 = 'GX_velocity_'+ file_name

name4 = 'GZ_velocity_'+ file_name

name5 = 'time_'+ file_name

name6 = 'Velocity_'+ file_name

# Save the data frame to an excel file

```

```
df1.to_excel(name1+'.xlsx',index=(False))
```

```
df2.to_excel(name2+'.xlsx',index=(False))
```

```
df3.to_excel(name3+'.xlsx',index=(False))
```

```
df4.to_excel(name4+'.xlsx',index=(False))
```

```
df5.to_excel(name5+'.xlsx',index=(False))
```

```
df6.to_excel(name6+'.xlsx',index=(False))
```

```
# Display the resulting DataFrame
```

```
print(df1)
```

```
print(df2)
```

```
print(df3)
```

```
print(df4)
```